

The generalized Nielsen-Ninomiya Theorem for the 17 wallpaper: Classification of 2D nodal superconductors, Dirac semimetals, and non-Hermitian nodal systems

Congcong Le,^{1,2,3,*} Zhesen Yang,^{4,5,2,*} Fan Cui,^{4,5} A. P. Schnyder,⁶ and Ching-Kai Chiu^{2,3,†}

¹Max Planck Institute for Chemical Physics of Solids, 01187 Dresden, Germany

²Kavli Institute for Theoretical Sciences, University of Chinese Academy of Sciences, Beijing 100190, China

³RIKEN Interdisciplinary Theoretical and Mathematical Sciences (iTHEMS), Wako, Saitama 351-0198, Japan

⁴Beijing National Laboratory for Condensed Matter Physics,

Institute of Physics, Chinese Academy of Sciences, Beijing 100190, China

⁵University of Chinese Academy of Sciences, Beijing 100049, China

⁶Max-Planck-Institute for Solid State Research, Heisenbergstr. 1, D-70569 Stuttgart, Germany

(Dated: May 16, 2022)

The Nielsen-Ninomiya Theorem has set up a ground rule for the minimal number of the topological points in a Brillouin zone. Notably, in the 2D Brillouin zone, chiral symmetry and space-time inversion symmetry can properly define topological invariants as charges characterizing the stability of the nodal points so that the non-zero charges protect these points. Due to the charge neutralization, the Nielsen-Ninomiya Theorem requires at least two stable topological points in the entire Brillouin zone. However, additional crystalline symmetries might duplicate the points. In this regard, for the wallpaper groups with crystalline symmetries, the minimal number of the nodal points in the Brillouin zone might be more than two. In this work, we determine the minimal numbers of the nodal points for the wallpaper groups in chiral-symmetric and space-time-inversion-symmetric systems separately and provide examples for new topological materials, such as topological nodal time-reversal-symmetric superconductors and Dirac semimetals. This generalized Nielsen-Ninomiya Theorem serves as a guide to search for 2D topological nodal materials. Furthermore, we show the Nielsen-Ninomiya Theorem can be extended to 2D non-Hermitian systems hosting topologically protected exceptional points and Fermi points for the 17 wallpaper groups.

PACS numbers:

I. INTRODUCTION

The study of various topologically protected points in lattice has deepened our understanding of profound knowledge in condensed matter physics [1–7]. In particular, the 2D nodal point, which is one type of these topological points, emerged in a variety of solid-state systems [8–12]. The manipulation of Dirac points in graphene has broadened our knowledge of strongly correlated systems [13–16] and topological phases [17–20]. Furthermore, nodal time-reversal symmetric superconductors host nodal points at zero energy revealing Majorana flat bands in the edges [21, 22]. While the nodal points require symmetry for protection, exceptional points in non-Hermitian systems are robust even without symmetry protection [23–25]. All of these special topological points in 2D Hermitian and non-Hermitian lattice follow the Fermion doubling theorem (Nielsen-Ninomiya theorem) [26–28] as a universal no-go theorem.

In Hermitian systems, the Nielsen-Ninomiya Theorem in 2D is different from the one in 1D and 3D. That is, symmetries are required to protect 2D nodal points; either space-time inversion symmetry or chiral symmetry can protect 2D Dirac nodes with *2-fold degeneracy* at any location in the Brillouin zone (BZ). Space-time inversion symmetry quantizes the Z_2 Berry phase in the 1D integral path [29], whereas chiral sym-

metry leads to a well-defined integer winding number in the 1D integral path [5, 11]. When the 1D integral path encircles a Dirac node, the non-zero integral invariant stabilizes the Dirac node. The reason is that if the Dirac node is gapped, the integral path can become contractible and then vanishes. Since this contradicts the robustness of the non-zero invariant, the invariant quantized by the symmetries protects the Dirac node. This robustness manifests the emergence of multiple 2D Dirac semimetals [30–33].

In chiral-symmetric systems, Dirac points with non-zero integer winding numbers are stable and fixed at zero energy, while in space-time inversion symmetric systems, Dirac points can be moved to any energy level and are the only stable nodal points due to the Z_2 invariant. On the other hand, in 2D non-Hermitian systems, robust Fermi points [34] and exceptional points [24] are characterized by other non-zero integer winding numbers even in the absence of any symmetries. Those topological points (nodal points, Fermi points, exception points) in the Hermitian and non-Hermitian lattices always obey the Nielsen-Ninomiya Theorem as the ground rule [25]. In other words, in a 2D lattice, a topological point inevitably accompanies at least another topological point since the total charges characterizing the topological points in the entire BZ must be neutralized. However, in the presence of other symmetries, this no-go theorem might not be that simple. Generally, a 2D lattice system belongs to one of the 17 wallpaper groups (WGs) and preserves on-site symmetries, such as time-reversal symmetry. The additional symmetries limit the possible number of the topological points and confine the points in designated locations in the BZ. In other

*These two authors contributed equally

†Electronic address: Corresponding: ching-kai.chiu@riken.jp

words, the minimal number of the topological points might be more than two; hence, the fermion “doubling” theorem is not a proper name for the generalization of the theorem; hence, we use Nielsen-Ninomiya theorem or no-go theorem for the name. In the literature, the generalized Nielsen-Ninomiya theorem has not been exhaustively studied for different wallpaper groups with or without time reversal symmetry. Due to the growing interest in topological materials, it is essential to set up the ground rule to understand the minimal multiplicity of the topological points for different crystalline symmetries and on-site symmetries.

To investigate the generalized no-go theorem, we consider the three distinct 2D platforms — nodal chiral-symmetric systems, space-time inversion symmetric semimetals, and non-Hermitian systems. That is, in the manuscript our generalized no-go theorem exhaustively includes any 2D lattice possessing the topological points characterized by \mathbb{Z} and \mathbb{Z}_2 invariants. For Hermitian lattices, we note that the fragile topology [35–37] or Dirac nodes protected by different crystalline symmetries [38, 39] is not considered here, and our focus is on the stable nodal points, even in the presence of trivial bands and 2-fold degenerate Dirac nodes protected by chiral symmetry or space-time inversion symmetry. First, we start with the minimal configurations and multiplicities of the nodal points at zero energy protected by chiral symmetry for all the 17 wallpaper groups in the BZ. The chiral-symmetric systems without and with different types of time reversal symmetry and particle-hole symmetry correspond to five of the ten Altland-Zirnbauer (AZ) symmetry classes [40–42]. These five AZ classes (AIII, BDI, DIII, CII, CI) preserving chiral symmetry must be treated separately for the generalized no-go theorem since different time reversal symmetries lead to different charges and configurations for the nodal points. Second, in space-time-reversal-symmetric semimetals the nodal points characterized by the \mathbb{Z}_2 invariants might have different minimal configurations for the generalized no-go theorem with \mathbb{Z} invariants. The reason is that the two nodal points with non-zero \mathbb{Z}_2 charges can be annihilated [43], whereas the ones with non-zero integer charges together are always intact. However, space-time inversion symmetry can be realized in the wallpaper groups preserving inversion symmetry. Hence, only ten wallpaper groups, which possess inversion symmetry, can be studied for the generalized no-go theorem. Lastly, in 2D non-Hermitian systems without symmetries, exceptional points and Fermi points are characterized by integer winding numbers [9, 25, 44, 45], whose mathematical structures are similar to the winding number quantized by chiral symmetry. In this regard, we directly extend the generalized no-go theorem of the nodal chiral-symmetric systems in class AIII to the topological points in the non-Hermitian systems for all the 17 wallpaper groups. In addition, in non-Hermitian systems, the transpose operation and the complex-conjugation operation are not equivalent [46]. When those operations combine with crystalline operations, combined crystalline symmetries emerge. We also expand the generalized no-go theorem for the combined crystalline symmetries.

This generalized no-go theorem provides a new approach to understand the topological phases beyond the methodology

of the symmetry indicators [47–51], which can detect some topological phases but cannot sense most of the nodal points at the general points in the BZ. Our generalization of the no-go theorem for the 17 wallpaper groups thoroughly shows the minimal configurations for the topological points at different locations of the BZ, particularly including the general points. Furthermore, this generalized theorem can be applied for any topological points characterized by \mathbb{Z} and \mathbb{Z}_2 invariants and governs various topological systems. For instance, spinless and spinful topological nodal time-reversal symmetric superconductors in class BDI and class DIII are two of the physical examples [22, 52]; the nodal points in the bulk Bogoliubov-de-Gennes Hamiltonian connect Majorana flat bands on the edges [21, 53, 54]. The generalized no-go theorem lists the minimal multiplicity and configurations of the nodal points for different symmetries. Furthermore, our theorem can be directly extended to 2D non-Hermitian systems and capture the minimal configuration of the exceptional points, which connect bulk Fermi arcs [55]. In addition, Dirac semimetals are another promising example [33, 38, 56–66]. For free fermion systems, space-time inversion symmetry protects Dirac points unfixed at any energy level. This theorem exhaustively provides the possible configurations of the Dirac points in 2D lattice and serves a guide to hunt new Dirac semimetals.

The remainder of this paper is organized as follows. In sec. II, before going through the technicality, we provide an overview of the no-go theorem for the 17 WGs in topological points Hermitian and non-Hermitian lattices. In sec. III, we thoroughly study the generalized no-go theorem for zero-energy nodal points protected by chiral symmetry. In sec. IV, using a similar approach, we extend the no-go theorem to Dirac nodes protected by space-time inversion symmetry for the 10 WGs possessing inversion symmetry. In sec. V, we show that the non-Hermitian no-go theorem for exceptional points and Fermi points inherits some features from the Hermitian chiral-symmetric one and distinctly have additional restrictions from rotation symmetries. Lastly, we conclude with a summary in Sec. VI. Some technical details have been relegated to appendices.

II. THE OVERVIEW OF THE NO-GO THEOREM FOR THE 17 WALLPAPER GROUPS

We begin with the overview of the generalized no-go theorem for 2D Hermitian and non-Hermitian lattices for the 17 wallpaper groups, and the following sections will serve all of the details. In general, in the 2D BZ, a stable topological point at \mathbf{k}_i is characterized by a non-zero charge $C(\mathbf{k}_i)$, and the charge can be a \mathbb{Z} or \mathbb{Z}_2 invariant. The key of the no-go theorem is that the summation of the charges carried by the topological points in the entire BZ must vanish as charge neutralization, i.e.,

$$\sum_{\mathbf{k}_i \in \text{BZ}} C(\mathbf{k}_i) = 0. \quad (1)$$

This neutralization equation directly leads to the well-known statement of the Nielsen-Ninomiya theorem [26–28] that a stable topological point must be accompanied by at least another topological point in the 2D BZ. To quantify the minimal multiplicity of the topological points, we define the absolute charge number

$$\nu_{\text{abs}} = \sum_{\mathbf{k}_i \in \text{BZ}} |C(\mathbf{k}_i)|. \quad (2)$$

In chosen symmetry class, the minimum of this number corresponds to the minimal multiplicity and configuration of the topological points. The standard Nielsen-Ninomiya theorem [26–28] shows $\nu_{\text{abs}} \geq 2$ and ν_{abs} is always an even number. We note that ν_{abs} can be an integer greater than one, even though the charge $C(\mathbf{k}_i)$ might have \mathbb{Z}_2 property. The reason is that the topological points may be at different locations and cannot be annihilated. Beyond the Nielsen-Ninomiya theorem, our generalized no-go theorem shows that for some WGs, ν_{abs} is always greater than 2 so that the minimal number of the topological points with charge weights is greater than 2. The main results of our generalized no-go theorem for Hermitian and non-Hermitian 2D lattices, which shows the minimal number of ν_{abs} , are summarized in Table I.

First, let us introduce the no-go theorem for 2D Hermitian lattices preserving chiral symmetry for the 17 WGs in Table I. Chiral symmetry makes the nodal points carrying non-zero \mathbb{Z} winding numbers [5, 11] stable and locked at zero energy. The 17 WGs are simplified to 11 equivalent sets based on point groups, and 5 AZ symmetry classes (AIII, BDI, DIII, CI, and CII) can also be divided into four categories, since BDI and CII share the same no-go theorem. Hence, the number of symmetry combinations is 44 effective WG symmetry classes. With translation symmetry, each WG is formed by rotation symmetry operation C_n or/and mirror symmetry operation M_x as generators. Here we fix the direction of the mirror M_x along $\overline{\Gamma X}$ for the rectangle (square) BZ and $\overline{\Gamma M}$ for the hexagonal BZs. The minimal configuration of the nodal points further depends on the algebra between the chiral symmetry operator S and the two generators C_n, M_x . In Table I, C_n^\pm represents the rotation symmetry operator commutes/anticommutes with S , while M_x^\pm indicates the mirror symmetry operator commutes/anticommutes with S . The numbers listed in the table represent the minimal absolute number ν_{abs} for each WG symmetry class. Since some symmetries can trivialize the nodal points, ‘0’ indicates the absence of the stable nodal points protected by chiral symmetry. Most of the remaining numbers represent the minimal numbers of the Dirac nodes with ± 1 charge, with the exceptions labeled by *; due to the symmetry constraints, the minimal configurations of the exceptions require the presence of nodal points with high charges, whose absolute values are greater than one $|C| > 1$. For example, in class CI in WG#10 with C_4^+ the unique minimal configuration for $\nu_{\text{abs}} = 4$ is given by one nodal point with +2 winding number and the other with -2 winding number.

For other Hermitian systems, stable nodal points protected by space-time inversion symmetry ($(C_2T)^2 = 1$) carry only ± 1 charge, due to the \mathbb{Z}_2 invariant of the Berry phase [29,

43]. That is, there is only one type of stable nodal points. Being different from topological points with \mathbb{Z} charges, two of the non-zero \mathbb{Z}_2 nodal points together are annihilated. In this regard, the no-go theorem with \mathbb{Z}_2 invariants is distinct from the theorem with \mathbb{Z} invariants. On the other hand, inversion symmetry is required in the WGs to form space-time inversion symmetry with time-reversal symmetry. Only 10 of the 17 WGs preserving inversion symmetry can possess the \mathbb{Z}_2 nodal points. Furthermore, the (anti)commutation relation between C_2T and the generators (C_n, M_x) does not affect the no-go theorem. In Table I, the numbers ν_{abs} marked by \diamond indicate the minimal numbers of the protected nodal points for the 10 WGs. We note that those numbers also represent the minimal absolute numbers ν_{abs} for chiral symmetric lattices in class AIII.

Lastly, for 2D non-Hermitian lattices, any symmetry is no longer required to protect topological points; robust Fermi points and exceptional points carrying non-zero charges naturally arise [9, 24, 25]. In the absence of the symmetry requirement for protection, the algebra between the symmetry operators is inapplicable to classify the minimal configuration of the non-Hermitian systems. Hence, the 17 WGs are the only symmetry classes in this classification. Since the charges of the Fermi points and exceptional points share the same \mathbb{Z} properties, these two distinct types of the topological points obey the same generalized rules of the no-go theorem. The non-Hermitian lattices and the Hermitian chiral-symmetric ones share \mathbb{Z} invariant, so the restriction of the nodal points in the chiral-symmetric systems with C_n^+, M_x^+ can be applied to the non-Hermitian for the 17 WGs. The only difference is that the charges of the non-Hermitian topological points at rotation centers, say C_n , must be the multiple of n . Following this additional rule, we note that the non-Hermitian no-go theorem does not always share the same minimal absolute numbers ν_{abs} with the chiral-symmetric lattices in class AIII. In Table I, the generalized no-go theorem for the non-Hermitian lattices is shown by the absolute charge numbers labeled by \bullet .

Table I serves as a dictionary showing the minimum of the absolute charge numbers ν_{abs} for the three distinct 2D lattice systems as the generalized no-go theorem. However, in the minimal configurations, topological points have to be located at specific momenta in the BZ. That is, the configuration of the topological points profoundly depends on their locations. The location-dependent multiplicities of the topological points are studied in great detail in the following sections. Furthermore, our generalized theorem lists all of the possible configurations of Dirac nodes; this prediction can lead to possible discoveries of new exotic Dirac materials. The following sections provide the tight-binding models for the potential realization and the detailed derivation of the generalized no-go theorem.

III. 2D HERMITIAN CHIRAL-SYMMETRIC LATTICES

We start with 2D Hermitian lattices preserving chiral symmetry. Since there are 5 AZ symmetry classes with chiral symmetry, the generalized no-go theorem for chiral symmetry is much more complicated than space-time-inversion-

TABLE I: **The minimum multiplicity list for topological points in Hermitian and non-Hermitian lattices.** The entire table exhaustively lists minimal ν_{abs} describing the minimal multiplicities of the nodal points at zero energy for each WG and AZ symmetry class preserving chiral symmetry. For each WG, one or two point group generators with signs indicate the algebra between the chiral symmetry operator and the generators. While ‘0’ indicates the absence of nodal points protected by chiral symmetry, non-zero ν_{abs} indicates the minimal number of Dirac points with ± 1 charges for most of the WG symmetry classes, with the exceptions labelled by *. That is, in the exceptions the minimal configurations require the presence of at least one high-ordered nodal point, of which the charge is not ± 1 . On the other hand, label \diamond indicates the minimal numbers of the Dirac nodes for space-time-inversion-symmetric lattices for 10 of the WGs. For non-Hermitian systems, label \bullet marks the minimal numbers of Fermi points and exceptional points for the 17 WGs.

WG	Generators	AIII	BDI/CI	DIII	CI
#1		2^\bullet	2	4	4
#2	C_2^+	4^\bullet	0	4	4
	C_2^-	2^\diamond	2	0	0
#3,4,5	M_x^+	2^\bullet	2	4	4
	M_x^-	2	2	4	4
#6,7	C_2^+ and M_x^+	4^\bullet	0	4	4
8,9	C_2^+ and M_x^-	4	0	4	4
	C_2^- and M_x^\pm	2^\diamond	2	0	0
#10	C_4^+	$4, 8^\bullet$	0	4	4^*
	C_4^-	4^\diamond	0	4	4
#11,12	C_4^+ and M_x^+	8^\bullet	0	8	8
	C_4^+ and M_x^-	4	0	4	4^*
	C_4^- and M_x^\pm	4^\diamond	0	4	4
#13	C_3^+	$2, 6^\bullet$	2	4^*	4^*
	C_3^-	0	0	0	0
#14	C_3^+ and M_y^+	$2, 6^\bullet$	2	12	12
	C_3^+ and M_y^-	6	6	4^*	4^*
	C_3^- and M_y^\pm	0	0	0	0
#15	C_3^+ and M_x^+	6^\bullet	6	12	12
	C_3^+ and M_x^-	2	2	4^*	4^*
	C_3^- and M_x^\pm	0	0	0	0
#16	C_6^+	$4^*, 12^\bullet$	0	4^*	4^*
	C_6^-	2^\diamond	2	0	0
#17	C_6^+ and M_x^+	12^\bullet	0	12	12
	C_6^+ and M_x^-	4^*	0	4^*	4^*
	C_6^- and M_x^+	6	6	0	0
	C_6^- and M_x^-	2^\diamond	2	0	0

symmetric systems and non-hermitian lattices. After going through the details of all the chiral symmetry classes, we directly extend these results of the no-go theorem to the two other cases.

A. Nodal points protected by chiral symmetry

We review the interplay of nodal points, chiral symmetry, and winding numbers by showing that the non-zero winding number quantized by chiral symmetry can protect the nodal point. Furthermore, we build the relation between winding numbers for two nodal points connected by crystalline symmetries or time reversal symmetry. This relation is an important building block for our no-go theorem.

Chiral symmetry is our focus symmetry protecting nodal points with non-zero winding numbers in this section. We consider an (effective) non-interacting system and the Bloch Hamiltonian preserving chiral symmetry obeys

$$S\mathcal{H}(\mathbf{k})S^{-1} = -\mathcal{H}(\mathbf{k}), \quad (3)$$

where unitary matrix S is defined as chiral symmetry operator. One of the ideal platforms to realize chiral symmetry is time-reversal symmetric superconductors [21, 22, 52–54]. Superconductor systems can be described by a Bogoliubov-de Gennes Hamiltonian [67] obeying particle-hole symmetry

$$C\mathcal{H}(-\mathbf{k})C^{-1} = -\mathcal{H}(\mathbf{k}), \quad (4)$$

where particle-hole symmetry operator C is antiunitary. The time-reversal symmetric Hamiltonian also satisfies

$$T\mathcal{H}(-\mathbf{k})T^{-1} = \mathcal{H}(\mathbf{k}), \quad (5)$$

where time-reversal symmetry operator T is also antiunitary. Consequently, the combination of particle-hole symmetry and time-reversal symmetry becomes chiral symmetry with chiral symmetry operator $S = CT$ as a unitary one.

When an eigenstate $|\Psi(\mathbf{k})\rangle$ possesses energy E , the chiral symmetry equation (3) leads to another eigenstate $S|\Psi(\mathbf{k})\rangle$ having energy $-E$; zero energy ($E = 0$) is a special point. Furthermore, it will be shown later that stable nodal points are locked in zero energy so we choose zero energy as Fermi level.

Here we review the definition of the winding number quantized by chiral symmetry. By choosing a proper basis, the chiral symmetry operator is written as $S = \tau_z \otimes \mathbb{I}_{n \times n}$ so the Hamiltonian is in the block off-diagonal form

$$\mathcal{H}(\mathbf{k}) = \begin{pmatrix} 0 & h(\mathbf{k}) \\ h^\dagger(\mathbf{k}) & 0 \end{pmatrix}. \quad (6)$$

Assuming $h(\mathbf{k})$ is invertible ($\det(h(\mathbf{k})) \neq 0$), we can define the winding number in a closed loop integral path in the BZ

$$\begin{aligned} \nu &= \frac{i}{2\pi} \oint d\mathbf{k} \cdot \text{Tr}[h^{-1}(\mathbf{k})\partial_{\mathbf{k}}h(\mathbf{k})] \\ &= \frac{i}{2\pi} \oint d\mathbf{k} \cdot \partial_{\mathbf{k}}\text{Tr}[\ln h(\mathbf{k})] \\ &= \frac{i}{2\pi} \oint d(\ln \det[h(\mathbf{k})]) \end{aligned} \quad (7)$$

By rewriting $\det h(\mathbf{k}) \equiv f(\mathbf{k})e^{i\alpha(\mathbf{k})}$, where $f(\mathbf{k})$ is a single-valued function and $\alpha(\mathbf{k})$ is a multivalued function, the winding number is given by

$$\nu = \frac{-1}{2\pi} \oint d\alpha(\mathbf{k}) \quad (8)$$

Since in the loop the start and end points of the integral are identical, $\oint d\alpha(\mathbf{k}) = 2\pi l$ and then the winding number ν is quantized. We note that the definition of the winding number is equivalent to the one using the flattened Hamiltonian (see Appendix B for the detail).

We demonstrate the interplay of nodal point protection, chiral symmetry, and winding number by using a simple 2×2 Hamiltonian

$$\mathcal{H}_n(\mathbf{k}) = \begin{pmatrix} 0 & (\Delta k_x + i\Delta k_y)^n \\ (\Delta k_x - i\Delta k_y)^n & 0 \end{pmatrix}, \quad (9)$$

where n is a positive integer, $\Delta k_x = k_x - k_{x0}$, $\Delta k_y = k_y - k_{y0}$. The nodal point appears at $\mathbf{K}_0 = (k_{x0}, k_{y0})$ in the BZ with $E = 0$. The energy dispersion $E = \pm\Delta k^n$ and $q = \Delta k e^{in\theta}$, where $\Delta k = \sqrt{\Delta k_x^2 + \Delta k_y^2}$. The meaning of the winding number is the change of $U(1)$ phase of $\det h(\mathbf{k})$ along the close loop $\Gamma(\mathbf{K}_0)$ encircling \mathbf{K}_0 in the counterclockwise direction. The chiral symmetry operator is given by $S = \tau_z$ and $\mathcal{H}(\mathbf{k})$ obeys chiral symmetry equation (3). Here we use the polar coordinate $\Delta k_x \equiv k_0 \cos \theta$ and $\Delta k_y \equiv k_0 \sin \theta$. With the integral path encircling \mathbf{K}_0 , by Eq. 7 the winding number $\nu(\mathbf{K}_0) = n$. ($n = \pm 1$ corresponds to a Dirac point.) This node is equivalent to $|n|$ Dirac nodes with $\nu = \text{sign}(n)$. Chiral symmetry quantizes the winding number and forbids the presence of τ_z destroying the nodal point. Moreover, the zero energy of the nodal point cannot be lifted, since the identity matrix, which is the only one changing the nodal point energy, is forbidden by chiral symmetry. In this regard, the non-zero winding number n indicates the presence of the stable nodal point. We note that without breaking chiral symmetry, the nodal point with winding number n can be deformed to several nodal points and the summation of the winding numbers for the nodal point is still n .

Likewise, the Hamiltonian having another nodal point with $-n$ winding number is written as

$$\mathcal{H}_{-n}(\mathbf{k}) = k_0^n e^{in\theta} \tau_+ + k_0^n e^{-in\theta} \tau_-, \quad (10)$$

When we merge these two systems ($\mathcal{H}_n(\mathbf{k})$ and $\mathcal{H}_{-n}(\mathbf{k})$), the Hamiltonian is given by

$$\mathcal{H}^\pm(\mathbf{k}) = k_0^n \cos n\theta \sigma_0 \otimes \tau_x + k_0^n \sin n\theta \sigma_z \otimes \tau_y, \quad (11)$$

which still preserves chiral symmetry with the symmetry operator $S = \sigma_0 \otimes \tau_z$. Since the total winding number for the nodal point vanishes, we simply find a symmetry-preserving mass term $m\sigma_y \otimes \tau_y$ destroying the nodal point and the gapped energy dispersion is given by $E = \pm\sqrt{k_0^{2n} + m^2}$. Namely, the two nodal points at the same locations with the opposite winding numbers are unstable.

A symmetry operator g acts on the \mathbf{k} -space in the following form

$$g\mathbf{k} = \begin{pmatrix} g_{11} & g_{12} \\ g_{21} & g_{22} \end{pmatrix} \begin{pmatrix} k_x \\ k_y \end{pmatrix}. \quad (12)$$

Suppose there exists a generic nodal point at \mathbf{K}_0 , which is protected by chiral symmetry but not necessarily described by the simple model (9). The winding number of the nodal point is given by

$$\nu(\mathbf{K}_0) = \frac{i}{2\pi} \oint_{\Gamma(\mathbf{K}_0)} \nabla_{\mathbf{k}}(\ln \det[h(\mathbf{k})]) \cdot d\mathbf{k}, \quad (13)$$

where $\Gamma(\mathbf{K}_0)$ indicates an infinitesimal loop of the integral encircling \mathbf{K}_0 counterclockwise. The symmetry results in the presence of a nodal point at $g\mathbf{K}_0$, while this symmetry operator can be time reversal or crystalline. To count the number of the nodal points in the BZ, it is important to study the relation between the two winding numbers ($\nu(\mathbf{K}_0)$, $\nu(g\mathbf{K}_0)$) of the two nodal points connected by the symmetry g ; the winding numbers ($\nu(\mathbf{K}_0)$, $\nu(g\mathbf{K}_0)$) are computed in the integral loops $\Gamma(\mathbf{K}_0)$ and $\Gamma(g\mathbf{K}_0)$ encircling \mathbf{K}_0 and $g\mathbf{K}_0$ points respectively as illustrated in Fig. 1.

The algebra of chiral symmetry operator and g symmetry operator determines the connection between the two winding numbers at \mathbf{K}_0 and $g\mathbf{K}_0$. The derivation details of the connections for crystalline symmetry operators and time reversal symmetry operators are given in appendix B. As we first consider crystalline symmetry, the Hamiltonian preserving crystalline symmetry obey (See appendix A for the derivation)

$$\mathcal{H}(g\mathbf{k}) = U_g^\pm(\mathbf{k})\mathcal{H}(\mathbf{k})U_g^{\pm\dagger}(\mathbf{k}), \quad (14)$$

where U_g^\pm represents the unitary crystalline symmetry operator in the momentum basis and \pm signs indicate (anti)commutation relation between the two symmetry operators ($U_g^\pm S \mp S U_g^\pm = 0$). We note that $\mathcal{H}(\mathbf{k})$ and $U(\mathbf{k})^\pm$, which are single-valued (appendix A), obey

$$\mathcal{H}(\mathbf{k} + \mathbf{G}_i) = \mathcal{H}(\mathbf{k}), \quad U(\mathbf{k} + \mathbf{G}_i)^\pm = U(\mathbf{k})^\pm, \quad (15)$$

where \mathbf{G}_i is a reciprocal lattice vector. In the following, we always use $+(-)$ to indicate that the chosen symmetry operator (anti)commutes with chiral symmetry operator (S). These two possible forms of U_g^\pm lead to the different connections of the winding numbers between \mathbf{K}_0 and $g\mathbf{K}_0$

$$\nu(g^\pm \mathbf{K}_0) = \pm \det(g^\pm) \nu(\mathbf{K}_0). \quad (16)$$

There are two types of crystalline symmetries in wallpaper groups — (glide) mirror symmetries and rotation symmetries. The mirror operators satisfy $\det g = -1$, whereas the rotation operators obey $\det g = 1$. For g^+ , the two nodal points (\mathbf{K}_0 and $g\mathbf{K}_0$) connected by the mirror symmetry possess the opposite winding numbers, while the nodal points linked by the rotation symmetry have the identical winding numbers. On the contrary, for g^- , the two winding numbers linked by the

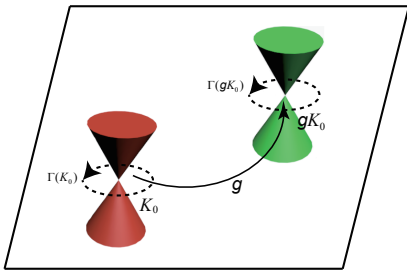


FIG. 1: (color online) The two Dirac points at \mathbf{K}_0 and $g\mathbf{K}_0$ are connected by symmetry g . The two dashed circles represent the counterclockwise integral loops $\Gamma(\mathbf{K}_0)$ and $\Gamma(g\mathbf{K}_0)$ for the winding number $\nu(\mathbf{K}_0)$ and $\nu(g\mathbf{K}_0)$ respectively.

T^\pm	C_n^\pm	M^\pm
$\nu(-\mathbf{K}_0) = \mp \nu(\mathbf{K}_0)$	$\nu(g\mathbf{K}_0) = \pm \nu(\mathbf{K}_0)$	$\nu(g\mathbf{K}_0) = \mp \nu(\mathbf{K}_0)$

TABLE II: Symmetry related winding numbers for nodal points. The operator labels T^\pm , C_n^\pm , M^\pm indicate time reversal, n -fold rotation, and mirror respectively. The signs $+(-)$ indicate the corresponding symmetry operator (anti)commuting with chiral symmetry operator S .

mirror operator are identical and the ones linked by the rotation operator have the different signs.

We note that the generic forms of the crystalline symmetry operators in Eq. 14 are momentum-dependent. That is, nonsymmorphic symmetry operations, which are glide mirror ones only in 2D systems, have the same winding number relations at \mathbf{K}_0 and $g\mathbf{K}_0$ with mirror symmetry operations. Therefore, in the next subsection when we classify the minimal multiplicities of the nodal points, we treat the WGs #(3, 4, 5) as one set together since the three WGs have the same effective mirror symmetries in momentum space, regardless of the glide operations. Similarly, WG #(6, 7, 8, 9) and #(11, 12) are respectively gathered to two sets for the classification of the generalized no-go theorem in the next subsection.

On the other hand, time reversal symmetry operator can commute (T^+) or anticommute (T^-) with chiral symmetry operator S . For T^\pm , the connection between the two winding numbers is given by (see the derivation in appendix B)

$$\nu(-\mathbf{K}_0) = \mp \nu(\mathbf{K}_0). \quad (17)$$

The winding number relations at \mathbf{K}_0 and $g\mathbf{K}_0$ for different symmetry operators are summarized in Table II. This table is our fundamental tool to study the minimal multiplicity of the nodal points for 17 WGs and 5 AZ symmetry classes possessing chiral symmetry.

B. Nodal points for the 17 wallpaper groups and the 5 AZ symmetry classes

Symmetries different from chiral symmetry crucially affect the minimal multiplicity of the stable nodal points in the BZ. For 2D lattice systems with chiral symmetry, symmetries can be classified by 17 WGs and 5 AZ symmetry classes. While the 17 WGs include various crystalline symmetries and translational symmetries in the two spatial directions, the AZ symmetry classes can only have non-spatial symmetries — chiral symmetry, time-reversal symmetry, and particle-hole symmetry. As we consider the combination of crystalline symmetries and AZ symmetry classes, there are 85 WG symmetry classes. However, we will show later that the number of the effective WG symmetry classes for the no-go theorem can be reduced. Let us first review the properties of the 17 WGs. The WGs are classified to four crystal systems (monoclinic, orthorhombic, square and hexagon) as well as five Bravais lattices. In the WGs, C_n and C_{nv} ($n=1,2,3,4,6$) are the only 10 types of the point groups, while mirror M and rotation C_n operations can be the only two generators for these point groups. The point

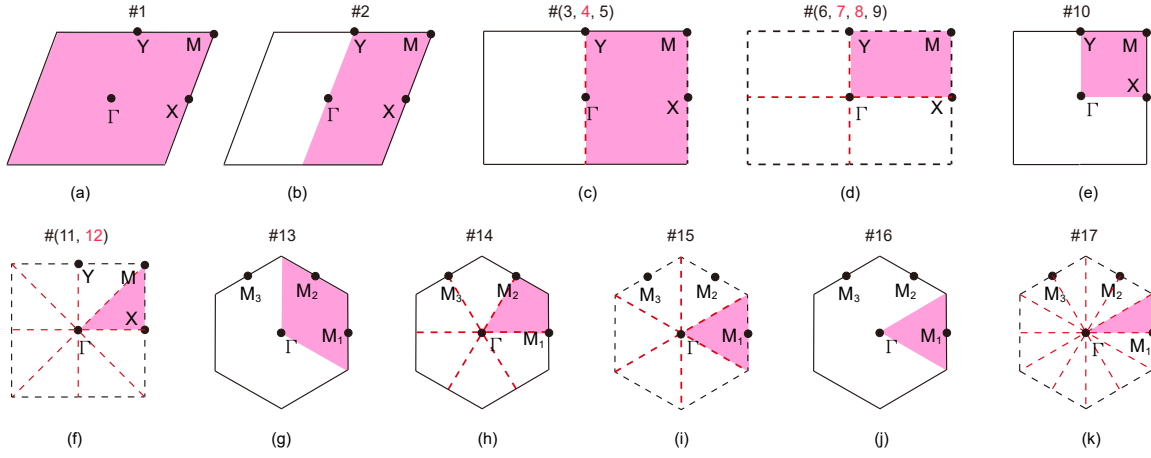


FIG. 2: (color online) **The irreducible BZs (purple) for the 17 Wallpaper groups.** Based on the crystalline symmetry operations, the 17 wallpaper groups are classified to 11 equivalent sets for the classification of the no-go theorem. The red numbers denote nonsymmorphic wallpaper groups. The black lines indicate the boundary of the BZ, the solid dots indicate TRI points, and the (red) dashed lines indicate mirror lines (inside the BZ).

symmetry groups can reduce the first BZ to the irreducible BZ as shown in Fig. 2, since the crystalline symmetry connects any point in the BZ from the irreducible BZ. In this regard, all of the nodal points in the irreducible BZ can be easily extended to the entire BZ by using those two generators of the point group. The irreducible BZ is our building block to study the minimal multiplicity and configuration of nodal points in the no-go theorem.

It has been shown in Table II that the algebra between the chiral symmetry operator and the other symmetry operators determines the winding numbers of the nodal points extended by the symmetry operators from the irreducible BZ. On the other hand, although the crystalline symmetry operators can be momentum-dependent, regardless of the algebra between the symmetry operators, different forms of the symmetry operators do not affect the winding numbers of the extended nodal points. For example, WG #3 and WG #4 only preserve reflection symmetry and reflection glide symmetry respectively and their symmetry operators are in different forms. Since these two symmetry operations flip momentum only in one direction in the same BZ, these two WGs are classified as the same set to discuss the no-go theorem. In this regard, the 17 WGs are classified to 11 equivalent sets for the no-go theorem as shown in Fig. 2. We note that although WG #14 and #15 have the same C_{3v} point group, their mirror lines are along Γ -M and Γ -K differently. Hence, these groups belong to the different sets for the no-go theorem.

The five AZ symmetry classes (AIII, BDI, DIII, CI, and CII), which preserve chiral symmetry, can possess nodal points characterized by winding numbers. By considering the 11 distinct sets of the WGs, we can directly study the no-go theorem for class AIII, since this symmetry class preserves only chiral symmetry. The remaining four symmetry classes have additional time reversal symmetry. Because chiral symmetry is the combination of time-reversal symmetry and particle-hole symmetry ($S = TC$), we treat particle-hole symmetry as redundancy. The AZ symmetry classes deter-

mine the algebra between the chiral operator and the time-reversal operator. While class BDI, CII have T^+ time-reversal operator, class DIII, CI have T^- time-reversal operator (see the proof in appendix C). In two of the following subsections, class BDI, CII have the same minimal configurations for each of the 17 WGs. In total, there are $44 (= 11 \times 4)$ effective WG symmetry classes for the generalized no-go theorem.

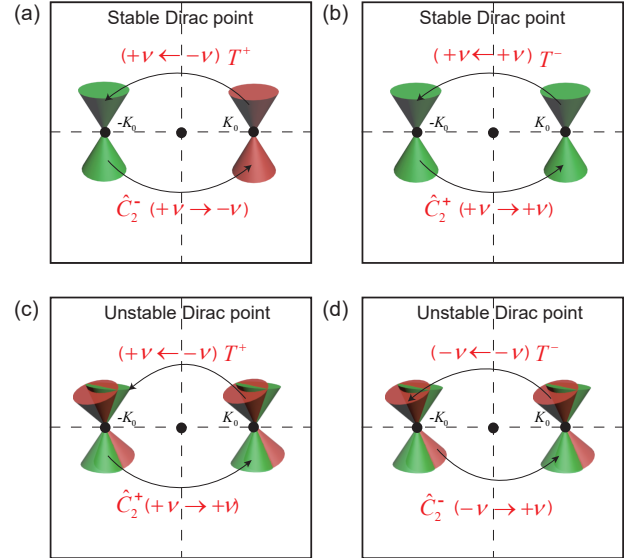


FIG. 3: (color online) The survival of nodal points protected by chiral symmetry in the presence of time-reversal symmetry and C_2 rotation symmetry. The green and red cones represent nodal points with +1 and -1 winding numbers respectively. (a,b) T^\pm time-reversal operator and C^\mp rotation operator act on the nodal point at \mathbf{K}_0 . The nodal point goes back to the same point with the same winding number. (c,d) T^\pm time-reversal operator and C^\pm rotation operator act on the nodal point at \mathbf{K}_0 . The two nodal points with the opposite winding number at the same point loses the protection from chiral symmetry.

Time reversal and C_2 symmetry operators both map nodal points at $\pm\mathbf{K}_0$ to ones at $\mp\mathbf{K}_0$ respectively. There are two possibilities of the operator algebra arrangements to determine the existence of the protected nodal points. We assume the winding number at \mathbf{K}_0 to be w and time reversal operation T^\pm leads to the winding number at $-\mathbf{K}_0$ to be $\mp w$. On the one hand, we use C_2^\mp operation, which correspond to the first operation T^\pm respectively, to map the winding number at $-\mathbf{K}_0$ back to the one at \mathbf{K}_0 as illustrated in Fig. 3(a,b). After the two symmetry operations, the winding number w at \mathbf{K}_0 is identical to the original one. Hence, this nodal point survives in the symmetry operations. On the other hand, after the T^\pm operation, we exchange the two algebra types of C_2 operations so that C_2^\pm correspond to the first operation T^\pm respectively as illustrated in Fig. 3(c,d). After the two symmetry operations, the mapping winding number $-w$ at \mathbf{K}_0 coexists with the original winding number w at the same location. Since the total winding number at \mathbf{K}_0 vanishes, T^\pm time reversal symmetry and C_2^\pm symmetry always force nodal points to lose the protection from chiral symmetry in the entire BZ. Thus, when a WG in some symmetry class preserves T^\pm and C_2^\pm symmetries, the number of nodal points protected by chiral symmetry is always zero. Similarly, in the presence of C_3^- symmetry, by performing three times of C_3^- rotation operation the nodal point moving back to $\mathbf{K}_0 = (C_3^-)^3\mathbf{K}_0$ has $w, -w$ winding number together. Since the total winding number vanishes at \mathbf{K}_0 , which can be any point in the BZ, a nodal point protected by chiral symmetry is absent in the entire BZ.

The trivialization of the nodal points can be extended to nodal points at symmetry-invariant points. According to Table II, any of T^\pm , C_n^\pm , and M^\pm operations leads to $\nu(\mathbf{K}_0) = -\nu(g\mathbf{K}_0)$. Hence, when a nodal point is located at the corresponding time-reversal, rotation, or mirror invariant points, its winding number must vanish and the nodal point does not have chiral symmetry protection.

The charge of the nodal point is defined by the winding number $C(\mathbf{K}_0) = \nu(\mathbf{K}_0)$ and the absolute charge number ν_{abs} is defined in Eq. 2. Given WG symmetry class and the algebra of the symmetry operators, the smallest number of the absolute charge number ν_{abs} indicates the minimal configuration of the nodal points. We note that the minimal configuration of nodal points in BZ might not be unique. Since the winding numbers of the nodal points have the weight in this indicator number, the minimal number of the nodal points cannot directly determine the minimal configuration. The only exception is the all of the nodal points in the BZ are Dirac node with $\nu = \pm 1$. In this case, the number of the Dirac nodes is equal to ν_{abs} .

Since a nodal point at a time-reversal invariant point inherits additional constraints from the ten-fold classification of the topological nodal superconductors [5, 11], we separate the classification of the no-go theorem to two categories — *off* and *at* time-reversal invariant (TRI) points. We note that class AIII, which does not have TRI points, is studied only in the *off*-TRI point case due to the absence of time-reversal symmetry.

C. Nodal points off time-reversal invariant points

According to the classification of topological semimetals and nodal topological superconductors [5, 11], for the five AZ symmetry classes preserving chiral symmetry, nodal points away from TRI points can be characterized by winding number. In the presence of crystalline symmetries, focusing on the irreducible BZs is sufficient to study the minimal configuration of the nodal points in entire BZ. The number of nodal points crucially depends on their locations in the irreducible BZ and the algebra between chiral operator and other symmetry operators. We provide the complete no-go theorem for nodal points away from TRI points in Table III by using the following four steps to find the minimal ν_{abs} of the nodal points in the different configurations.

(a) We check if the symmetries force nodal points to possess zero winding number. For example, when the system preserves T^\pm time-reversal symmetry and C_2^\pm symmetry, there are no nodal points protected by chiral symmetry. Allowing nodal points with non-zero winding number, the symmetries do not restrict the value of the winding number away from any TRI points. To find the minimal configuration of the nodal points, we first place one Dirac point with winding number $\nu = 1$ in the irreducible BZ but not at TRI points.

(b) Different placements of the Dirac point lead to different configurations of the Dirac points in the entire BZ. We separately consider the location of the Dirac point at *mirror lines, rotation centers, and general points*. Commonly, rotation centers are in mirror lines, although K and K' points for WG#14 are two of the exceptions. If the Dirac point is located at a symmetry-invariant point, we have to further check if the symmetry corresponding to the invariant point trivializes the Dirac point. For example, according to Table II, M^+ forces the winding number of the Dirac point at the mirror line to vanish since $\mathbf{K}_0 = M^+\mathbf{K}_0$ and $\nu(\mathbf{K}_0) = -\nu(M^+\mathbf{K}_0)$. If the non-zero winding number survives, we can continue to discuss the configuration of the nodal points.

(c) Using the symmetry operation (rotation, mirror, or time-reversal), we extend the nodal point from the irreducible BZ to the remaining area of the BZ. Following table II, we determine the winding numbers of the extended nodal points based on the algebra between the chiral symmetry operator and the symmetry operators for the extension.

(d) Since the summation over the winding numbers of all the nodal points in the entire BZ must vanish as the key result of the original Nielsen-Ninomiya theorem (I) (see appendix D for the proof)

$$\sum_i \nu(\mathbf{K}_0^i) = 0, \quad (18)$$

we have to check if the summation is zero after the extension of nodal points. If so, this configuration has the minimal configuration of the nodal points. If not, we add an additional nodal point and repeat step (b,c) until the total winding number vanishes (18). We note that when we place a new nodal point, its winding number is usually chosen to be either +1 or -1 to neutralize the entire BZ and to have minimal ν_{abs} but exceptions are possible.

TABLE III: **The absolute winding number ν_{abs} for nodal points protected by chiral symmetry away from TRI points.** The table exhaustively provides the values of ν_{abs} for all the possible minimal configurations for each WG symmetry class. The two point group generators (M_x^\pm, C_n^\pm) with signs indicates the algebra between the chiral symmetry operator and the generators. While '0' indicates the absence of nodal points protected chiral symmetry, the non-zero number ν_{abs} indicates the minimal number of Dirac points with ± 1 winding numbers. Label \sim above some numbers indicates the minimal configuration is unique and label $*$ indicates some nodal points possess high charges ($|\nu| > 1$). Furthermore, label \circ indicates that the Dirac points are in the effective mirror lines ($T * M$ invariant lines), and label \bullet indicates that Dirac nodes can be located in ordinary and effective mirror lines.

WG	Generators	AIII	BDI/CII T^+	DIII/CI T^-
#1		2	$\tilde{2}$	4
#2	C_2^+ C_2^-	4 $\tilde{2}$	0 $\tilde{2}$	4 0
#3,4,5	M_x^+ M_x^-	$\tilde{2}$ 2 mirror lines (MLs) or 4	$\tilde{2}^\circ$ MLs or $\tilde{4}$ $\tilde{2}$ MLs or $\tilde{4}$	$\tilde{4}$ 4 \bullet MLs or 8
#6,7	C_2^+ and M_x^+	$\tilde{4}$	0	$\tilde{4}$
8,9	C_2^+ and M_x^- C_2^- and M_x^\pm	4 MLs or 8 $\tilde{2}$ MLs or $\tilde{4}$	0 $\tilde{2}$ MLs or $\tilde{4}$	4 MLs or 8 0
#10	C_4^+ C_4^-	$\tilde{4}(\Gamma, M, X, Y)$ or 8 $\tilde{4}$	0 0	8 $\tilde{4}$
#11,12	C_4^+ and M_x^+ C_4^+ and M_x^- C_4^- and M_x^\pm	$\tilde{8}$ $\tilde{4}(\Gamma, M, X, Y)$ or 8 MLs or 16 $\tilde{4}$ MLs or $\tilde{8}$	0 0 0	$\tilde{8}$ 8 MLs or 16 $\tilde{4}$ MLs or $\tilde{8}$
#13	C_3^+ C_3^-	$\tilde{2}(K, K')$ or $\tilde{6}(K, K', \Gamma, M_{1/2/3})$ or $\tilde{6}^*(\Gamma, M_{1/2/3})$ or 6 0	$\tilde{2}(K, K')$ or $\tilde{6}$ 0	12 0
#14	C_3^+ and M_y^+ C_3^+ and M_y^- C_3^- and M_y^\pm	$\tilde{2}(K, K')$ or $\tilde{6}$ 6 MLs or $\tilde{6}(K, K', \Gamma, M_{1/2/3})$ or $\tilde{6}^*(\Gamma, M_{1/2/3})$ or 12 0	$\tilde{2}(K, K')$ or $\tilde{6}^\circ$ MLs or $\tilde{12}$ $\tilde{6}$ MLs or $\tilde{12}$ 0	$\tilde{12}$ 12 \bullet MLs or 24 0
#15	C_3^+ and M_x^+ C_3^+ and M_x^- C_3^- and M_x^\pm	$\tilde{6}$ $\tilde{2}(K, K')$ or 6 MLs or $\tilde{6}(K, K', \Gamma, M_{1/2/3})$ or $\tilde{6}^*(\Gamma, M_{1/2/3})$ or 12 0	$\tilde{6}^\circ$ MLs or $\tilde{12}$ $\tilde{2}(K, K')$ or $\tilde{6}$ MLs or $\tilde{12}$ 0	$\tilde{12}$ 12 \bullet MLs or 24 0
#16	C_6^+ C_6^-	$\tilde{4}^*(K, K', \Gamma)$ or $\tilde{6}(K, K', \Gamma, M_{1/2/3})$ or $\tilde{6}^*(\Gamma, M_{1/2/3})$ or 12 $\tilde{2}(K, K')$ or $\tilde{6}$	0 $\tilde{2}(K, K')$ or $\tilde{6}$	12 0
#17	C_6^+ and M_x^+ C_6^+ and M_x^- C_6^- and M_x^+ C_6^- and M_x^-	$\tilde{12}$ $\tilde{4}^*(K, K', \Gamma)$ or $\tilde{6}(K, K', \Gamma, M_{1/2/3})$ or $\tilde{6}^*(\Gamma, M_{1/2/3})$ or 12 MLs or 24 $\tilde{6}$ MLs or $\tilde{12}$ $\tilde{2}(K, K')$ or $\tilde{6}$ MLs or $\tilde{12}$	0 0 $\tilde{6}$ MLs or $\tilde{12}$ $\tilde{2}(K, K')$ or $\tilde{6}$ MLs or $\tilde{12}$	$\tilde{12}$ 12 MLs or 24 0 0

Table III shows that the smallest absolute winding numbers ν_{abs} subtly depend on WG symmetry class, locations of the nodal points, and algebra between the symmetry operators. In particular, choosing different locations of the first Dirac point in the irreducible BZ in step (c) leads to different configurations of nodal points. Table III shows all of the minimal nodal point configurations in the BZ for each WG with the five symmetry classes. Namely, the different locations of the nodal points correspond to different numbers ν_{abs} even if the nodal points are away from TRI points.

Now we consider a specific WG symmetry class to demonstrate the aforementioned approach for the generalized no-go theorem by using WG#15 with C_3^+ , M^- in class BDI/CII (T^+) as an example. (a) The symmetries do not kill winding numbers of any nodal points. (b) There are three types of the locations to place the first nodal point — rotation centers (Γ, K, K'), mirror lines ($\Gamma\bar{K}, \Gamma\bar{K}'$), and general points. Let us first focus on the rotation centers by placing a Dirac point at K with +1 winding number, since Γ is a TRI point, which will be discussed in the next subsection. (c) Time-reversal

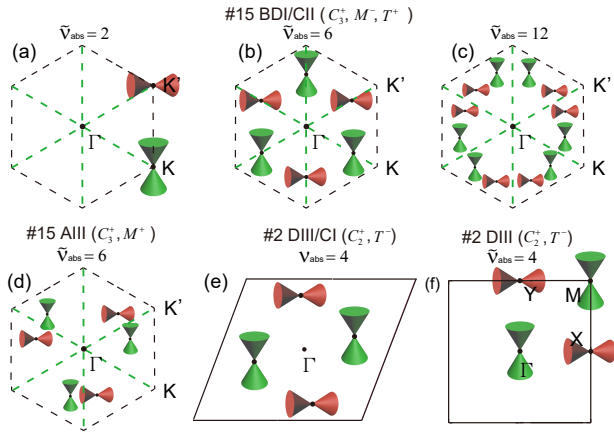


FIG. 4: (color online) Examples of the configuration for nodal points away from TRI points. The green and red cones represent nodal points with +1 and -1 winding numbers respectively, while the dashed lines indicate the mirror lines. (a-c) show that the nodal points are in the three different types of the locations — rotation centers, mirror lines, and general points. (a-d) The configurations are unique, since any two nodal points in the BZ can be connected by symmetries. (e) does not have the unique configuration since the two red nodal points with $\nu = -1$ connected by the symmetries can move freely without affecting the green nodal points with $\nu = 1$. (f) four Dirac points located at (Γ, M, X, Y) are the minimal configuration for WG#2 with C_2^+ .

symmetry T^+ maps the Dirac point at K to the Dirac point at K' with -1 winding number. (d) The total winding number at K and K' is zero. Hence, the Dirac points at K, K' are the minimal configuration as shown in Fig. 4(a) and $\nu_{\text{abs}} = 2$ is the absolute winding number.

Alternatively, when the first Dirac point with -1 winding number is placed at one point of the mirror lines $(\bar{\Gamma}K, \bar{\Gamma}K')$, not K, K' , C_3^+ rotation symmetry generates 2 additional copies of the Dirac points with the same winding number. Furthermore, from these 3 Dirac points, time-reversal symmetry produces other 3 Dirac points with -1 winding numbers as shown in Fig. 4(b). Since the total winding number of the six Dirac points vanishes, the six Dirac points are the minimal configuration for mirror lines. Similarly, for the first Dirac point located at a general point, as illustrated in Fig. 4(c) mirror symmetry doubles the number of the six Dirac points, which are extended by time-reversal symmetry and C_3 rotation symmetry. In this case, $\nu_{\text{abs}} = 12$. For the three types of the nodal point locations, each nodal point can connect any other nodal point through symmetries. That is, once we fix the location of the first Dirac point, all of the nodal point locations are determined. Hence, for this WG symmetry class with T^+, C_3^+, M_x^- , the configurations of the nodal points are unique. Although the sign change for all of the winding numbers leads to another configuration, we treat that the configuration with the sign flipping is identical to the original one. To mark the uniqueness, we put \sim on the minimal absolute number 12 in Table III.

Let us consider another example for WG#15 in class AIII with C_3^+, M^+ . Reflection symmetry M^+ enforces vanishing

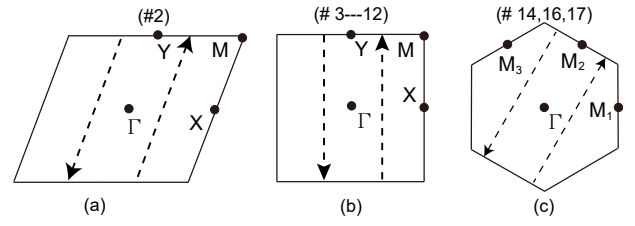


FIG. 5: The dashed lines are the integral paths of the winding numbers through the entire BZs. Due to C_2^+ rotation symmetry or M^- reflection symmetry, the two winding numbers of the separate dashed lines, which are quantized, in each BZ are identical. Through the integral path deformation, the summation of the two winding numbers is identical to (a,b) $\nu(\Gamma) + \nu(Y)$ and (c) $\nu(\Gamma) + \nu(M_2)$.

winding number for any nodal point located at a mirror line $(\bar{\Gamma}K, \bar{\Gamma}K')$. In this regard, nodal points protected by chiral symmetry can survive only at general points and then we place the first Dirac point with +1 winding number at a general point. Using reflection symmetry and C_3 rotation symmetry, there are 3 Dirac points with +1 winding number and other three with -1 winding number; this minimal configuration of the nodal points with $\nu_{\text{abs}} = 6$ is unique as shown in Fig. 4(d).

Another example is WG#2 in class DIII, CI with T^- and C_2^+ . (a) With these symmetries, nodal points with non-zero winding numbers survive. (b) We place a Dirac point with +1 winding number at a general point (say K_0). (c) These two symmetries (T^-, C_2^+) lead to another Dirac point with +1 winding number at $-K_0$. (d) However, the total winding number is two so we have to place another Dirac point with -1 winding number at another general point. Due to the symmetries, there are two Dirac points with -1 winding numbers. With the four Dirac points as shown in Fig. 4(e), the total winding number is neutralized. The Dirac points with the opposite winding numbers are not directly connected by the symmetries so that we can freely choose their locations even when the Dirac points with $\nu = 1$ are spatially fixed. Hence, the configuration is not unique.

Most of the WG symmetry classes follow the aforementioned recipe to search for the minimal configuration of the protected nodal points. However, for class AIII there are some exceptions, which are nodal points located in the special points (Γ, M, X, Y) and (Γ, M_i) for the two types of the BZs respectively. An additional step of the recipe has to be considered in these special cases.

(e) The winding number with the integral path through the entire BZ (the dash lines in Fig. 5) must be quantized. Rotation symmetry (C_2) and mirror symmetry (m) can connect the two winding numbers with these two integral paths. For C_2^+ and m^- , these two winding numbers with the two symmetry related paths are identical. Furthermore, by considering nodal points located at the aforementioned special points, these two paths together can deform to two infinitesimal circles surrounding two of the special points, and the winding numbers are unchanged. Hence, the total winding number of the two special points must be even. For the WGs (#2, 6-12) possessing C_2^+ generator, the winding numbers in two of the

special points obey

$$\nu(\Gamma) + \nu(Y) = 0 \pmod{2}, \nu(\Gamma) + \nu(X) = 0 \pmod{2}, \quad (19)$$

where n and m are integers; for the WGs (#3 – 9, 11, 12) possessing m_x^- generator, the constraint is reduced to

$$\nu(\Gamma) + \nu(Y) = 0 \pmod{2}, \quad (20)$$

On the other hand, the hexagonal BZ has different special points. For WGs (#14, 17) possessing m_y^- generator and WGs (#16, 17) possessing C_2^+ generator, we have

$$\nu(\Gamma) + \nu(M_i) = 0 \pmod{2}. \quad (21)$$

Thus, in this final step we have to check if the configuration of the nodal points satisfies Eqs. 19, 20, or 21 for the corresponding WG symmetry classes. If so, the minimal configuration is found. If not, step (b,c,d) are need to be repeated until the constraint conditions are fulfilled.

Let us use WG#2 with C_2^+ in class AIII as an example. We place two Dirac points with ± 1 winding number at Γ and M separately. Although the entire BZ is neutralized, Eq. 19 is violated. In fact, no matter how the two Dirac points are located at two of the rotation invariant points (Γ, X, Y, M), Eq. 19 does not hold. The only way is to have four Dirac points placed at the four invariant points separately and Fig. 4(f) illustrates one of the valid minimal configuration.

D. Nodal points at time-reversal invariant points

The TRI points are special for nodal points. Since TRI points obey $\mathbf{K}_0 = -\mathbf{K}_0$, in the presence of T^+ time reversal symmetry the winding number of the nodal point at this invariant point vanishes. The reason is that based on table II T^+ gives the opposite winding number at the same point. Class BDI/CII with T^+ never possesses a nodal point with non-zero winding number at any time-reversal invariant points. Hence, we discuss the no-go theorem for only two non-trivial AZ symmetry classes — DIII and CI. The absolute numbers ν_{abs} of the minimal configurations for the WG symmetry class are shown in Table IV. This non-trivial property is consistent with the classification of topological semimetals and nodal topological superconductors [5, 11], which shows that in these two AZ symmetry classes the nodal points at TRI points can be characterized by non-zero winding number. Namely, class DIII and CI correspond to \mathbb{Z} and $2\mathbb{Z}$ invariants respectively.

Class AIII and CII may possess protected nodal points, since according to the classification table, nodal points in class AIII and CII can be characterized by \mathbb{Z} and \mathbb{Z}_2 invariants respectively. However, TRI points are absent in class AIII, which has been exhaustively studied in the previous subsection. In addition, although in class CII the non-zero \mathbb{Z}_2 invariant can protect the nodal point, here we focus on only nodal points protected by winding numbers. Hence, class AIII and CII are excluded in the no-go theorem for TRI nodal points.

The recipe to find the smallest absolute winding number ν_{abs} for each WG symmetry class is identical to the previous

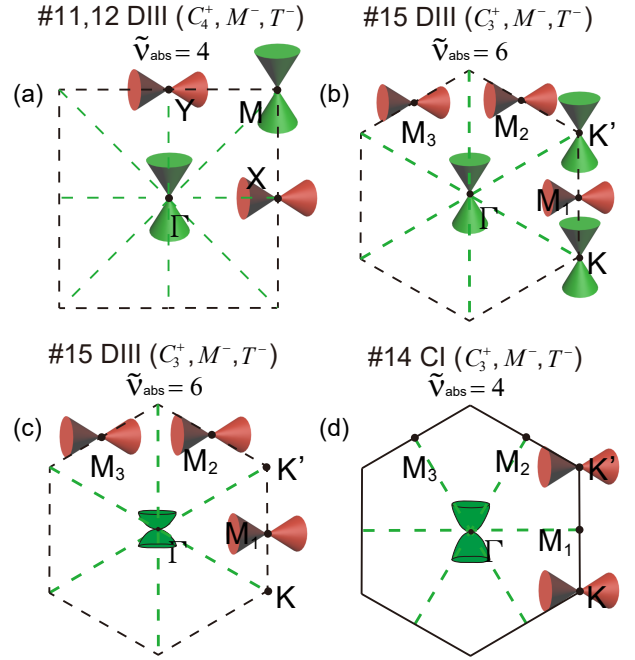


FIG. 6: (color online) **Examples of the configuration for nodal points at the TRI points.** The green and red cones with linear dispersions represent nodal points with $+1$ and -1 winding numbers respectively, the green cones with quadratic and cubic dispersions represent nodal points with $+2$ and $+3$ winding numbers in (d) and (c) respectively. The dashed lines indicate the mirror lines.

subsection for off-time-reversal-invariant-point. Additional cares are needed for class DIII with $T^2 = -1$ and for class CI with $T^2 = +1$. First, due to $T^2 = -1$, the Kramers' degeneracy leads to double degeneracy for each band at all of the TRI points. In addition, chiral symmetry pairs two energy bands with $\pm E$. Hence, for the odd number of the energy band pairs in the system there must exist an energy band pair at $E = 0$ at all of the four time-reversal invariant points in the BZ. Since we assume that nodal lines are absent, the nodal points always appear at the four time-reversal invariant points. On the other hand, since in class CI $2Z$ invariant given by the classification table [5, 11] indicates that the winding number of the nodal point located at a TRI point must be even. Hence, in step (b) the winding number of the first nodal point should be chosen to be $+2$, instead of $+1$. The Kramers' degeneracy in class DIII and even winding numbers in class CI automatically fulfill the constraints in Eq. 19, 20, 21 in step (e). The remaining steps to find the minimal configuration of the nodal points are identical to the previous subsection.

We demonstrate three examples to show how to find the minimal configurations of the nodal points. We first consider WG#11, 12 with C_4^+ and M^- in class DIII ($(T^-)^2 = -1$). These two WGs share the same point groups. In the BZ, Γ, X, Y, M are TRI points and three of them (except for Y) are in the irreducible zone as shown in Fig. 2(g). As discussed previously, due to the Kramers' degeneracy, in class DIII once a nodal point at $E = 0$ appears at one of the TRI points, all of the TRI points must be nodal points. Since C_4^+ rotation sym-

TABLE IV: **The absolute winding number ν_{abs} for nodal points protected by chiral symmetry at TRI points.** The table shows the minimal ν_{abs} for the 17 WGs in class DIII and BDI. Mark \sim above the numbers indicates that the minimal configuration is unique. The two point group generators (C_n^\pm, M_x^\pm) with signs indicate the algebra between the chiral symmetry operator and the generators; $\nu_{\text{abs}} = 0$ indicates the absence of nodal points protected by chiral symmetry. In the table there are some cases that nodal points are forced to be placed at K, K' , which are not TRI points, due to the charge neutralization. In some cases, high-ordered nodal points with $|\nu| > 1$ must be present in the minimal configurations; hence, we use * to distinguish the particular cases from the case possessing only Dirac nodes.

WG	Generators	DIII T^-	CI T^-
#1		$\tilde{4}(\Gamma, M, X, Y)$	4^*
#2	C_2^+	$\tilde{4}(\Gamma, M, X, Y)$	4^*
	C_2^-	0	0
#3,4,5	M_x^+	0	0
	M_x^-	$\tilde{4}(\Gamma, M, X, Y)$	4^*
#6,7,8,9	C_2^+ and M_x^+	0	0
	C_2^+ and M_x^-	$\tilde{4}(\Gamma, M, X, Y)$	4^*
	C_2^- and M_x^\pm	0	0
#10	C_4^+	$\tilde{4}(\Gamma, M, X, Y)$	$\tilde{4}^*(\Gamma, M)$ or 8^*
	C_4^-	0	$\tilde{4}^*(X, Y)$
#11,12	C_4^+ and M_x^+	0	0
	C_4^+ and M_x^-	$\tilde{4}(\Gamma, M, X, Y)$	$\tilde{4}^*(\Gamma, M)$ or 8^*
	C_4^- and M_x^\pm	0	0
#13	C_3^+	$\tilde{4}^*(K, K', \Gamma), \tilde{6}(K, K', \Gamma, M_{1/2/3}),$ or $\tilde{6}^*(\Gamma, M_{1/2/3})$	$\tilde{4}^*(K, K', \Gamma), \tilde{12}^*\{(K, K', \Gamma, M_{1/2/3}),$ or $(\Gamma, M_{1/2/3})\}$
	C_3^-	0	0
#14	C_3^+ and M_y^+	0	0
	C_3^+ and M_y^-	$\tilde{4}^*(K, K', \Gamma), \tilde{6}(K, K', \Gamma, M_{1/2/3}),$ or $\tilde{6}^*(\Gamma, M_{1/2/3})$	$\tilde{4}^*(K, K', \Gamma), \tilde{12}^*\{(K, K', \Gamma, M_{1/2/3}),$ or $(\Gamma, M_{1/2/3})\}$
	C_3^- and M_y^\pm	0	0
#15	C_3^+ and M_x^+	0	0
	C_3^+ and M_x^-	$\tilde{4}^*(K, K', \Gamma), \tilde{6}(K, K', \Gamma, M_{1/2/3}),$ or $\tilde{6}^*(\Gamma, M_{1/2/3})$	$\tilde{4}^*(K, K', \Gamma), \tilde{12}^*\{(K, K', \Gamma, M_{1/2/3}),$ or $(\Gamma, M_{1/2/3})\}$
	C_3^- and M_x^\pm	0	0
#16	C_6^+	$\tilde{4}^*(K, K', \Gamma), \tilde{6}(K, K', \Gamma, M_{1/2/3}),$ or $\tilde{6}^*(\Gamma, M_{1/2/3})$	$\tilde{4}^*(K, K', \Gamma), \tilde{12}^*\{(K, K', \Gamma, M_{1/2/3}),$ or $(\Gamma, M_{1/2/3})\}$
	C_6^-	0	0
#17	C_6^+ and M_x^+	0	0
	C_6^+ and M_x^-	$\tilde{4}^*(K, K', \Gamma), \tilde{6}(K, K', \Gamma, M_{1/2/3}),$ or $\tilde{6}^*(\Gamma, M_{1/2/3})$	$\tilde{4}^*(K, K', \Gamma), \tilde{12}^*\{(K, K', \Gamma, M_{1/2/3}),$ or $(\Gamma, M_{1/2/3})\}$
	C_6^- and M_x^\pm	0	0

metry or M^- mirror symmetry forces the winding numbers at X, Y to be identical. The only minimal configuration is formed by Dirac points with +1 winding numbers at Γ, M and ones with -1 winding numbers at X, Y as shown in Fig. 6(a).

Another example is WG#15 in class DIII with T^- , C_3^+ , M^- . The four points (Γ, M_1, M_2, M_3) are TRI points in the hexagonal zone as shown in Fig. 2(j). The Kramers' degeneracy leads to nodal points located at these four points together. Due to C_3^+ rotation symmetry, M_1, M_2, M_3 possess the same winding number (say -1). However, Γ with +1 winding number cannot neutralize the entire zone. Therefore, we place two Dirac point with +1 winding numbers at K, K'

and the total winding number vanishes as shown in Fig. 6(b). However, the minimal configuration with ν_{abs} is not unique. Alternatively, we choose a nodal point with +3 winding number at Γ and three Dirac points with -1 winding number at three M_i points as shown in Fig. 6(c); this choice is the other minimal configuration.

We consider WG#14 in class CI with T^- , C_3^+ , M^- as the last example. We place the first nodal point at Γ . Since in class CI any nodal point at a TRI point must possess even winding number, the simplest choice for the nodal point at Γ is +2 winding number. With C_3^+ rotation symmetry, a nodal point in the most area of the BZ has three copies with the same wind-

ing number, except for K', K, Γ . Therefore, a Dirac point with -1 winding number is placed at K . Due to T^- time-reversal symmetry or M^- reflection symmetry, another Dirac point appear at K' with -1 winding number. The total winding number vanishes and as shown in Fig. 6(d) this configuration with $\nu_{\text{abs}} = 4$ is minimal.

E. Examples

The symmetry constraints control the configurations of the nodal points protected by chiral symmetry. Table III,IV provide all of the possible minimal configurations for each WG symmetry class. The minimal configurations can be building blocks to understand realistic systems possessing the nodal points. Here we study several examples in condensed matter systems to show that the examples of the nodal points cannot escape from the predicted configurations in our generalized no-go theorem.

Off time-reversal invariant points

Nodal points protected by chiral symmetry away from TRI points can be realized in 2D Dirac materials and time reversal symmetric superconductors. 2D Dirac materials, such as graphene, may preserve accidental chiral (sublattice) symmetry, whereas time reversal symmetric superconductors naturally preserve chiral symmetry stemming from intrinsic time reversal symmetry and particle-hole symmetry.

1. *D-wave superconductors: WG#11 in class CI*

We first consider a two-dimensional nodal Cu-based superconductor with *d*-wave pairing [68, 69] with spin $SU(2)$ symmetry. The Bogoliubov-de Gennes Hamiltonian [70] in the 2×2 Nambu basis can be written in the second quantization form of

$$H = \sum_{\mathbf{k}} \psi^\dagger(\mathbf{k}) \mathcal{H}(\mathbf{k}) \psi(\mathbf{k}) = \sum_{\mathbf{k}} \hat{\psi}^\dagger(\mathbf{k}) [\varepsilon(\mathbf{k})\tau_z + \Delta(\mathbf{k})\tau_x] \hat{\psi}(\mathbf{k}), \quad (22)$$

where $\hat{\psi}(\mathbf{k}) = (\hat{c}_{\mathbf{k},\uparrow}, \hat{c}_{-\mathbf{k},\downarrow}^\dagger)$, $\varepsilon(\mathbf{k}) = -2t_1(\cos k_x + \cos k_y) - 4t_2 \cos k_x \cos k_y - \mu$, and $\Delta(\mathbf{k}) = \Delta_0(\cos k_x - \cos k_y)$. We choose the parameters as $t_1 = 0.25$, $t_2 = -0.05$, $\mu = -0.18$ and $\Delta_0 = 0.1$. First, the system preserves particle-hole symmetry (4) with $C = \tau_y \mathcal{K}$. Secondly, time-reversal symmetry (5) is also preserved with $T = \mathcal{K}$. By combining the two symmetry operators above, chiral symmetry (3) is also preserved with $S = \tau_y$. We have $C^2 = -1$ and $T^2 = 1$ corresponding to class CI, which is consistent with the symmetry class of time-reversal symmetric superconductor with spin $SU(2)$ symmetry in the literature [42]; furthermore, the time-reversal operator T^- anti-commutes with the chiral symmetry operator S . On the other hand, the system belongs to WG#11 possessing C_{4v} point group symmetry with generators $C_4 = \tau_z$ and $M_x = \tau_0$, which obey $C_4 H_{BdG}(k_x, k_y) C_4^{-1} = H_{BdG}(-k_y, k_x)$

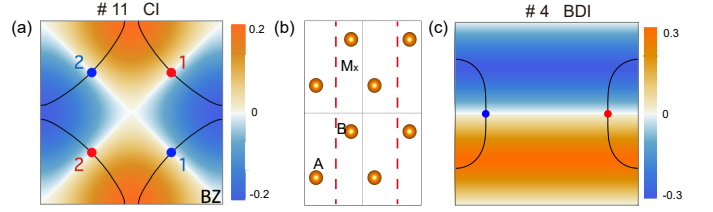


FIG. 7: (color online) Time-reversal symmetric superconductors possess protected nodal points. The colorbar from blue to yellow indicates the value of the order parameter $\Delta(\mathbf{k})$, and the black lines represent the Fermi lines in the absence of the superconductivity. Their crossings form the nodal points with $\nu = +1$ (red) and $\nu = -1$ (blue). (a) The *d*-wave SC belonging to WG#11 in class CI has 4 nodal points in the BZ. (b) The crystal structure for the toy model of the glide-reflection symmetric superconductor belongs to WG#4 in class BDI. (c) There are 2 nodal points with $\nu = \pm 1$ in the BDI superconductor.

and $M_x H_{BdG}(k_x, k_y) M_x^{-1} = H_{BdG}(-k_x, k_y)$, and the (anti)commutation relations of the generator operators are given by C_4^- and M_x^+ .

This *d*-wave SC has four nodes located at the mirror lines as shown in Fig. 7(a). The Hamiltonian of the low energy expansion near the four nodal points $\mathbf{k}_{0\pm} = (0.44\pi, \pm 0.44\pi)$, $\mathbf{k}'_{0\pm} = (-0.44\pi, \mp 0.44\pi)$ are in the form of

$$\begin{aligned} \mathcal{H}_\pm^r(\mathbf{k}) &\simeq \alpha(\delta k_{x\pm} \mp \delta k_{y\pm})\sigma_x + \beta(\delta k_{x\pm} \pm \delta k_{y\pm})\sigma_y, \\ \mathcal{H}_\pm^l(\mathbf{k}) &\simeq -\alpha(\delta k'_{x\pm} \pm \delta k'_{y\pm})\sigma_x - \beta(\delta k'_{x\pm} \mp \delta k'_{y\pm})\sigma_y, \end{aligned} \quad (23)$$

where $\delta \mathbf{k}_\pm = \mathbf{k} - \mathbf{k}_{0\pm}$, $\delta \mathbf{k}'_\pm = \mathbf{k} - \mathbf{k}'_{0\pm}$, $\alpha = 0.98$, and $\beta = 0.45$. Since chiral symmetry is still preserved with $S = \sigma_z$ and the linear dispersions lead to the four Dirac points with ± 1 winding numbers, with the low-energy Hamiltonians $H_\pm^{r/l}(\mathbf{k}) = \delta k_i A_{ij} \delta k_j$, $\text{sign}(\det A)$ corresponds to ± 1 winding numbers of the Dirac points. Therefore, $\nu = +1$ for \mathbf{k}_{0+} , \mathbf{k}'_{0+} and $\nu = -1$ for \mathbf{k}_{0-} , \mathbf{k}'_{0-} as shown in Fig. 7(a).

Back to our no-go theorem in Table III, for WG #11 with C_4^- and M_x^+ in class CI, we have $\nu_{\text{abs}} = 4$ for nodal points located at mirror lines. This is consistent with the presence of the 4 nodal points with ± 1 winding numbers in the *d*-wave SC model. By using C_4^- and M_x^+ operations, we can generate the same distribution of the four Dirac points.

2. *Glide reflection symmetric superconductors: WG#4 in class BDI*

The classification of our no-go theorem depends on point groups, regardless of symmorphic and non-symmorphic symmetries. Glide reflection symmetry is the only type of the non-symmorphic symmetries in the 17 wallpaper groups. We study a toy model of a 2D glide plane symmetric superconductor in class BDI. Fig. 7 (b) shows 2D orthorhombic lattice of non-symmorphic WG#4 with A and B sites in the primitive cell. The glide reflection symmetry, which is the only crystalline symmetry in WG#4, has its operator $\hat{g}_\delta =$

$\{M_x|\delta = (0, \frac{b}{2})\}$ exchanging site A and B with a reflection M_x in the x direction and half-lattice-constant movement along the y direction. Then, we provide a toy model of the spinless fermion in the lattice

$$H_{\text{BdG}}(\mathbf{k}) = (\epsilon(\mathbf{k}) - \mu)\tau_z\sigma_0 + \beta(\mathbf{k})\tau_z\sigma_x + \gamma(\mathbf{k})\tau_z\sigma_y - \Delta(\mathbf{k})\tau_y\sigma_0, \quad (24)$$

in the basis of $\psi(\mathbf{k}) = (C_{\mathbf{k},A}, C_{\mathbf{k},B}, C_{-\mathbf{k},A}^\dagger, C_{-\mathbf{k},B}^\dagger)^T$, where $\epsilon(\mathbf{k}) = m_0 + 2t_2 \cos(k_x) + 2t_3 \cos(k_y)$, $\beta(\mathbf{k}) = 2t_1 \cos(\frac{k_y}{2}) \cos(k_x + \frac{k_y}{2})$, $\gamma(\mathbf{k}) = 2t_1 \cos(\frac{k_y}{2}) \sin(k_x + \frac{k_y}{2})$, and superconductor gap $\Delta(\mathbf{k}) = \Delta_0 \sin(k_y)$. We choose the parameters as $t_1 = 1.2$, $t_2 = 0.2$, $t_3 = 0.3$, $m_0 = 2$, $\mu = 0$ and $\Delta_0 = 0.3$ so that two nodal points appear at $(\pm 2\pi/3, 0)$.

The spinless superconductor system naturally preserves particle-hole symmetry (4) with its operator $C = \tau_x\sigma_0\mathcal{K}$ and time-reversal symmetry (5) with its operator $T = \tau_0\sigma_0\mathcal{K}$. Hence, this belongs to class BDI and chiral symmetry (3) is preserved with $S = \tau_x\sigma_0$. By using chiral symmetry operator, the winding numbers for nodal points at $(\pm 2\pi/3, 0)$ are given by ± 1 ; time-reversal symmetry T^+ connects these two nodal points with the opposite winding numbers. Due to the glide reflection symmetry, the BdG Hamiltonian obeys $M_g H(k_x, k_y) M_g^{-1} = H(-k_x, k_y)$, where the symmetry operator $M_g = e^{-i\frac{k_y}{2}} (\cos(\frac{k_y}{2})\tau_0\sigma_x + \sin(\frac{k_y}{2})\tau_0\sigma_y)$. Since this operator M_g^+ commutes with S , M_g^+ also connects the two nodal points with the opposite winding numbers. Away from TRI points, the two nodal points with ± 1 winding numbers are consistent with Table III for WG#4 in class BDI.

3. Graphene: WG#17 in class BDI

It is known that there are two Dirac points in the graphene model, which can be simply described by the p_z orbital containing nearest neighbor hoppings [71]. The spinless Hamiltonian in the basis of (C_k^A, C_k^B) can be written as

$$H_g(\mathbf{k}) = \begin{pmatrix} 0 & h_{12}(\mathbf{k}) \\ h_{12}^*(\mathbf{k}) & 0 \end{pmatrix} \quad (25)$$

where $h_{12}(\mathbf{k}) = t \left[e^{i(\frac{1}{2}k_y - \frac{\sqrt{3}}{6}k_x)} + e^{i\frac{\sqrt{3}}{3}k_x} + e^{i(-\frac{1}{2}k_y - \frac{\sqrt{3}}{6}k_x)} \right]$ and t is hopping parameter. Since the system preserves sublattice chiral symmetry $S = \sigma_z$, time reversal symmetry $T = \mathcal{K}$, effective particle-hole symmetry $C = \sigma_z\mathcal{K}$, we have class BDI with T^+ . We note that the graphene is a non-interacting electron system in this case so the effective particle-hole symmetry, which stems from the combination of the sublattice symmetry and time reversal symmetry, is unrelated to superconductivity. On the other hand, the graphene belongs to WG#17 with two generators $M_x^- = \sigma_x$ and $C_6^- = \sigma_x$. The crystalline symmetries lead to

$$M_x H_g(-k_x, k_y) M_x^{-1} = H_g(k_x, k_y), \quad (26)$$

$$C_6 H_g\left(\frac{k_x}{2} + \frac{\sqrt{3}k_y}{2}, \frac{k_y}{2} - \frac{\sqrt{3}k_x}{2}\right) C_6^{-1} = H_g(k_x, k_y). \quad (27)$$

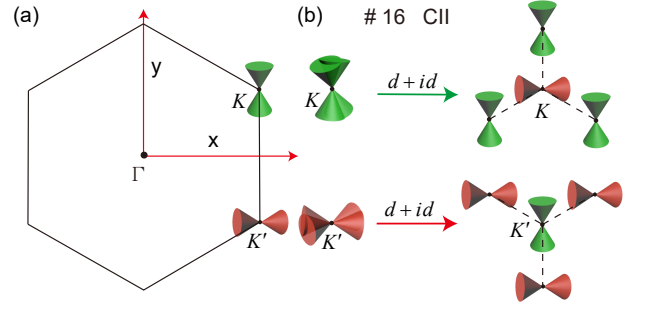


FIG. 8: (color online) The nodal points in the graphene without or with $d + id$ -wave SC. (a) The graphene Hamiltonian H_g hosts two Dirac nodes at K, K' . (b) By introducing $d + id$ -wave SC pairing, each of the nodal points at K, K' become four separate Dirac nodes. by using K point as an example, three of them move along $\overline{K\Gamma}$ with $\nu = 1$ in the three directions and the remaining Dirac point stays at K with $\nu = -1$.

The nodal points are present at $K : (2\pi/\sqrt{3}, 2\pi/3)$ and $K' : (2\pi/\sqrt{3}, -2\pi/3)$ with $+1$ and -1 winding numbers respectively. Table III indicates $\nu_{\text{abs}} = 2$ at K, K' for WG#17 with M_x^- and C_6^- . It is not surprising that our no-go theorem covers the two Dirac points in the graphene.

4. $d + id$ superconductors: WG#17 in class CII

We add $d + id$ -wave superconductor pairing in the graphene. Its BdG Hamiltonian in the basis of $\Psi(k) = (C_{k\uparrow}^A, C_{k\uparrow}^B, C_{-k\downarrow}^A, C_{-k\downarrow}^B)^\dagger$ is written as [72]

$$H_{\text{BdG}}(\mathbf{k}) = \begin{pmatrix} 0 & h_{12}(\mathbf{k}) & 0 & \Delta(\mathbf{k}) \\ h_{12}^*(\mathbf{k}) & 0 & \Delta(-\mathbf{k}) & 0 \\ 0 & \Delta^*(-\mathbf{k}) & 0 & -h_{12}^*(-\mathbf{k}) \\ \Delta^*(\mathbf{k}) & 0 & -h_{12}(-\mathbf{k}) & 0 \end{pmatrix}, \quad (28)$$

where the $d + id$ -wave pairing by nearest-neighbor antiferromagnetic exchange coupling in a honeycomb lattice [73] is

$$\Delta(\mathbf{k}) \equiv \frac{\Delta_0}{3} e^{i\frac{k_x}{\sqrt{3}}} \left[2 \cos\left(-\frac{k_y}{2} + \frac{2\pi}{3}\right) e^{-i\frac{\sqrt{3}k_x}{2}} + 1 \right]. \quad (29)$$

Since this spinless SC model stems from the spinful system with spin $SU(2)$ symmetry, we have particle-hole symmetry with $C = \tau_y\sigma_0\mathcal{K}$ and $C^2 = -1$ [42]. The SC system inherits chiral symmetry from the graphene with $S = \tau_0\sigma_z$; hence, effective time reversal symmetry is preserved with $T^+ = \tau_y\sigma_z\mathcal{K}$, although the physical time-reversal symmetry is broken in the $d + id$ -wave superconductor. Furthermore, the graphene structure leads to the same WG#17 with two extended generators $M_x^- = \tau_y\sigma_y$ and

$$C_6^- = \begin{pmatrix} 1 & 0 \\ 0 & e^{i2\pi/3} \end{pmatrix} \otimes \sigma_x. \quad (30)$$

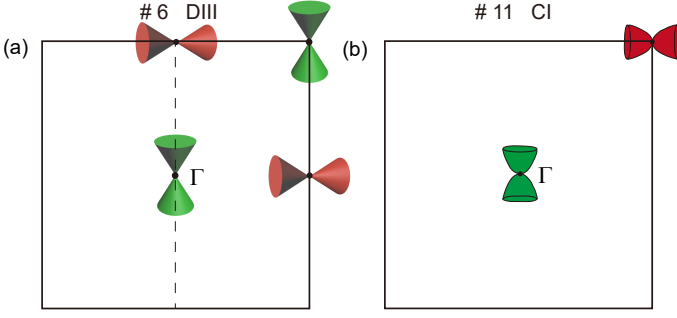


FIG. 9: (color online) The nodal points at TRS points (a) class DIII with C_2^+ and M_x^- , and (b) class CI.

Therefore, the Hamiltonian $H_{BdG}(\mathbf{k})$ preserves reflection symmetry (26) and 6-fold rotation symmetry (27). The systems belong to WG#17 with M_x^- and C_6^- in class CII in Table III.

Back to nodal points, when the superconducting gap vanishes, in the BdG Hamiltonian each of K and K' possesses two Dirac points with the same winding numbers — one from particle part and the other from the hole part. Let us focus on K possessing the two Dirac points with +1 winding number. As the superconductor gap gradually increases from zero, a Dirac nodal point with -1 winding number stays at K and three Dirac nodal points with +1 winding number move away from K along three $\overline{\Gamma K}$ lines separately as illustrated in Fig. 8(b). The reason is that the combination symmetry of the time-reversal T^+ and the reflection M_x^- symmetries locks the three Dirac points at $\overline{\Gamma K}$. The total winding number of the four Dirac points near K is still 2, whereas the four Dirac points near K' with the opposite winding numbers have the identical distribution. The SC system possesses three Dirac points with -1 winding numbers in the three *effective* mirror lines ($\overline{\Gamma K}$) and three Dirac points with -1 winding numbers the three mirror lines ($\overline{\Gamma K'}$), while two other Dirac points with +1 and +1 are located at K and K' . On the other hand, for WG#17 with M_x^- and C_6^- in class CII Table III shows $\nu_{\text{abs}} = 2$ in K, K' and $\nu_{\text{abs}} = 6$ in the mirror lines. Thus, the table of the no-go theorem shows the building blocks of the nodal points for this $d + id$ wave superconductor.

At time-reversal symmetry points

The key difference between nodal points located at and away from TRI points is that time reversal symmetry imposes an additional constraint at TRI points. For class DIII, nodal points exhibit Kramers' degeneracy at TRI points, while for class BDI, the winding numbers of the nodal points are always even. We provide several examples to show these special properties.

5. $p + ip$ superconductors: WG#6 in class DIII

To illustrate the Dirac points at TRI points, we study an effective Hamiltonian of a $p + ip$ wave superconductor with

C_{2v} point group symmetry in the rectangular lattice

$$H(\mathbf{k}) = a \sin k_x \sigma_x + b \sin k_y \sigma_y. \quad (31)$$

Particularly, we remove the diagonal term so that the Hamiltonian preserves chiral symmetry (3) with $S = \sigma_z$. Four Dirac points are located at TRI momenta $(0,0)$, $(0,\pi)$, $(\pi,0)$, (π,π) because Kramers' degeneracy and chiral symmetry force two-fold degenerate states with zero energy at all of the TRI points. The system preserves time reversal symmetry (5) with $T^- = i\sigma_y \mathcal{K}$ and particle-hole symmetry (4) with $C = \sigma_x \mathcal{K}$. Since $T^2 = -1$ and $C^2 = +1$, the system belongs to class DIII. On the other hand, the system possesses C_{2v} point group symmetry with generators $C_2 = \sigma_z$ and $M_x = \sigma_y$, which obey $C_2 H(\mathbf{k}) C_2^{-1} = H(-\mathbf{k})$ and $M_x H(k_x, k_y) M_x^{-1} = H(-k_x, k_y)$, and the algebra of the crystalline symmetry operators is given by C_2^+ and M_x^- . According to Table II, the algebra of the symmetry operators (T^-, M_x^-, C_2^+) does not trivialize winding numbers at TRI points, where nodal points are located.

Table IV shows that in class DIII WG #6 with C_2^+ and M_x^- has $\nu_{\text{abs}} = 4$ indicating 4 nodal points with ± 1 winding numbers at TRI points. As expected, the distribution of the nodal points in the model is in agreement with the generalized no-go theorem. Furthermore, we find that the winding number of the system is in the form of $\nu = \frac{i}{2\pi} \oint h^{-1} dh$, with

$$h(\mathbf{k}) = a \sin k_x - ib \sin k_y. \quad (32)$$

By choosing the integral path encircling one of the nodal points, we obtain $\nu = +1$ for the nodes at $(0,0)$ and (π,π) , whereas $\nu = -1$ for the nodes at $(0,\pi)$ and $(\pi,0)$.

6. Quadratic nodal superconductors: WG#11 in class CI

The symmetries in class CI force nodal points at TRI points to have even winding numbers. Since $T^2 = 1$, Kramers' degeneracy is absent at TRI points; hence, unlike class DIII, it is not necessary that all of the TRI points in the BZ possess nodal points at zero energy when the number of the energy band pairs is odd. To demonstrate these properties, we consider a simple 2D tight-binding Hamiltonian

$$H(\mathbf{k}) = (\cos k_y - \cos k_x) \sigma_x + \sin k_x \sin k_y \sigma_y. \quad (33)$$

The system preserves chiral symmetry (3) with $S = \sigma_z$, time-reversal symmetry (5) with $T = \sigma_x \mathcal{K}$, and particle-hole symmetry (4) with $C = \sigma_y \mathcal{K}$. Furthermore, the Hamiltonian obeys $C_4 H(k_x, k_y) C_4^{-1} = H(-k_y, k_x)$ and $M_x H(k) M_x^{-1} = H(-k_x, k_y)$, where symmetry operators $C_4^+ = \sigma_z$ and $M_x^- = \sigma_x$. Since $T^2 = 1$ and $C^2 = -1$, the system belongs to SG#11 in class CI.

Two nodal points with quadratic energy dispersions are located at TRI momenta $\Gamma: (0,0)$ and $M: (\pi,\pi)$. The Hamiltonian of the low energy expansion near the nodal points Γ and M is in the form of

$$H_{\Gamma/M}(\delta\mathbf{k}) \simeq \pm \frac{1}{2} (\delta k_x^2 - \delta k_y^2) \sigma_x + \delta k_x \delta k_y \sigma_y, \quad (34)$$

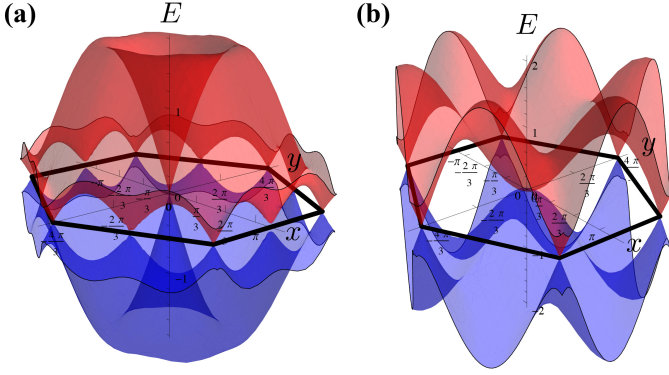


FIG. 10: (color online) The energy dispersion of the hexagonal BZ for the nodal points located at TRI points. (a) Three Dirac points with $\nu = 1$ are separately located at Γ, K, K' , whereas other three with $\nu = -1$ are separated located at M_1, M_2, M_3 . (b) One nodal point with quadratic dispersion at Γ carries -2 winding number, while the remaining two Dirac points with $\nu = 1$ is separately located at K, K' .

where $\delta\mathbf{k} = \mathbf{k} - \mathbf{k}_{\Gamma/M}$ indicates momentum expansion at the nodal points. Using $S = \sigma_z$, we have the values of the winding number $\nu_{\Gamma} = 2$ and $\nu_M = -2$. The distribution of the nodal points with ± 2 winding numbers is consistent with table IV for WG#11 in class CI with C_4^+ and M_x^- .

7. Six Dirac nodes: WG#17 in class DIII

We provide a 2-band tight binding model possessing six Dirac nodes located at high symmetry points ($\Gamma, K, K', M_1, M_2, M_3$) as shown in Fig. 6(b). Importantly, the Dirac semimetal is first predicted in the manuscript and has never been observed. Starting with each site having spin-1/2 degree of freedom in triangular lattice, we consider only the nearest neighbor hoppings with the Pauli matrices depending on the directions. The Hamiltonian in the real space is written in the form of the second quantization

$$\hat{H}_6 = \frac{1}{2} \sum_{\mathbf{r}} \left\{ iD_{\mathbf{r}+a\hat{y}}^\dagger \sigma_y D_{\mathbf{r}} + iD_{\mathbf{r}+C_6(a\hat{y})}^\dagger C_6(\sigma_y) D_{\mathbf{r}} + iD_{\mathbf{r}+C_6^2(a\hat{y})}^\dagger C_6^2(\sigma_y) D_{\mathbf{r}} + h.c. \right\}, \quad (35)$$

where the rotation operator obeys $C_6(\hat{x}) = (\hat{x} + \sqrt{3}\hat{y})/2$ and $C_6(\hat{y}) = (\hat{y} - \sqrt{3}\hat{x})/2$. Furthermore, the rotation operation C_6 acting on σ_x and σ_y exhibits the same basis changing as \hat{x} and \hat{y} . We rewrite the Hamiltonian in the momentum space

$$H_6(\mathbf{k}) = \begin{pmatrix} 0 & h_6(\mathbf{k}) \\ h_6^*(\mathbf{k}) & 0 \end{pmatrix}, \quad (36)$$

where $h_6(\mathbf{k}) = -i \sin k_y - i \sin(-(k_y + \sqrt{3}k_x)/2)e^{-2\pi i/3} - i \sin((-k_y + \sqrt{3}k_x)/2)e^{2\pi i/3}$. Since chiral symmetry with $S = \sigma_z$, time reversal symmetry with $T = \sigma_y \mathcal{K}$, and particle-hole symmetry with $C = \sigma_x \mathcal{K}$ are preserved, $T^2 = -1$ and $C^2 = 1$

lead to class DIII. Moreover, the system preserves reflection symmetry $M_x H_6(-k_x, k_y) M_x^{-1} = H_6(k_x, k_y)$ with $M_x = \sigma_y$ and $C_6 H_6(k_x/2 + \sqrt{3}k_y/2, k_y/2 - \sqrt{3}k_x/2) C_6^{-1} = H_6(k_x, k_y)$ with

$$C_6 = \begin{pmatrix} e^{-\pi i/6} & 0 \\ 0 & e^{\pi i/6} \end{pmatrix} \quad (37)$$

Based on the algebra between the crystalline symmetry operators and the chiral symmetry operator, the model belongs to WG#17 with M_x^- and C_6^+ . The energy dispersion in Fig. 10(a) shows that three Dirac nodes with $\nu = 1$ are located at Γ, K, K' and the other three with $\nu = -1$ are located at M_1, M_2, M_3 . We note that this tight-binding model can be used in any WG symmetry class possessing the same minimal configuration of the nodal points in Tables III, IV. For example, the model can be attached to another breaking the time reversal symmetry and the C_2 rotation symmetry but preserving the remaining symmetries. The WG symmetry class, which is class AIII with C_3^+ and M_x^- , possesses the six nodal points ($\Gamma, K, K', M_{1/2/3}$) as predicted in Table III.

8. Quadratic node at Γ : WG#17 in class CI

We build a tight binding model hosting a quadratic node at Γ and two Dirac nodes at K, K' separately. Consider each site has spin-1/2 degree of freedom in triangular lattice. The 2×2 Hamiltonian in the real space is written as

$$\hat{H}_4 = \frac{1}{2} \sum_{\mathbf{r}} \left\{ D_{\mathbf{r}+a\hat{y}}^\dagger \sigma_y D_{\mathbf{r}} + D_{\mathbf{r}+C_3(a\hat{y})}^\dagger C_3(\sigma_y) D_{\mathbf{r}} + D_{\mathbf{r}+C_3^2(a\hat{y})}^\dagger C_3^2(\sigma_y) D_{\mathbf{r}} + h.c. \right\}, \quad (38)$$

where $C_3 = C_6^2$. In this regard, the Hamiltonian in the momentum space is given by

$$H_4(\mathbf{k}) = \begin{pmatrix} 0 & h_4(\mathbf{k}) \\ h_4^*(\mathbf{k}) & 0 \end{pmatrix}, \quad (39)$$

where $h_4(\mathbf{k}) = -i(\cos k_y + \cos((k_y + \sqrt{3}k_x)/2)e^{-2\pi i/3} + \cos((-k_y + \sqrt{3}k_x)/2)e^{2\pi i/3})$. The symmetry class corresponds to CI, since one can check that chiral symmetry with $S = \sigma_z$, time reversal symmetry with $T = \sigma_x \mathcal{K}$, and particle-hole symmetry with $C = \sigma_y \mathcal{K}$ are preserved. Moreover, the system preserves reflection symmetry $M_x H_4(-k_x, k_y) M_x^{-1} = H_4(k_x, k_y)$ with $M_x^- = \sigma_y$ and $C_6 H_4(k_x/2 + \sqrt{3}k_y/2, k_y/2 - \sqrt{3}k_x/2) C_6^{-1} = H_4(k_x, k_y)$ with

$$C_6 = \begin{pmatrix} e^{\pi i/3} & 0 \\ 0 & e^{-\pi i/3} \end{pmatrix}. \quad (40)$$

As shown in Fig. 10(b), one quadratic node with $\nu = -2$ is located at Γ , while two Dirac nodes with $\nu = 1$ are separately located at K, K' .

This tight-binding model can be used for the same minimal configuration in different WGs(#13 – 17) in class CI as listed in Table IV and in class AIII as listed in Table III. That is, since $H_4(\mathbf{k})$ belongs to WG#17 in class CI, we can simply break selected symmetries without destroying the Dirac nodes so that the WG symmetry class can be changed to any of the aforementioned symmetry classes with the same minimal configuration. However, the only problem is that $H_4(\mathbf{k})$ cannot be directly transformed from class CI to class DIII, although the same minimal configuration with $\nu_{\text{abds}} = 4$ in class DIII is listed in Table III. Instead, we provide the 4-band tight-binding model $H_{4 \times 4}(\mathbf{k})$, which belongs to WG#17 in class DIII, having the same minimal configuration in Appendix E.

The tight-binding models $H_6(\mathbf{k}), H_4(\mathbf{k}), H_{4 \times 4}(\mathbf{k})$ in the example and Appendix E are new types of topological nodal systems, which have not been predicted and observed till now. Being different from graphene, the new nodal systems can host a Dirac node at $\Gamma, M_{1,2,3}$ or a quadratic node at Γ . Furthermore, for hexagonal BZ (WGs(#13 – 17)) these three models are the only building blocks for any minimal configuration with nodal points located at TRI points. For example, a nodal point carries $\nu = 3$ at Γ and three nodal points separately at $M_{1,2,3}$ carry $\nu = -1$ as the minimal configuration belonging to WG#17 in class DIII. This configuration can be realized by putting $H_6(\mathbf{k})$ and $H_{4 \times 4}(\mathbf{k})$ together.

IV. DIRAC NODES PROTECTED BY TIME-SPACE INVERSION SYMMETRY

For 2D lattices, chiral symmetry is not the only symmetry protecting nodal points. Space-time inversion symmetry, which is the combination of time-reversal symmetry and inversion symmetry, is another option and its symmetry operator obeying $(C_2T)^2 = \pm 1$ represents the two distinct types of the space-time inversion symmetry. Particularly, the space-time inversion symmetry with $(C_2T)^2 = 1$ can protect nodal points. While chiral symmetry intrinsically appears in time-reversal-symmetric superconductors, the space-time inversion symmetry with $(C_2T)^2 = 1$ can naturally arise in most of the inversion-symmetric materials preserving time-reversal symmetry; the symmetry-preserving Hamiltonian in the momentum space obeys

$$V_{\mathbf{k}} H^*(\mathbf{k}) V_{\mathbf{k}}^* = H(\mathbf{k}), \quad (41)$$

where the symmetry operator $C_2T = V_{\mathbf{k}} \mathcal{K}$ and $V_{\mathbf{k}} V_{\mathbf{k}}^* = 1$. In this regard, to search for new Dirac materials it is important to study the generalized no-go theorem of the space-time inversion symmetry for different WGs. However, this no-go theorem is distinct from the aforementioned theorem of the chiral symmetry, because there are two main differences between chiral symmetry and space-time inversion symmetry. First, the \mathbb{Z}_2 Berry phase quantized by space-time inversion symmetry characterizes the stability of the Dirac nodes, while the \mathbb{Z} winding number quantized by chiral symmetry characterizes the stability of the node points. Second, the Dirac

nodes protected by space-time inversion symmetry can move freely at any energy level, whereas the node points protected by chiral symmetry are locked at zero energy.

To preserve space-time inversion symmetry, we consider inversion symmetry C_2 and time-reversal symmetry T both are preserved. That is, to simplify the problem, we consider type-II magnetic wallpaper groups ($G+TG$). Since crystalline symmetry operator C_2 and time-reversal symmetry operator T always commute, we have $+1 = (C_2T)^2 = C_2^2 T^2 = T^2$ corresponding to class AI. Furthermore, only 10 of the 17 WGs preserve inversion symmetry and their corresponding point groups are C_n and C_{nv} with $n = 2, 4, 6$. Hence, the generalized no-go theorem of space-time inversion symmetry in class AI is much simpler than the one of chiral symmetry.

To study the generalized no-go theorem of space-time inversion symmetry, in the following we review that the symmetry quantizes the \mathbb{Z}_2 Berry phase, and build the relation between the \mathbb{Z}_2 Berry phases for two nodal points connected by crystalline symmetries or time reversal symmetry. Then, we discuss the minimal configurations of the Dirac nodes for different WGs by borrowing the idea from the discussion of chiral symmetry. Lastly, we implement the no-go theorem on the study of the two-dimensional Dirac semimetal materials.

A. \mathbb{Z}_2 Berry phases

For the space-time inversion symmetry, the Berry phase characterizing the nodal points is the key to its generalized no-go theorem. The Berry phase for the nodal point K_0 can be in form of

$$\gamma(\mathbf{K}_0) = \sum_{n \in \text{occupied}} \oint_{\Gamma(\mathbf{K}_0)} \mathbf{A}_n(\mathbf{k}) \cdot d\mathbf{k}, \quad (42)$$

where $\mathbf{A}_n(\mathbf{k}) = i \langle \mathbf{u}_n(\mathbf{k}) | \partial_{\mathbf{k}} | \mathbf{u}_n(\mathbf{k}) \rangle$ is the Berry connection, $|\mathbf{u}_n(\mathbf{k})\rangle$ is the periodic function of the Bloch wavefunction, the summation is for all the occupied states below the energy level of \mathbf{K}_0 , and $\Gamma(\mathbf{K}_0)$ is the closed integral path encircling K_0 . In the literature, the space-time inversion symmetry quantizes this Berry phase with the only two possible values $(0, \pi)$ as an \mathbb{Z}_2 invariant [74] (see the derivation in appendix F). Comparing with the definition of the winding number in Eq. 13, we find the wavefunction of the Berry phase can go through gauge transformation so that $\gamma(\mathbf{K}_0) = 0, 2\pi$ are equivalent. On the contrary, for chiral symmetry, any two different winding numbers correspond inequivalent topological systems. Furthermore, since $\gamma(\mathbf{K}_0) = \pm\pi$ are identical, choosing the orientation of the integral path does not affect the value of the Berry phase.

As the Berry phase $\gamma(\mathbf{K}_0) = \pi$, the integral path cannot smoothly shrink to a single point and then vanish, due to the singularity of the nodal point. This leads to the protection of the nodal point against gap opening without breaking space-time inversion symmetry. This protected nodal point with the lowest order of energy dispersion is a Dirac node. Although there exists a high-ordered nodal point with $\gamma = \pi$, without breaking the symmetry, the node can be smoothly deformed to a Dirac node [35]. This is the reason that space-time inversion

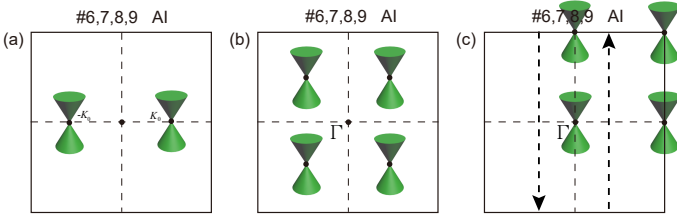


FIG. 11: (color online) The minimum number of nodal points (a) at the mirror lines, (b) at general points and (c) at TRI points in the WG#6, 7, 8, 9. The dashed lines are the integral paths of the quantized Berry phase through the entire BZs. Due to C_2 rotation symmetry or m reflection symmetry, the quantized Berry phases of the separate dashed lines are identical.

symmetry is the essential symmetry for Dirac materials. Here we focus on Dirac nodes only.

Next, in order to include all the nodal points in the BZ, we consider the relation between the two \mathbb{Z}_2 Berry phases $(\gamma(\mathbf{K}_0), \gamma(g\mathbf{K}_0))$ of two nodal points connected by crystalline symmetry or time-reversal symmetry g and this symmetry operation can be symmorphic or nonsymmorphic. The berry phase at $g\mathbf{K}_0$ point is given by

$$\gamma(g\mathbf{K}_0) = \sum_{n \in \text{occupied}} \oint_{\Gamma(g\mathbf{K}_0)} \mathbf{A}_n(\mathbf{k}) \cdot d\mathbf{k} \quad (43)$$

Since the value of the Berry phase is either 0 or π , it is expected that the two Berry phases connected by the symmetry g are identical

$$\gamma(g\mathbf{K}_0) = \gamma(\mathbf{K}_0) \quad (44)$$

(see the proof in appendix F). While the relations of the winding numbers connected by a symmetry in Table II are complicated, we find that this simple relation for the Berry phases can be easily applied for the generalized no-go theorem.

B. Minimal configurations of nodal points

The \mathbb{Z}_2 property of the Berry phase significantly simplifies the process to find the minimal configurations of Dirac nodes as the generalized no-go theorem, when we compare this with the complexity of chiral symmetry. The five steps for nodal points protected by chiral symmetry can be simplified for space-time inversion symmetry. Let us first provide the recipe for Dirac nodes not located at TRI points.

(a) We start to place a Dirac node with $\gamma = \pi$ at any location of the irreducible BZ, except for TRI points, as shown in Fig. 2. Similarly, different placement leads to different minimal configuration; hence, we have to consider all placement possibilities. Moreover, the Dirac node always survives at any location even if crystalline symmetries or time-reversal symmetry is introduced. The reason is that the symmetry operation does not bring the opposite charge at the same momentum point. This ubiquity of the Dirac node is different from the chiral-symmetric systems, since the symmetries can trivialize

nodal points protected by chiral symmetry at some locations with zero winding number in total.

(b) This step is similar to the one for chiral symmetry. That is, using all of the symmetry operations, we duplicate the node point inside of the irreducible BZ to the remaining area of the BZ. We note that space-time inversion symmetry is used to quantize the Berry phase, only one of time-reversal symmetry and inversion symmetry can duplicate the Dirac node. We always use inversion for duplication unless mention otherwise.

(c) Finally, we have to check if the summation of the Berry phases from all the Dirac nodes in the BZ obeys

$$\sum_i \gamma(\mathbf{K}_0^i) = 0 \pmod{2\pi}, \quad (45)$$

which is the Nielsen-Ninomiya theorem for the \mathbb{Z}_2 charges. The derivation is similar with the one for the \mathbb{Z} charges in appendix D. Since inversion symmetry is always preserved, the duplication in step (b) leads to even number of the Dirac nodes. Hence, the summation condition is naturally satisfied. This is the end of searching for the minimal configuration of the Dirac nodes.

On the other hand, for the Dirac node placed at one of the TRI points, the procedure is identical to the point off TRI points till step (c). Inversion symmetry cannot lead to even number of the Dirac nodes, since inversion symmetry operation cannot duplicate any nodal point located at a TRI point. Therefore, we have to add another Dirac node and repeat the procedure for the charge neutralization. At the same time, we need to make sure the constraint conditions similar to Eq. 19,20,21 for specific Dirac nodes are satisfied. That is, the Berry phases at some TRI points obey

$$\gamma(\Gamma) + \nu(Y) = 0 \pmod{2\pi}, \gamma(\Gamma) + \nu(X) = 0 \pmod{2\pi}, \quad (46)$$

for WG#2, 6 – 12 and

$$\nu(\Gamma) + \nu(M_i) = 0 \pmod{2\pi}, \quad (47)$$

for WG#16, 17. The reason is that the two quantized Berry phases calculated in the two dashed lines as shown Fig. 5 must be quantized separately and identical due to C_2 rotation symmetry and the two integral paths together can be deformed to the paths encircling two TRI points; hence, the summation of these two Berry phases, characterizing two TRI points, must vanish. Once the summation condition (45) holds, searching for the minimal configurations ends.

After considering all possible placement of Dirac nodes, we can build Table V to show the minimal numbers and configurations of the Dirac nodes for the ten WGs with time-reversal symmetry. Furthermore, the minimal configurations in Table V are the basic building blocks for any configuration of Dirac nodes in any Dirac semimetals. That is, the combinations of the minimal configurations exhaustively cover all possible configurations of Dirac nodes, due to the absence of the high-ordered nodes.

Now let us use WG#6, 7, 8, 9 to demonstrate the procedure obtaining the three minimal configurations of the Dirac nodes with Hamiltonians. (a) We place a Dirac point with $\gamma = \pi$ in

TABLE V: **The minimal configurations of Dirac nodes protected by PT-symmetry off- points for the 10 WGs preserving C_2 symmetry.** The table exhaustively provides all the possible minimal configurations with the minimal numbers. The minimal numbers for off-TRI points without location specification indicate Dirac points located at general points, while the minimal numbers for at-TRI points without location specification indicate Dirac points located at all the TRI points.

WG	Generators	Off-TRI	At-TRI	Materials
#2	C_2	2	4	
#6,7,8,9	C_2 and m_x	2(mirror lines) or 4	4	Pmmn boron[75], 6,6,12-graphyne[61]
#10	C_4	4	4	
#11,12	C_4 and m_x	4(mirror lines) or 8	4	Square-graphyne[76]
#16	C_6	2(K,K') or 6	$4(M_{1,2,3}, \Gamma)$	
#17	C_6 and m_x	2(K,K') or 6(mirror lines) or 12	$4(M_{1,2,3}, \Gamma)$	β -graphyne[61], TiB ₂ [77], NiPSe ₂ [78]

one of the mirror lines at momentum \mathbf{K}_0 . (b) Since C_2 inversion symmetry is the only symmetry for duplication, the duplicated Dirac node is located at $-\mathbf{K}_0$. (c) There are two Dirac nodes with $\gamma = \pi$ as shown in Fig. 11(a), the total Berry phase in the BZ is neutralized. Hence, the presence of the two Dirac nodes is the minimal configuration. The example Hamiltonian is given by $H_2(\mathbf{k}) = (\cos k_x + 1 - \cos k_y)\sigma_x + \sin k_y\sigma_y$. The two Dirac nodes with $\nu = \pi$ are located at $(\pm\pi/2, 0)$ in the M_y mirror line. It is easy to check the Hamiltonian preserving space-time inversion symmetry, inversion symmetry, and mirror symmetry with $C_2T = \mathcal{K}$, $C_2 = \sigma_x$, $M_y = \sigma_x$ respectively. On the other hand, if the first Dirac node is placed at a general point, C_2 inversion symmetry and M_x mirror generate 3 other Dirac nodes as shown in Fig. 11(b). Hence, there are 4 Dirac nodes as the minimal configuration. The Hamiltonian $H_4(\mathbf{k}) = \cos k_x\sigma_x + \cos k_y\sigma_y$ is a simple example. Four Dirac nodes with $\nu = \pi$ are located at $\pm(\pi/2, \pi/2)$ and $\pm(\pi/2, -\pi/2)$ respectively. The three symmetries are preserved with symmetry operators $C_2T = \mathcal{K}$, $C_2 = \mathbb{I}$, $M_x = \mathbb{I}$. Thus, according to the two cases, the minimal number of the Dirac nodes off TRI points is either 2 or 4 as listed in Table V.

When we place a Dirac node at TRI point, say Γ , any symmetry is unable to duplicate the Dirac point, which violates the neutralization (45). Furthermore, the distribution of the Dirac nodes must obey the additional condition (46) so that two other Dirac nodes have to be present at X and Y respectively. Due the charge neutralization (45), another Dirac must appear at M . Thus, there are four Dirac nodes separately located at the four TRI points as shown in Fig. 11(c). The example Hamiltonian is identical to Eq. 31 ($H_{\text{TRI}}(\mathbf{k}) = a \sin k_x\sigma_x + b \sin k_y\sigma_y$). It is known that $H_{\text{TRI}}(\mathbf{k})$ preserves chiral symmetry, inversion symmetry, and mirror symmetry with symmetry operators $S = \sigma_z$, $C_2 = \sigma_z$, $M_x = \sigma_y$. Also, space-time inversion symmetry is preserved with $C_2T = \sigma_x\mathcal{K}$. Four Dirac nodes with $\nu = 1$ are located at the four TRI points (Γ, X, Y, M).

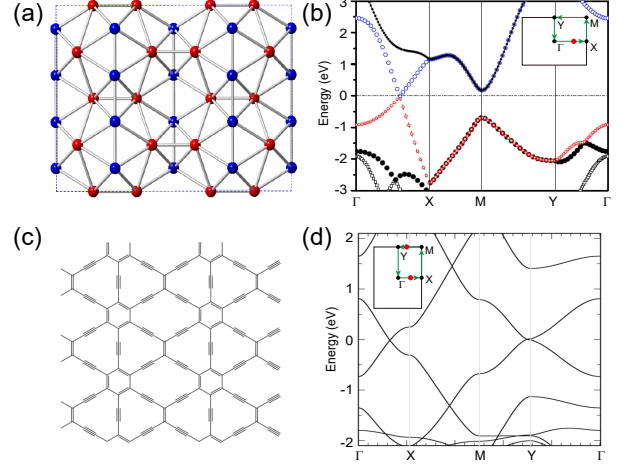


FIG. 12: (color online) The crystal and band structures of (a, b) Pmmn boron[75], (c, d) 6,6,12-graphyne [61]. The red dots denote the locations of Dirac points.

C. Examples

Over hundreds of 2D and quasi-2D materials, graphene[57–59], silicene and germanene[60], and several graphynes[61, 62] have been predicted to be Dirac materials. Particularly, Dirac cones in graphene have been truly confirmed experimentally. Since graphene preserves time-space inversion symmetry and chiral (sublattice) symmetry, its Dirac nodes are under double protection. However, chiral symmetry is fragile for most of the free-fermion materials, while space-time inversion symmetry can be naturally preserved. By implementing our generalized no-go theorem (Table V), we review Dirac semimetals in the literature [79], and show that the minimal configurations of our theorem includes the configurations of the Dirac nodes in the material examples.

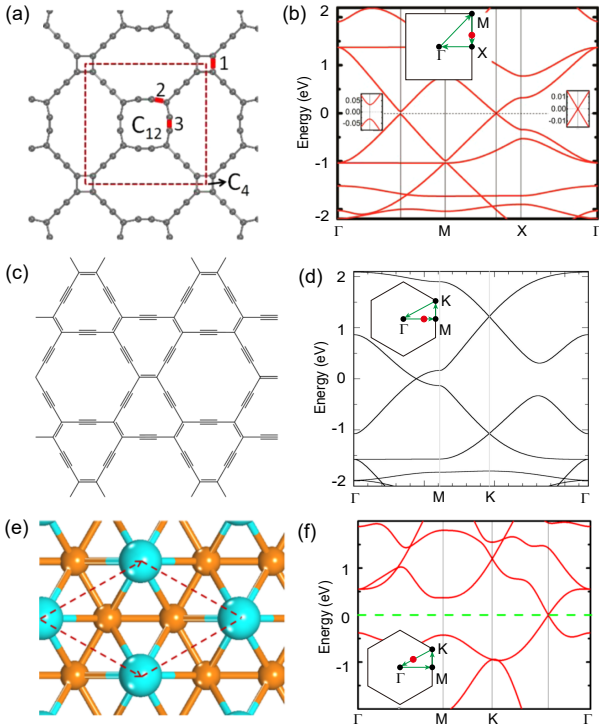


FIG. 13: (color online) The crystal and band structures of (a, b) Square-graphyne[76], (c, d) β -graphyne[61], (e, f) TiB_2 [77]. The red dots denote the locations of Dirac points

(a) WG#6 – Pmmn boron and 6,6,12-graphyne: The Pmmn boron with WG#6 is a 2D layer structure as shown in Fig.12(a). Fig.12(b) shows two Dirac points connected by C_2 rotational symmetry in the mirror line $\Gamma\bar{X}$ in agreement with Table V. Similarly, 6,6,12-graphyne also belongs to WG#6, see Fig.12(c). Two Dirac nodes connected by C_2 rotational symmetry are separately located in the mirror line $\Gamma\bar{X}$, while two others are present in the mirror line $\bar{Y}\bar{M}$. The material possesses the combination of the two minimal configurations of the Dirac nodes in Table V.

(b) WG#11 – Square-graphyne: The crystal structure of S-graphyne in Fig.13(a) indicates the system belongs to WG#11. Fig.13(b) shows a Dirac point located at $\bar{X}\bar{M}$ as the mirror line. C_4 rotation symmetry produces three other Dirac nodes in the mirror lines. The total number of the Dirac nodes is four in agreement with Table V.

(c) WG#17 – β -graphyne and TiB_2 : Fig. 13(c) shows that the crystal structures of β -graphyne belongs to WG#17. For β -graphyne, the band structure in Fig. 13(d) shows that a Dirac point located in the mirror line $\Gamma\bar{M}$, and there are six Dirac points in the BZ due to C_6 rotation symmetry. On the other hand, TiB_2 is a 3D layer structure described by layer group P6/mmm. The 2D projection in Fig. 13(e) shows the subgroup of the layer group is WG#17. In the band structure of Fig. 13(f), six Dirac nodes are located in the six different mirror lines ($\Gamma\bar{K}$ and $\Gamma\bar{K}'$) are connected by C_6 rotational symmetry. Indeed, the number of the Dirac nodes is consistent with Table V.

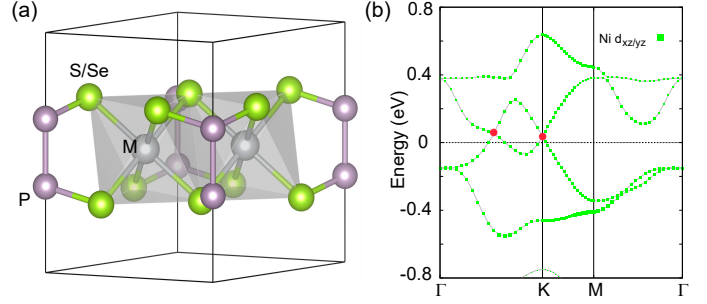


FIG. 14: (color online) The crystal and band structures of the monolayer NiPSe_3 [78]. The red dots denote Dirac points located at non-zero energy.

(d) WG#17 – NiPSe_2 : The monolayer NiPSe_3 belongs to the layer group $\text{P}\bar{3}1\text{m}$ including point group D_{3d} and its crystal structure is shown in Fig. 14(a). Although the layer does not include C_2 rotation symmetry, its inversion symmetry can be treated as an effective C_2 symmetry after the monolayer is projected to the 2D plane. Hence, the 2D projection belongs to WG#17, which is a subgroup of $\text{P}\bar{3}1\text{m}$ with additional C_2 rotation symmetry. Since the monolayer in the paramagnetic state preserves time reversal symmetry and spin-orbital coupling is absent, the system is equivalent to two identical subsystems preserving time reversal symmetry with its symmetry operator $T = \mathcal{K}$. Hence, space-time inversion symmetry (C_2T) is preserved to protect Dirac nodes.

Near the Fermi level, the valence and conduction bands are predominantly attributed to the $\text{Ni-}3d_{xz/yz}$ orbitals. With $\text{Ni-}3d_{xz/yz}$ orbitals and two bases of the sublattice the effective 4-band tight binding model [78, 80] can capture the Dirac points near Fermi level. The band structures of the effective model (Fig. 14(b)) show that two Dirac nodes are separately located at K and K' as well as six Dirac nodes are separately located at three $\Gamma\bar{K}$ lines and three $\Gamma\bar{K}'$ lines. By choosing the integral path of nodal points, we obtain \mathbb{Z}_2 Berry phase $\nu = \pi$ for every Dirac point. The total number of Dirac points for this system is the sum of the two minimum number [$2(K, K')$ and 6 MLs] in Table V.

V. 2D NON-HERMITIAN LATTICES

Beyond the Hermitian systems, non-Hermitian physics [9, 23–25, 44, 46, 81–128], has emerged in a variety of quantum platforms, such as open quantum systems [83], wave systems with gain and loss [23, 84–87] and interacting electron systems [101]. The origin of non-Hermitian terms can stem from the self-energy correction of the Green's function [83, 99–101] as an example. We focus on a 2D non-Hermitian lattice model in periodic boundary condition. The eigenenergy of the system can be complex $E_n(\mathbf{k}) = \varepsilon_n(\mathbf{k}) + i\Gamma_n(\mathbf{k})$, where the real part $\varepsilon_n(\mathbf{k})$ represents the renormalized band dispersion and the imaginary part $\Gamma_n(\mathbf{k})$ represents the inverse of quasi-particle lifetime, which is affected by environment dissipation [83] or many body interacting [99–101].

In a 2D non-Hermitian Hamiltonian $\mathcal{H}_{nH}(\mathbf{k})$, Fermi points (FPs) and exceptional points (EPs) can be topologically protected and immune to any perturbations [9, 25, 101]. The topological invariants, which identify the robustness of these two distinct points, share the mathematical similarity of the winding number [25] characterizing Dirac nodes in Hermitian chiral symmetric systems. In this regard, the non-Hermitian no-go theorems for FPs and EPs can smoothly inherit the Hermitian no-go theorem. Due to the constraints of the WGs, the minimal number of the protected points might be greater than 2. We first study the no-go theorem for the EPs and then extend the discussion to the FPs.

In the following, we first review the topological invariants of EPs and then show that the relation of the EPs connected by crystalline symmetries is identical to the chiral-symmetric lattices. Being different from the Hermitian chiral-symmetric systems, rotation symmetry in the non-Hermitian systems imposes an additional constraint on EPs located at rotation centers. Finally, we generalize the corresponding no-go theorems to the 17 WGs. Likewise, the no-go theorem of FPs follows the same recipe in the next subsection.

A. Non-Hermitian exceptional points

In 2D non-Hermitian BZ, degeneracy points can be topological stable points and are categorized into exceptional (defective) points and non-defective points. That is, at an EP the corresponding eigenstates coalesce [129] (become identical), while at a non-defective degeneracy point the eigenstates remain distinct. It has been shown that without any symmetry a degeneracy point can be characterized by an integer discriminant number (ν_{disc}) and this non-zero number leads to the robustness of the degeneracy point [25]. However, the presence of the EPs with high topological charges ($|\nu_{\text{disc}}| > 1$) or non-defective degeneracy points requires fine-tuned parameters. In the presence of arbitrarily small perturbations, these points can be easily deformed to EPs with $\nu_{\text{disc}} = \pm 1$. Since the only EPs with $\nu_{\text{disc}} = \pm 1$ are stable, we focus on the physics of these EPs. In the literature [25], the EPs obey the Fermion doubling theorem

$$\sum_j \nu_{\text{disc}}(\mathbf{K}_{\text{EP}}^j) = 0, \quad (48)$$

where \mathbf{K}_{EP}^j is the momentum of the EP in the BZ.

Before extending the no-go theorem of the EPs to the 17 wallpaper groups, let us review the definition of the discriminant number $\nu_{\text{disc}}(\mathbf{K}_{\text{EP}})$. For a generic m -band non-Hermitian Hamiltonian $\mathcal{H}_{nH}(\mathbf{k})$, the characteristic equation determines all of the eigenenergies

$$f(E, \mathbf{k}) = \det[E - \mathcal{H}_{nH}(\mathbf{k})] = \prod_{\alpha=1}^m [E - E_{\alpha}(\mathbf{k})] = 0, \quad (49)$$

where $E_{\alpha}(\mathbf{k})$ is the band dispersion of the α -th band and is the roots of the polynomial $f(E, \mathbf{k})$. To identify EPs, we use the discriminant of the polynomial $f(E, \mathbf{k})$

$$\text{Disc}_E[\mathcal{H}_{nH}](\mathbf{k}) = \prod_{\alpha < \beta} [E_{\alpha}(\mathbf{k}) - E_{\beta}(\mathbf{k})]^2. \quad (50)$$

The EP momentum \mathbf{K}_{EP} corresponds to the vanishing of the discriminant $\text{Disc}_E[\mathcal{H}_{nH}](\mathbf{K}_{\text{EP}}) = 0$. We note that although this equation can also identify non-defective degeneracy points, the points are unstable and can be easily deformed to EPs [25]. The discriminant $\text{Disc}_E[\mathcal{H}_{nH}](\mathbf{k})$ for EPs and $\det[h(\mathbf{k})]$ for Hermitian Dirac nodes share similar mathematical roles. That is, when the discriminant vanishes, its vanishing real and imaginary parts form 0D points in the 2D BZ. Furthermore, the important property of the discriminant is a single-valued function of \mathbf{k} . The reason is that the discriminant, which is the determinant of the Sylvester matrix of the polynomials $f(E, \mathbf{k})$ and $\partial_E f(E, \mathbf{k})$ [130–132], inherits the single-valued property from the Hamiltonian $\mathcal{H}_{nH}(\mathbf{k})$. In this regard, by comparing with the winding number (13) for the Dirac node, one can define the discriminant number

$$\nu_{\text{disc}}(\mathbf{K}_{\text{EP}}) = \frac{i}{2\pi} \oint_{\Gamma(\mathbf{K}_{\text{EP}})} d\mathbf{k} \cdot \nabla_{\mathbf{k}} \ln \text{Disc}_E[\mathcal{H}_{nH}](\mathbf{k}), \quad (51)$$

where the integration path $\Gamma(\mathbf{K}_{\text{EP}})$ is a loop encircling \mathbf{K}_{EP} counterclockwise. Due to the single-valued discriminant function, the discriminant number is always an integer. Since the topological numbers from the two distinct origins (chiral-symmetric systems and EPs) share the same mathematical structure, we can derive the doubling theorem for EPs by following the same recipe in chiral-symmetric system (Appendix D). That is, the sum over the discriminant numbers of all the EPs vanishes as previously shown in Eq. 48.

1. Conditions from crystalline symmetries

To extend the EP no-go theorem to the 17 wallpaper groups, we study the relation of the discriminant numbers for EPs connected by symmetries. It is known that the two symmetry generators C_n and M form the 17 wallpaper groups, with crystalline symmetry operator matrix $U_g(\mathbf{k})$. The symmetry-preserved Hamiltonian obeys

$$\mathcal{H}_{nH}(g\mathbf{k}) = U_g(\mathbf{k})\mathcal{H}_{nH}^{\eta}(\mathbf{k})U_g^{-1}(\mathbf{k}), \quad (52)$$

where $\eta = 1$ for the conventional crystalline symmetry. The crystalline symmetry generators can be extended to the combination symmetry of crystalline operation and complex-conjugation/transpose [46]. In this regard, $U_g(\mathbf{k})\mathcal{K}^t$, $U_g(\mathbf{k})\mathcal{K}^*$, and $U_g(\mathbf{k})\mathcal{K}^{\dagger}$ indicate the combination symmetry operator of the crystalline operation and the transpose/complex-conjugation/conjugate-transpose respectively. The corresponding Hamiltonians obey the symmetry equation above with $\eta = t, *, \dagger$. Hence, conventional (U_g), transpose ($U_g\mathcal{K}^t$), conjugation ($U_g\mathcal{K}^*$), and conjugate-transpose ($U_g\mathcal{K}^{\dagger}$) crystalline generators correspond to the four types of the symmetries.

For $\eta = 1, t$, using the symmetry equation, we have $E_n(g\mathbf{k}) = E_n(\mathbf{k})$. Similarly, for $\eta = *, \dagger$, $E_n(g\mathbf{k}) = E_n^*(\mathbf{k})$. In the following discussion, we label g to indicate $U_g(\mathbf{k})$ and $U_g(\mathbf{k})\mathcal{K}^t$ representations and \bar{g} to indicate $U_g(\mathbf{k})\mathcal{K}^{*/\dagger}$ representations. We are interested in WGs formed by one or two generators and the generators can either g or \bar{g} . The generators

are either rotation or mirror. To be specific, the WG with one generator is in form of g or \bar{g} , while the WG with two generators is in form of (C_n, M) , (C_n, \bar{M}) , (\bar{C}_n, M) , (\bar{C}_n, \bar{M}) . We study the no-go theorem for the WGs in those forms and build Table VI in the following. Particularly, the EP no-go theorem for the 17 WGs correspond to the cases with the generator g .

We use examples to illustrate the distinct combination symmetries above. Consider a Hermitian Hamiltonian $\mathcal{H}_H(\mathbf{k}) = \mathcal{H}_H^\dagger(\mathbf{k})$ which preserves inversion symmetry, i.e. $\mathcal{H}_H(-\mathbf{k}) = U_I \mathcal{H}_H(\mathbf{k}) U_I^{-1}$. When a non-Hermitian term $i\lambda(\mathbf{k})\Gamma$ (which is typically a perturbation) is added, where $\lambda(\mathbf{k}) = \lambda(-\mathbf{k})$ is a real even function and Γ is a Hermitian matrix, the Hamiltonian becomes $\mathcal{H}_{nH}(\mathbf{k}) = \mathcal{H}_H(\mathbf{k}) + i\lambda(\mathbf{k})\Gamma$. One can easily check that when $[\Gamma, U_I]_\pm = 0$, the corresponding inversion symmetry representation becomes $U_I U_I \mathcal{K}^\dagger$, respectively. On the other hand, $U_I(\mathbf{k})\mathcal{K}^*$ is equivalent to time reversal symmetry operator. We start with a Hermitian Hamiltonian preserving time reversal symmetry ($\mathcal{H}_H(-\mathbf{k}) = U_I(\mathbf{k})\mathcal{H}_H^*(\mathbf{k})U_I^{-1}(\mathbf{k})$). Similarly, when a non-Hermitian perturbation is introduced, the Hamiltonian reads $\mathcal{H}_{nH}(\mathbf{k}) = \mathcal{H}_H(\mathbf{k}) + i\lambda(\mathbf{k})\Gamma$. As $[\Gamma, U_I]_\pm = 0$, transpose inversion symmetry ($U_I(\mathbf{k})\mathcal{K}^\dagger$)/time-reversal symmetry ($U_I(\mathbf{k})\mathcal{K}^*$) is preserved respectively.

Before build the no-go theorem for g and \bar{g} in Table VI, we use the absolute number ν_{abs} to indicate the minimal configuration of the EPs, where $\nu_{\text{abs}} = \sum_{\mathbf{k}_{\text{EP}}^i \in \text{BZ}} |\nu_{\text{disc}}(\mathbf{k}_{\text{EP}}^i)|$. For all of the WGs, ν_{abs} can indicate the number of the EPs with $\nu_{\text{disc}} = \pm 1$ in the minimal configuration. For the non-unique cases (ν_{abs} without \sim), EPs with higher charges ($|\nu_{\text{disc}}| > 1$) can be present in the minimal configurations.

(a) We first consider the conventional crystalline symmetries and the transpose ones and their generators are all indicated by g . Since no global symmetries are required to protect EPs in 2D non-Hermitian systems, unlike Hermitian Hamiltonian preserving chiral symmetry, there is no algebra between crystalline symmetry operators and other global symmetry operators. By using the symmetry equation (52), the Hamiltonians at these two points possess the identical characteristic polynomial

$$\begin{aligned} \det[E - \mathcal{H}_{nH}(\mathbf{k})] &= \det[E - U_g(\mathbf{k})\mathcal{H}_{nH}^{1/t}(\mathbf{k})U_g^{-1}(\mathbf{k})] \\ &= \det[E - \mathcal{H}_{nH}(g\mathbf{k})]. \end{aligned} \quad (53)$$

Hence, the discriminants at these two points are identical

$$\text{Disc}_E[\mathcal{H}_{nH}](\mathbf{k}) = \text{Disc}_E[\mathcal{H}_{nH}](g\mathbf{k}). \quad (54)$$

As symmetry g connects two EPs ($g\mathbf{K}_{\text{EP}}$ and \mathbf{K}_{EP}), the relation of the discriminant numbers at these two points is given by

$$\begin{aligned} \nu_{\text{disc}}(g\mathbf{K}_{\text{EP}}) &= \frac{i}{2\pi} \oint_{\Gamma(\mathbf{K}_{\text{EP}})} \det(g) d(\ln(\text{Disc}_E[\mathcal{H}_{nH}](g\mathbf{k}))) \\ &= \frac{i}{2\pi} \oint_{\Gamma(\mathbf{K}_{\text{EP}})} \det(g) d(\ln(\text{Disc}_E[\mathcal{H}_{nH}](\mathbf{k}))) \\ &= \det(g) \nu_{\text{disc}}(\mathbf{K}_{\text{EP}}) \end{aligned} \quad (55)$$

The explicit relations between the two EPs for the two differ-

ent types of the crystalline symmetries are given by

$$\nu_{\text{disc}}(\hat{C}_n \mathbf{K}_{\text{EP}}) = \nu_{\text{disc}}(\mathbf{K}_{\text{EP}}), \nu_{\text{disc}}(\hat{M} \mathbf{K}_{\text{EP}}) = -\nu_{\text{disc}}(\mathbf{K}_{\text{EP}}), \quad (56)$$

which are identical to the relation of the generators C_n^+ and M^+ in Table II for the Hermitian chiral-symmetric systems without any time-reversal symmetry. Thus, as shown in Table VI, the list of the EP no-go theorem for the 17 WGs formed by U_g and $U_g \mathcal{K}^t$ can inherit the cases of C_n^+ and M^+ in class AIII in Table III, except for EPs located at rotation centers.

Consider n -fold rotation symmetry C_n . Being different from the Hermitian chiral symmetric systems, the charge of the non-Hermitian EP at a rotation center, say \mathbf{K}_{EP}^r , is limited by an additional restriction. In order to show the restriction, in the expression (51) of the discriminant number, the integral path Γ enclosing \mathbf{K}_{EP}^r is divided into n integral paths related by the C_n rotation symmetry

$$\Gamma(\mathbf{K}_{\text{EP}}^r) = \cup_{l=0}^{n-1} \hat{C}_n^l \Gamma_{1/n}(\mathbf{K}_{\text{EP}}^r), \quad (57)$$

where $\Gamma_{1/n}(\mathbf{K}_{\text{EP}}^r)$ denotes the one n -th of the closed integral path $\Gamma(\mathbf{K}_{\text{EP}}^r)$ with the two end points \mathbf{k}_o and $\hat{C}_n \mathbf{k}_o$. After decomposing the integral of the winding number to n separate integral paths, we can reorganize the discriminant number equation

$$\begin{aligned} \nu_{\text{disc}}(\mathbf{K}_{\text{EP}}^r) &= \frac{i}{2\pi} \int_{\Gamma_{1/n}(\mathbf{K}_{\text{EP}}^r)} \sum_{l=1}^{n-1} d(\ln(\text{Disc}_E[\mathcal{H}_{nH}](\hat{C}_n^l \mathbf{k}))) \\ &= n \times \frac{i}{2\pi} \oint_{\Gamma_{1/n}(\mathbf{K}_{\text{EP}}^r)} d(\ln(\text{Disc}_E[\mathcal{H}_{nH}](\mathbf{k}))) \\ &= nj. \end{aligned} \quad (58)$$

where j is an integer. The second line stems from that the symmetry relation (52) between the two points $(\mathbf{k}, \hat{C}_n \mathbf{k})$ leads to $\text{Disc}_E[\mathcal{H}_{nH}](\mathbf{k}) = \text{Disc}_E[\mathcal{H}_{nH}](\hat{C}_n \mathbf{k})$. Since the integrands at \mathbf{k}_o and $\hat{C}_n \mathbf{k}_o$ are identical, the integral path of $\Gamma_{1/n}(\mathbf{K}_{\text{EP}}^r)$ is effectively closed so that the integral is quantized. Hence, as an EP is located at a n -fold rotation symmetry center, its discriminant number is a multiple of n . This constraint for the value of the discriminant number does not allow the EPs to inherit some of the minimal configurations from the chiral symmetric systems. For example, for WG#10 with C_4^+ , one of the chiral symmetric minimal configurations is that four Dirac points with ± 1 charges quantized can be separately located at Γ, X, Y, M , which are rotation centers. However, the C_4 rotation symmetry from WG#10 forbids any non-Hermitian EP with ± 1 charge to appear at any rotation center. Hence, this configuration is excluded in Table VI. We note that the non-Hermitian cases in Table I only shows the no-go theorem for the 17 conventional WGs (C_n, M_x) .

(b) Consider the conjugation crystalline symmetries and the conjugate-transpose ones; their generators are all indicated by \bar{g} . By using the symmetry equation (52), we can directly connect the determinant at \mathbf{k} and $\bar{g}\mathbf{k}$

$$\begin{aligned} \det[E - \mathcal{H}_{nH}(\bar{g}\mathbf{k})] &= \det[E - U_{\bar{g}}(\mathbf{k})\mathcal{H}_{nH}^{*/t}(\mathbf{k})U_{\bar{g}}^{-1}(\mathbf{k})] \\ &= \det[E - \mathcal{H}_{nH}^*(\mathbf{k})]. \end{aligned} \quad (59)$$

The conjugation adds an additional minus sign to the relation equation (55) between the two symmetry-connected discriminant numbers

$$\nu_{\text{PF}}(\bar{g}\mathbf{K}_{\text{EP}}) = -\det(\bar{g})\nu(\mathbf{K}_{\text{EP}}) \quad (60)$$

Hence, in Table VI the EP no-go theorem for the conjugate 17 WGs (\bar{C}_n, \bar{M}) corresponds to the Hermitian no-go theorem for C_n^- and M^- in class AIII as listed in Table III.

(c) For a WG containing two generators, there are four groups based on the combinations — $(C_n, M), (C_n, \bar{M}), (\bar{C}_n, M), (\bar{C}_n, \bar{M})$. The last two can be easily extended by the recipe above. Due to the relations between the symmetry-connected EPs (55,60), the non-Hermitian no-go theorem for $C_n, \bar{M}/\bar{C}_n, M$ inherits the Hermitian no-go theorem for $C_n^+, M^-/C_n^-, M^+$ in class AIII. However, we note that the constraint (58) for EP at rotation centers also excludes some minimal configurations from the inheritance of C_n^+ .

2. Examples

To host EPs, the minimal dimension of the non-Hermitian Hamiltonian must be 2×2 , since at least two states coalesce. First, we calculate the explicit form of the discriminant for a generic 2×2 non-Hermitian Hamiltonian

$$\mathcal{H}_{2 \times 2}(\mathbf{k}) = h_0(\mathbf{k})\sigma_0 + h_x(\mathbf{k})\sigma_x + h_y(\mathbf{k})\sigma_y + h_z(\mathbf{k})\sigma_z. \quad (61)$$

The eigenenergies are given by $E_{\pm} = h_0 \pm \sqrt{h_x^2 + h_y^2 + h_z^2}$. Using Eq. 50, we have a simple form of the discriminant

$$\begin{aligned} \text{Disc}_E[\mathcal{H}_{2 \times 2}](\mathbf{k}) &= (E_+ - E_-)^2 \\ &= 4(h_x^2 + h_y^2 + h_z^2) = 4(h_0^2 - \det \mathcal{H}_{2 \times 2}). \end{aligned} \quad (62)$$

This form is employed to compute the discriminant for the following examples.

(a) We start with a 2×2 off-diagonal Hamiltonian

$$\mathcal{H}(\mathbf{k}) = \begin{pmatrix} 0 & 1 \\ \cos k_x + \cos k_y + i(\cos k_x - \cos k_y) & 0 \end{pmatrix}. \quad (63)$$

The Hamiltonian preserves the following symmetries

$$\bar{C}_4 \mathcal{H}^*(k_x, k_y) \bar{C}_4^{-1} = \mathcal{H}(k_y, -k_x), \quad (64)$$

$$M_x \mathcal{H}(k_x, k_y) M_x^{-1} = \mathcal{H}(-k_x, k_y), \quad (65)$$

where $\bar{C}_4 = \sigma_0$ and $M_x = \sigma_0$. Table VI shows the minimal configuration of WG#11 is either 4 EPs at the mirror lines or 8 EPs at general points.

To find EPs in this model, we obtain the discriminant $\text{Disc}_E[\mathcal{H}](\mathbf{k}) = 4[\cos k_x + \cos k_y + i(\cos k_x - \cos k_y)]$ by using Eq. 62. As the discriminant vanishes, the Hamiltonian becomes a Jordan canonical form and the two eigenstates coalesce as an EP. In this regard, the four EPs are located at

$(\pm\pi/2, \pm\pi/2)$ and $(\pm\pi/2, \mp\pi/2)$ in the mirror lines. To compute the discriminant number of the EPs, we particularly consider the EP at $(\pi/2, \pi/2)$. Near the EP, the leading order of the discriminant is given by

$$\text{Disc}_E[\mathcal{H}](\mathbf{k}) = -(1+i)dk_x - (1-i)dk_y + O(d\mathbf{k}^2), \quad (66)$$

where $dk_{x/y} = k_{x/y} - \pi/2$. By the definition (51) of the discriminant number, we have $\nu_{\text{disc}} = +1$ for the EP at $(\pi/2, \pi/2)$. The \bar{C}_4 rotation symmetry extends to this EP to the remaining three by implementing the discriminant number relation (60). Hence, the EPs at $(\pm\pi/2, \pm\pi/2)/(\pm\pi/2, \mp\pi/2)$ possess $+1/-1$ charge.

(b) Consider a non-Hermitian Hamiltonian preserving C_4 rotation symmetry and \bar{M}_x reflection symmetry

$$\mathcal{H}(\mathbf{k}) = \begin{pmatrix} 0 & 1 \\ (h(\mathbf{k}) - m)(h(\mathbf{k}) + m) & 0 \end{pmatrix}, \quad (67)$$

where $h(\mathbf{k}) = \cos k_x - \cos k_y + i \sin k_x \sin k_y$. We can check that the Hamiltonian obeys

$$C_4 \mathcal{H}(k_x, k_y) C_4^{-1} = \mathcal{H}(k_y, -k_x), \quad (68)$$

$$\bar{M}_x \mathcal{H}^*(k_x, k_y) \bar{M}_x^{-1} = \mathcal{H}(-k_x, k_y), \quad (69)$$

where $C_4 = \sigma_0$ and $\bar{M}_x = \sigma_0$. According to Table VI, for WG#11 there are three types of the EP minimal configurations — two EPs at Γ , M with $\nu_{\text{disc}} = \pm 4$, eight EPs at mirror lines with $\nu_{\text{disc}} = \pm 1$, and sixteen EPs at general points with $\nu_{\text{disc}} = \pm 1$.

To study EPs in this model, we use Eq. 62 and then obtain the discriminant $\text{Disc}_E[\mathcal{H}](\mathbf{k}) = 4(h(\mathbf{k}) - m)(h(\mathbf{k}) + m)$. First, starting with $m = 0$, we find two EPs are located at Γ and M . The discriminant near these two points can be written as

$$\text{Disc}_E[\mathcal{H}](\mathbf{k}) = (k_x - ik_y)^4 + O(\mathbf{k}^5) \quad (70)$$

$$= (dk_{x\pi} + idk_{y\pi})^4 + O(d\mathbf{k}_{\pi}^5), \quad (71)$$

where $dk_{x\pi} = k_x - \pi$, $dk_{y\pi} = k_y - \pi$. Therefore, by using the definition (51) of the discriminant number, $\nu_{\text{disc}} = +4$ for the EP at Γ and $\nu_{\text{disc}} = -4$ for the EP at M . This minimal configuration possesses the EPs located at the C_4 rotation centers. The C_4 rotation symmetry (58) forces the discriminant numbers to be a multiple of 4.

When we increase m from 0, the EP at Γ is split into four EPs at $(0, \pm \cos^{-1}(1 - m))$ and $(\pm \cos^{-1}(1 - m), 0)$ in the mirror lines. Since the original EP at Γ possesses $+4$ discriminant number and the four EPs connected by the C_4 rotation symmetry share the same charge, each EP has $+1$ discriminant number. Similarly, the EP at M is split into four EPs at $(\pm \cos^{-1}(-1 + m), 0)$ and each EP possesses -1 discriminant number.

(c) Being a fundamental 2D example with non-trivial band topology, the Chern insulator has been widely studied in Hermitian topological band theory. One of the simplest Hermitian Hamiltonians describing the Chern insulator [133] is given by

$$\begin{aligned} \mathcal{H}_C(\mathbf{k}) &= \sin k_x \sigma_x + \sin k_y \sigma_y \\ &+ (\cos k_x + \cos k_y + M) \sigma_z. \end{aligned} \quad (72)$$

TABLE VI: **The minimal absolute topological number ν_{abs} for non-Hermitian “Exceptional points” and “Fermi Points”.** In the column of rotation centers, \times indicates the absence of the topological points with non-zero charges in the rotation centers, while the labels of the rotation centers with $n\mathbb{Z}$ indicates the topological number must be the multiple of integer n . Label \sim above some absolute numbers ν_{abs} indicates the minimal configuration is unique.

WG	Generators	Rotation centers	ν_{abs}
#1		No centers	2
#2	C_2	$(\Gamma, X, Y, M) : 2\mathbb{Z}$	4
	\bar{C}_2	\times	$\tilde{2}$
#3,4,5	M_x	\times	$\tilde{2}$
	\bar{M}_x	No centers	2 mirror lines (MLs) or 4
#6,7,8,9	C_2 and M_x	\times	$\tilde{4}$
	C_2 and \bar{M}_x	$(\Gamma, X, Y, M) : 2\mathbb{Z}$	4 MLs or 8
	\bar{C}_2 and M_x/\bar{M}_x	\times	$\tilde{2}$ MLs or $\tilde{4}$
#10	C_4	$(\Gamma, X, Y, M) : 4\mathbb{Z}$	8
	\bar{C}_4	\times	$\tilde{4}$
#11,12	C_4 and M_x	\times	$\tilde{8}$
	C_4 and \bar{M}_x	$(\Gamma, X, Y, M) : 4\mathbb{Z}$	8 MLs or 16
	\bar{C}_4 and M_x/\bar{M}_x	\times	$\tilde{4}$ MLs or $\tilde{8}$
#13	C_3	$(\Gamma, K, K') : 3\mathbb{Z}$	$\tilde{6}$
	\bar{C}_3	\times	0
#14	C_3 and M_y	\times	$\tilde{6}$
	C_3 and \bar{M}_y	$(\Gamma, K, K') : 3\mathbb{Z}$	6 MLs or 12
	\bar{C}_3 and M_y/\bar{M}_y	\times	0
#15	C_3 and M_x	\times	$\tilde{6}$
	C_3 and \bar{M}_x	$(\Gamma, K, K') : 3\mathbb{Z}$	6 MLs or 12
	\bar{C}_3 and M_x/\bar{M}_x	\times	0
#16	C_6	$(\Gamma, K, K') : 6\mathbb{Z} \ \& \ (M_{1/2/3}) : 2\mathbb{Z}$	12
	\bar{C}_6	\times	$\tilde{6}$
#17	C_6 and M_x	\times	$\tilde{12}$
	C_6 and \bar{M}_x	$(\Gamma, K, K') : 6\mathbb{Z} \ \& \ (M_{1/2/3}) : 2\mathbb{Z}$	12 MLs or 24
	\bar{C}_6 and M_x/\bar{M}_x	\times	$\tilde{6}$ MLs or $\tilde{12}$

In the region $0 < |M| < 2$, the nonzero Chern number leads to the presence of the chiral edge states and the quantized conductance. Then we add on-site dissipations uniformly to the Chern insulator so that the Hamiltonian becomes non-Hermitian

$$\mathcal{H}_{\text{nC}}(\mathbf{k}) = \mathcal{H}_{\text{C}}(\mathbf{k}) - i\gamma_z \sigma_z - i\gamma_0 \sigma_0, \quad (73)$$

where $\gamma_0 \pm \gamma_z$ are the on-site dissipations for the different orbitals. Due to the dissipative nature, $\gamma_0 \pm \gamma_z$ must be greater than zero, namely $\gamma_0 \pm \gamma_z \geq 0$. The reason is that due to the dissipative energies $-i(\gamma_0 \pm \gamma_z)$, the corresponding time evolution operator on each site exhibits exponential decay trend ($e^{-(\gamma_0 \pm \gamma_z)t}$) as time evolves.

In the presence of the on-site dissipation, this non-Hermitian Chern insulator preserves the following two symmetries $C_4 \mathcal{H}_{\text{nC}}(k_x, k_y) C_4^{-1} = \mathcal{H}_{\text{nC}}(k_y, -k_x)$ and $M_x \mathcal{H}_{\text{nC}}^t(k_x, k_y) M_x^{-1} = \mathcal{H}_{\text{nC}}(-k_x, k_y)$, where $C_4 = e^{i\pi\sigma_z/4}$ and $M_x = \sigma_z$, which belongs to WG#11. That is, the minimal number of EPs with charge ± 1 is given by 8 according to Table VI.

By Eq. 62, the discriminant can be written in the explicit form

$$\text{Disc}_E[\mathcal{H}](\mathbf{k}) = -4[\sin^2 k_x + \sin^2 k_y + (\cos k_x + \cos k_y + M - i\gamma_z)^2]. \quad (74)$$

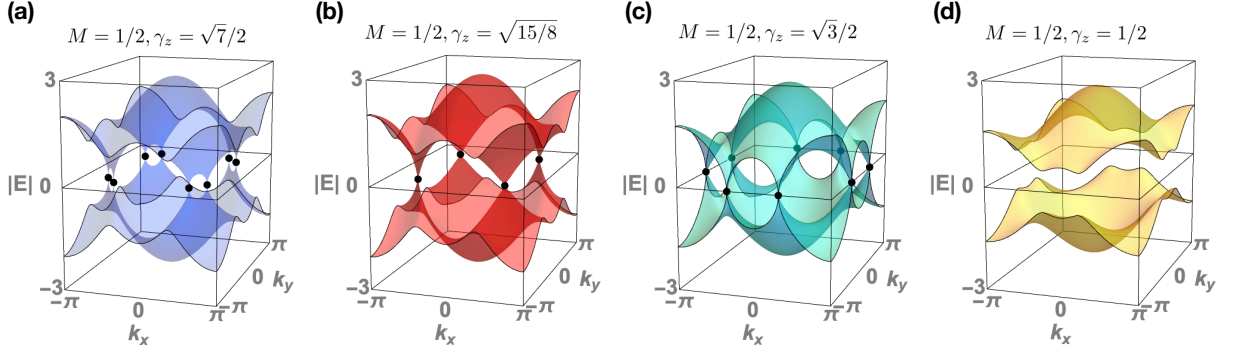


FIG. 15: The spectrum of the dissipative Chern insulator shows the locations of the EPs. (a) Eight EPs with $\nu_{\text{abs}} = \pm 1$ appear as $\sqrt{3}/2 < \gamma_z < \sqrt{15}/8$. (b,c) The eight EPs merge to four EPs with $\nu_{\text{abs}} = 0$ as $\gamma = \sqrt{15}/8$ and $\gamma = \sqrt{3}/2$ respectively. (d) In the region of $|\gamma_z| < \sqrt{3}/2$, the non-Hermitian phase with a line gap is topological.

To demonstrate the evolution of the EPs, we particularly choose $\gamma_0 = 0$ and $M = 1/2$ and start with $\gamma_z = \sqrt{7}/2$. The vanishing discriminant determines eight EPs in the 2D BZ — $(\pm 2\pi/3, \pm\pi/2)$, $(\pm 2\pi/3, \mp\pi/2)$, $(\pm\pi/2, \pm 2\pi/3)$, $(\pm\pi/2, \mp 2\pi/3)$ as shown in Fig. 15(a). Knowing one of the EP discriminant numbers, we can obtain the other discriminant numbers by using C_4 rotation symmetry and M_x transpose reflection symmetry, because the symmetry relations (56) connect the discriminant numbers of the eight EPs. The function of the discriminant is expanded to the linear order near $\mathbf{k}_1 = (2\pi/3, \pi/2)$

$$\text{Disc}_E[\mathcal{H}](\mathbf{k}) = -2\sqrt{3}\left(1 - i\sqrt{7}\right)\left(k_x - \frac{2\pi}{3}\right) + 4i\sqrt{7}\left(k_y - \frac{\pi}{2}\right) + O\left((\mathbf{k} - \mathbf{k}_1)^2\right) \quad (75)$$

Using the definition (51) of the discriminant number, we have $\nu_{\text{disc}}(\mathbf{k}_1) = 1$. In this regard, the C_4 rotation symmetry duplicates the three EPs at $(-2\pi/3, -\pi/2)$, $(\pm\pi/2, \pm 2\pi/3)$ with $\nu_{\text{disc}}(\mathbf{k}_1) = 1$, while M_x transpose reflection symmetry leads to the four remaining EPs with $\nu_{\text{disc}}(\mathbf{k}_1) = -1$. The presence of the eight EPs is the minimal configuration consistent with Table VI.

On the one hand, as we increase γ_z to $\sqrt{15}/8$, the two EPs from $(2\pi/3, \pi/2)$ and $(\pi/2, 2\pi/3)$ are merged into one EP at $(\cos^{-1}(-1/4), \cos^{-1}(-1/4))$ as shown in Fig. 15(b). The charge at the merging point is neutralized. The C_4 rotation symmetry duplicates the merging to the six remaining EPs; there are four EPs with zero discriminant numbers located at $(\pm \cos^{-1}(-1/4), \pm \cos^{-1}(-1/4))$ and $(\pm \cos^{-1}(-1/4), \mp \cos^{-1}(-1/4))$. When $\gamma_z > \sqrt{15}/8$, the four neutralized EPs vanish and the non-Hermitian system has a line gap.

On the other hand, as γ_z is decreased to $\sqrt{3}/2$, the two EPs at $(\pm 2\pi/3, \pi/2)$ merged into one EP at $(\pi, \pi/3)$ and the merge neutralizes the charge. Similarly, by merging the six remaining EP are reduced to three neutralized EPs separately located at $(\pi, -\pi/3)$ and $(\pm\pi/3, \pi)$ as shown in Fig. 15(c). As $\gamma_z < \sqrt{3}/2$, the four EPs vanish and the bulk spectrum has a line gap as shown in panel (d). In the open boundary condition the robust edge states connect the two separate bulk region in

the complex plane; hence, this gapped phase is topologically non-trivial [24].

In short, $|\gamma_z| < \sqrt{3}/2$ is the topological region, while $\gamma_z > \sqrt{15}/8$ is the trivial region. As $\sqrt{3}/2 < \gamma_z < \sqrt{15}/8$, the 8 EPs with $\nu_{\text{disc}} = \pm 1$ represent the topological phase transition region. Therefore, the EP minimal configurations listed in Table VI can indicate the topological phase transition for the non-Hermitian line-gap phases.

B. Non-Hermitian FPs

We briefly introduce the topological protection for FPs in 2D non-Hermitian models, which was recently studied in the literature [9, 25]. Next, we directly extend our new no-go theorem of the 17 WGs to the FPs.

The FPs are the direct generalization of Fermi surface from Hermitian to non-Hermitian systems. We first recall the Fermi surface defined for a Hermitian Hamiltonian $\mathcal{H}_H(\mathbf{k})$. In the 2D BZ the Fermi surface, which is determined by $\det[\mathcal{H}_H(\mathbf{k}) - \mu] = 0$, is 1D closed lines. Given a chemical potential μ and a non-Hermitian Hamiltonian $\mathcal{H}_{\text{NH}}(\mathbf{k})$, the non-Hermitian Fermi surface is located at \mathbf{k} satisfying $E_n(\mathbf{k}) - \mu = 0$. That is, the two constraints of the equation in the real and imaginary parts form two separate closed lines in the BZ and the Fermi surface is the crossing points of the two lines; hence, we call FPs for Fermi surface in 2D non-Hermitian systems. This is different from 1D Fermi lines in 2D Hermitian systems, since there exists a well-defined invariant characterizing any non-Hermitian FP in the BZ. To identify all of the FPs \mathbf{K}_{FP} in the BZ, we use determinant

$$\det[\mathcal{H}_{\text{NH}}(\mathbf{K}_{\text{FP}}) - \mu] = \prod_n (E_n(\mathbf{K}_{\text{FP}}) - \mu) = 0. \quad (76)$$

These FPs \mathbf{K}_{FP} can be characterized by winding number as an invariant

$$\nu_{\text{FP}}(\mathbf{K}_{\text{FP}}) = \frac{i}{2\pi} \oint_{\Gamma(\mathbf{K}_{\text{FP}})} \nabla_{\mathbf{k}} (\ln \det[\mathcal{H}_{\text{NH}}(\mathbf{k}) - \mu]) \cdot d\mathbf{k}, \quad (77)$$

where $\Gamma(\mathbf{K}_{\text{FP}})$ is a loop counterclockwise encircling the FP at \mathbf{K}_{FP} . Since in a proper basis the Hamiltonian $\mathcal{H}_{nH}(\mathbf{k})$ is single-valued in the entire BZ and the integrand is a singularity at the FP, the winding number ν_{FP} of the FP is always quantized as an integer. For any non-zero winding number, the integral loop is not contractable so that the FP \mathbf{K}_{FP} inside the loop is a stable singularity point, which cannot be removed. Furthermore, only FPs with non-zero winding numbers are singularities in the entire BZ.

Here we point out that the (non-Hermitian) FPs and the (Hermitian) Dirac points share the identical mathematical structure. In order to see this, we map the non-Hermitian Hamiltonian $\mathcal{H}_{nH}(\mathbf{k})$ to a Hermitian Hamiltonian with chiral symmetry [134]

$$\mathcal{H}_H(\mathbf{k}) = \begin{pmatrix} 0 & \mathcal{H}_{nH}(\mathbf{k}) - \mu \\ \mathcal{H}_{nH}^\dagger(\mathbf{k}) - \mu^* & 0 \end{pmatrix}. \quad (78)$$

The zero energy nodes of the Hermitian Hamiltonian $\mathcal{H}_H(\mathbf{k})$ appear when the determinant of the off-diagonal matrix vanishes $\det[\mathcal{H}_{nH}(\mathbf{k}) - \mu] = 0$. The equation is exactly identical to Eq. 76 determining the non-Hermitian FPs. Furthermore, the definitions of the topological invariants (13) for the Hermitian nodes and the non-Hermitian FPs are the same. Hence, these non-Hermitian FPs in $\mathcal{H}_{nH}(\mathbf{k})$ are mathematically equivalent to the nodal points in $\mathcal{H}_H(\mathbf{k})$ with the same winding numbers. The no-go theorem for chiral symmetry can be directly extended to the non-Hermitian FP no-go theorem [25] described by

$$\sum_j \nu_{\text{FP}}(\mathbf{K}_{\text{FP}}^j) = 0 \quad (79)$$

This charge neutralization manifests that in the BZ an FP with non-zero winding number must be accompanied by another FP with the opposite winding number.

1. Conditions from crystalline symmetries

To study the relations of FPs connected by symmetries, we consider four types of the combination crystalline symmetries — conventional crystalline, transpose crystalline, complex-conjugation, and conjugate-transpose symmetries. We use g to indicate the generators of the first two symmetries ($U_g, U_g \mathcal{K}^t$), while \bar{g} is used to indicate the generators of the last two symmetries ($U_g^*, U_g \mathcal{K}^\dagger$). Transferring from the EP no-go theorem for the 17 WGs to the FP cases, we simply replace the discriminant in the integrand of the discriminant number (51) by determinant for the FP winding number (77)

$$\text{Disc}_E[\mathcal{H}_{nH}](\mathbf{k}) \rightarrow \det[\mathcal{H}_{nH}(\mathbf{k}) - \mu]. \quad (80)$$

It is straightforward that the FP no-go theorem follows the same rules of the EPs as listed in Table VI and we use the absolute number $\nu_{\text{abs}} = \sum_{\mathbf{k}_{\text{FP}}^i \in \text{BZ}} |\nu_{\text{FP}}(\mathbf{k}_{\text{FP}}^i)|$ to express the FP no-go theorem. The reason of the identical rules is that

the relations between two FPs (\mathbf{K}_{FP} and $g\mathbf{K}_{\text{FP}}$) connected by the symmetries are identical to the EP cases (55,60)

$$\nu_{\text{FP}}(g\mathbf{K}_{\text{FP}}) = \det(g)\nu(\mathbf{K}_{\text{FP}}) \quad (81)$$

$$\nu_{\text{FP}}(\bar{g}\mathbf{K}_{\text{FP}}) = -\det(\bar{g})\nu(\mathbf{K}_{\text{FP}}) \quad (82)$$

and for C_n the charges of the FPs at rotation centers (\mathbf{K}_{FP}^r) are limited by the same constraint (58)

$$\nu_{\text{FP}}(\mathbf{K}_{\text{FP}}^r) = nj. \quad (83)$$

The only difference between the FPs and the EPs is that the chemical potential has to be included in the symmetry equations (52) to build the FP connections. For g ,

$$\begin{aligned} \det[\mathcal{H}_{nH}(g\mathbf{k}) - \mu] &= \det[U_g \mathcal{H}_{nH}^{1/t}(\mathbf{k}) U_g^{-1} - \mu] \\ &= \det[\mathcal{H}_{nH}(\mathbf{k}) - \mu]. \end{aligned} \quad (84)$$

The chemical potential μ can be any complex number, then the FP relation (81) still holds. On the other hand, for \bar{g} , there is an additional complex conjugation so that

$$\begin{aligned} \det[\mathcal{H}_{nH}(\bar{g}\mathbf{k}) - \mu] &= \det[U_{\bar{g}} \mathcal{H}_{nH}^{*/\dagger}(\mathbf{k}) U_{\bar{g}}^{-1} - \mu] \\ &= \det[\mathcal{H}_{nH}(\mathbf{k}) - \mu^*]^*, \end{aligned} \quad (85)$$

To satisfy the FP relation (82), the chemical potential must be real; hence, the Fermi energy of the FP has to be a real number.

2. Examples

We use three examples to demonstrate that our no-go theorem in table VI covers the minimal configurations of the non-Hermitian FPs.

(a) We first consider a one-band model with the Hamiltonian

$$E(\mathbf{k}) - \mu = \cos k_x - \cos k_y - \mu + i \sin k_x \sin k_y, \quad (86)$$

where μ is the chemical potential and imposed to be real to preserve \bar{M} symmetry. By checking the symmetries, the Hamiltonian obeys

$$C_2 E(k_x, k_y) C_2^{-1} = E(-k_x, -k_y), \quad (87)$$

where $C_2 = 1$, and

$$\bar{M}_x E(k_x, k_y) \bar{M}_x^{-1} = E(-k_x, k_y), \quad (88)$$

where $\bar{M}_x = \mathcal{K}^*$. Hence, the system belongs to WG#6 with C_2 and \bar{M}_x . When $\mu = 0$, two FPs are located at $(0, 0)$ and (π, π) separately. By expanding the energy near these points, we have

$$E(\mathbf{k}) = -(k_x - ik_y)^2/2 + O(\mathbf{k}^2) \quad (89)$$

$$= -(dk_{x\pi} + idk_{y\pi})^2/2 + O(dk_{\pi}^2), \quad (90)$$

where $dk_{x\pi} = k_x - \pi$, $dk_{y\pi} = k_y - \pi$. Hence, by using the winding number equation (77) of the FP, the FP at $(0, 0)$ possesses +2 charge, while the one at (π, π) possesses -2 charge.

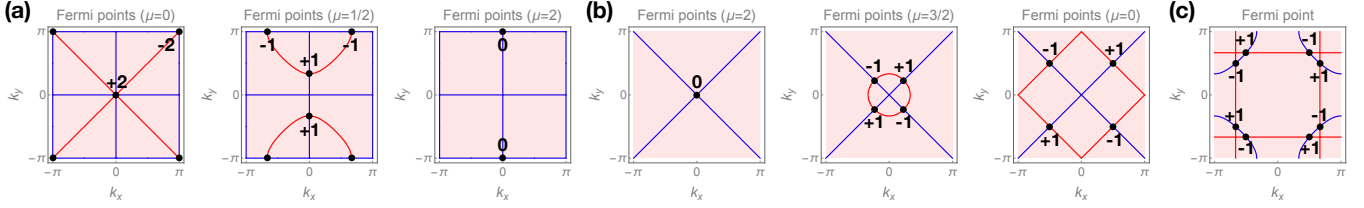


FIG. 16: FPs with non-zero charges (ν_{abs}) are located at the crossings of the red lines ($\text{Re}(\det(H(\mathbf{k}) - \mu)) = 0$) and the blue lines ($\text{Im}(\det(H(\mathbf{k}) - \mu)) = 0$). (a) Two FPs with $\nu_{\text{abs}} = \pm 2$ at the rotation centers are split into four FPs with $\nu_{\text{abs}} = \pm 1$ in the mirror lines. Finally, these FPs merge to one FP with $\nu_{\text{abs}} = 0$. (b) A FP with $\nu_{\text{abs}} = 0$ is split into four FPs with $\nu_{\text{abs}} = \pm 1$ in the mirror lines. (c) Eight FPs $\nu_{\text{abs}} = \pm 1$ are the general points.

The even numbers of the charges at the C_2 rotation centers is consistent with the rotation constraint (83).

Now we adjust the value of the chemical potential to $0 < \mu < 2$. The two FPs at $\mu = 0$ are split into four FPs located at $(0, \pm \cos^{-1}(1 - \mu))$, $(\pm \cos^{-1}(-1 + \mu), \pi)$ as shown in Fig. 16(a). The FPs at $(0, \pm \cos^{-1}(1 - \mu))$, which inherit the charge from the FP at $(0, 0)$, both have $+1$ winding number. Similarly, the FPs at $(\pm \cos^{-1}(-1 + \mu), \pi)$ have -1 winding number. The distribution of the four FPs at the mirror lines is consistent with WG#6 with C_2 and \bar{M}_x in Table VI. Finally, as $\mu = 2$, the four FPs merge at $(0, \pi)$ and the total charge of this single FP is neutralized.

(b) For the second example, we change the one-band model to

$$E(\mathbf{k}) - \mu = \cos k_x + \cos k_y - \mu + i(\cos k_x - \cos k_y) \quad (91)$$

The Hamiltonian obeys

$$\bar{C}_4 E(k_x, k_y) \bar{C}_4^{-1} = E(k_y, -k_x), \quad (92)$$

$$M_x E(k_x, k_y) M_x^{-1} = E(-k_x, k_y), \quad (93)$$

where $C_4^* = \mathcal{K}^*$ and $M_x = 1$. Hence, the system belongs to WG#10 with \bar{C}_4 and M_x .

We start with the chemical potential $\mu = 2$. The FP satisfying $E(\mathbf{K}_{\text{PF}}) = \mu$ is located at $(0, 0)$. Because this is the only FP in the entire system, to preserve the charge neutralization (79) the winding number of this FP must be zero. Then as μ is decreased, the FP at $(0, 0)$ is split into four FPs located at $(\pm \cos^{-1} \frac{\mu}{2}, \pm \cos^{-1} \frac{\mu}{2})$ and $(\pm \cos^{-1} \frac{\mu}{2}, \mp \cos^{-1} \frac{\mu}{2})$ as shown in Fig. 16(b). To identify the charge of the FP, we particularly consider the FP at $(\pi/2, \pi/2)$ for $\mu = 0$. The leading order of the energy with respect to the chemical potential can be written as

$$E(\mathbf{k}) - \mu = -(1 + i)dk_x - (1 - i)dk_y + O(dk^2), \quad (94)$$

where $dk_{x/y} = k_{x/y} - \pi/2$. By using the definition (77) of the winding number, the charge of the FP at $(\pi/2, \pi/2)$ is given by $+1$. The \bar{C}_4 rotation and reflection symmetries extend to this FP to the remaining three with the winding number relation (82). Hence, the FPs at $(\pm \cos^{-1} \frac{\mu}{2}, \pm \cos^{-1} \frac{\mu}{2}) / (\pm \cos^{-1} \frac{\mu}{2}, \mp \cos^{-1} \frac{\mu}{2})$ possess $+1/-1$ charge.

(c) Consider a non-Hermitian Chern insulator and its Hamiltonian $H_C(\mathbf{k})$ is written in Eq. 73. It has been shown

in EP example (c) that the Chern insulator Hamiltonian preserves C_4 rotation symmetry and M_x mirror symmetry with $C_4 = e^{i\pi\sigma_z/4}$ and $M_x = \sigma_z$. Even in the presence of the complex chemical potential, the symmetries are still preserved. According to Table VI, the minimal number of FPs with charge ± 1 is given by 8. To show the distribution of the FPs concretely, consider $\gamma_0 = 0$, $\gamma_z = \sqrt{3}/2$, $M = 1/2$, and $\mu = 1$. Therefore, the Fermi momentum \mathbf{K}_{FP} is determined by $\det(\mathcal{H}_C(\mathbf{K}_{\text{FP}}) - 1) = 0$. One of the FPs is located at $\mathbf{K}_{\text{FP}}^{++} = (\pi/2, 2\pi/3)$. Near this point, we expand the determinant to the leading order

$$\det(\mathcal{H}_C(\mathbf{k}) - \mu) = -i\frac{\sqrt{3}}{2}dk_x + \frac{\sqrt{3}-3i}{2}dk_y + O(dk^2), \quad (95)$$

where $dk_x = k_x - \pi/2$ and $dk_y = k_y - 2\pi/3$. The linear terms determine the winding number $\nu(\mathbf{K}_{\text{FP}}^{++}) = -1$. The C_4 rotation symmetry generates other three FPs with $\nu = -1$ located at $(-\pi/2, -2\pi/3)$, $(\mp 2\pi/3, \pm \pi/2)$. Furthermore, the transverse reflection symmetry extends 4 additional FPs with $\nu = +1$ located at $(\pm \pi/2, \mp 2\pi/3)$ and $(\pm 2\pi/3, \pm \pi/2)$ as shown in Fig. 16(c).

VI. CONCLUSION

The stable topological points in 2D lattices arise in chiral-symmetric, space-time-inversion-symmetric, and non-Hermitian systems. In the presence of crystalline symmetries and time-reversal symmetry, the minimal number of the topological points might be more than two beyond the original no-go theorem (the fermion doubling theorem [25–28]). We exhaustively study the generalized no-go theorem for the three distinct types of lattice systems and list the minimal numbers of the topological points with the configurations for given wallpaper groups. This theorem provides an alternative scheme to classify the nodal topological materials and includes the nodal topological points located at general points in BZ, which might be overlooked in the symmetry indicator schemes [47–51].

This generalized no-go theorem is the fundamental rule for forming Dirac semimetals, nodal time-reversal-symmetric topological superconductors, and non-Hermitian lattices with exceptional points or Fermi points. The examples in the manuscript show that the topological materials in the literature must obey this ground rule, such as graphene and d-wave

superconductors. In addition, the theorem predicts several new Dirac semimetals, such as six Dirac nodes in a hexagonal lattice (36) and a quadratic node with two Dirac nodes (39). Following this guidance, we can reveal and realize new types of novel nodal topological materials with topological nodal points. In particular, these Dirac semimetals in our prediction can be new platforms of twisted bilayers for strong correlations [135] and potentially possess Majorana bound states with superconductivity [136]. On the other hand, the non-Hermitian topology of Fermi points and exceptional points is captured by \mathbb{Z} invariants. Unlike the Hermitian Dirac nodes, the charges of those non-Hermitian topological points at the rotation center, say C_n rotation, must be multiple of n . Although \mathbb{Z} invariants also protect Dirac nodes in chiral-symmetric lattices, the non-Hermitian no-go theorem is distinct from the Hermitian one.

VII. ACKNOWLEDGEMENT

We thank Chen Fang, Akira Furusaki, Guang Bian, and Qiang Zhang for the helpful discussions and comments.

Appendix A: Hamiltonian properties

In certain basis, each entry of the Hamiltonian can be a single-valued function of momentum \mathbf{k} ; this single-valued property is the key to prove the fermion no-go theorem. On the other hand, the symmetry equations for the Hamiltonian through crystalline symmetry play an essential role to determine the minimal number of the topological points in the BZ. To set up these foundations of the generalized no-go theorem, we prove these two features above for 2D lattice systems in this appendix.

We intentionally choose the annihilation operator in the momentum basis in the unit cell convention

$$\phi_{\alpha a}(\mathbf{k}) = \frac{1}{\sqrt{N}} \sum_{\mathbf{R}_n} e^{-i\mathbf{k}\cdot\mathbf{R}_n} \psi_{\alpha}(\mathbf{R}_n + \mathbf{r}_a), \quad (\text{A1})$$

where \mathbf{R}_n is the central position of the n -th unit cell, N is the number of the unit cell. Label a indicates different spatial locations of atoms and \mathbf{r}_a is the location of the atom, whereas label α indicates non-spatial dependent index, such as spin. In this convention, the phase in the Fourier transformation does not have \mathbf{r}_a -dependence and the location-dependence of the annihilation operator $\phi_{\alpha a}$ is absorbed in index a . By the definition, the annihilation operator has periodicity

$$\phi_{\alpha a}(\mathbf{k} + m_1 \mathbf{G}_1 + m_2 \mathbf{G}_2) = \phi_{\alpha a}(\mathbf{k}), \quad (\text{A2})$$

where \mathbf{G}_i is the reciprocal lattice vector and m_i is an integer; therefore, $\phi_{\alpha a}(\mathbf{k})$ is single-valued in the BZ. On the other hand, the Hamiltonian in the form of the second quantization in momentum basis is written as

$$\hat{H} = \sum_{\mathbf{k}} \phi_{\beta b}^{\dagger}(\mathbf{k}) H_{\beta b, \alpha a}(\mathbf{k}) \phi_{\alpha a}(\mathbf{k}). \quad (\text{A3})$$

Thus, each entry $H_{\beta b, \alpha a}(\mathbf{k})$ in the free fermion Hamiltonian is a single-valued function of momentum in the BZ.

Consider crystalline symmetry operator with translation τ acts on the annihilation operator

$$\begin{aligned} g_{\tau} \psi_{\alpha a}(\mathbf{R}_n + \mathbf{r}_a) &= \sum_{\beta} W_{\alpha\beta} \psi_{\beta}(g_{\tau}(\mathbf{R}_n + \mathbf{r}_a)) \\ &= \sum_{\beta} W_{\alpha\beta} \psi_{\beta}(\mathbf{R}'_n{}^{ab} + \sum_b V_{ab} \mathbf{r}_b) \\ &= \sum_{\beta, b} W_{\alpha\beta} V_{ab} \psi_{\beta}(g\mathbf{R}_n + \mathbf{r}_b + n_1^b g\mathbf{a}_1 + n_2^b g\mathbf{a}_2), \end{aligned} \quad (\text{A4})$$

where $W_{\alpha\beta}$ is a constant transformation unitary matrix for crystalline operation, such as spin rotation and the orbital phase changes. We note that the crystalline operator also alters the location of the annihilation operator

$$g_{\tau}(\mathbf{R}_n + \mathbf{r}_a) = \mathbf{R}'_n + \sum_b V_{ab} \mathbf{r}_b, \quad (\text{A5})$$

where \mathbf{R}'_n is the central location of another unit cell. Matrix V_{ab} directly switches the original atom location to another and does not mix other atoms locations. That is, each entry in V_{ab} is either 0 or 1. In this regard, V_{ab} and the summation of b in Eq. A4 can be moved out of the parenthesis. In general, $\mathbf{R}'_n{}^{ab} \neq g\mathbf{R}_n$, where crystalline operator for position vector g acts on \mathbf{R}_n without translation and the invariant point of the operation (rotation center or reflection) is in the original point; hence, we have

$$\mathbf{R}'_n{}^{ab} = g\mathbf{R}_n + n_1^{ab} g\mathbf{a}_1 + n_2^{ab} g\mathbf{a}_2, \quad (\text{A6})$$

where integer n_i^{ab} , which depends on the atom location, indicates the number of the unit cell shift after the crystalline symmetry operation and \mathbf{a}_i is the primitive vector obeying

$$\mathbf{k} \cdot (n_1 \mathbf{a}_1 + n_2 \mathbf{a}_2) = k_1 n_1 + k_2 n_2, \quad (\text{A7})$$

where $\mathbf{k} = (k_1 \mathbf{G}_1 + k_2 \mathbf{G}_2)/2\pi$. Since the crystalline symmetry is preserved, $g\mathbf{a}_i$ is still the primitive vector; the last two terms in the equation above represent the shift of the unit cell.

We can discuss the g acts on the annihilation operator in the momentum space

$$\begin{aligned} g_{\tau} \phi_{\alpha a}(\mathbf{k}) &= \frac{1}{\sqrt{N}} \sum_{\mathbf{R}_n} e^{-i\mathbf{k}\cdot\mathbf{R}_n} g_{\tau} \psi_{\alpha}(\mathbf{R}_n + \mathbf{r}_a) \\ &= \frac{1}{\sqrt{N}} \sum_{\mathbf{R}_n, \beta, b} e^{-i\mathbf{k}\cdot\mathbf{R}_n} W_{\alpha\beta} V_{ab} \psi_{\beta}(\mathbf{R}'_n{}^{ab} + \mathbf{r}_b) \\ &= \frac{1}{\sqrt{N}} \sum_{\mathbf{R}_n, \beta, b} e^{-ig\mathbf{k}\cdot g\mathbf{R}_n} W_{\alpha\beta} V_{ab} \psi_{\beta}(\mathbf{R}'_n{}^{ab} + \mathbf{r}_b) \\ &= \frac{1}{\sqrt{N}} \sum_{\mathbf{R}_n, \beta, b} e^{-ig\mathbf{k}\cdot(\mathbf{R}'_n{}^{ab} - n_1^{ab} g\mathbf{a}_1 - n_2^{ab} g\mathbf{a}_2)} W_{\alpha\beta} V_{ab} \psi_{\beta}(\mathbf{R}'_n{}^{ab} + \mathbf{r}_b) \\ &= \frac{1}{\sqrt{N}} \sum_{\mathbf{R}_n, \beta, b} e^{ig\mathbf{k}\cdot(n_1^{ab} g\mathbf{a}_1 + n_2^{ab} g\mathbf{a}_2)} W_{\alpha\beta} V_{ab} e^{-ig\mathbf{k}\cdot\mathbf{R}'_n{}^{ab}} \psi_{\beta}(\mathbf{R}'_n{}^{ab} + \mathbf{r}_b) \\ &= \frac{1}{\sqrt{N}} \sum_{\beta, b} e^{i(k_1 n_1^{ab} + k_2 n_2^{ab})} W_{\alpha\beta} V_{ab} \phi_{\beta b}(g\mathbf{k}) \end{aligned} \quad (\text{A8})$$

To simplify the expression of the crystalline symmetry operation, we can define the single-valued \mathbf{k} -dependent unitary matrix

$$U_{\alpha\alpha,\beta\beta}^\dagger(\mathbf{k}) = e^{i(k_1 n_1^{ab} + k_2 n_2^{ab})} W_{\alpha\beta} V_{ab}. \quad (\text{A9})$$

The annihilation operator and creation operator can be rewritten in the economic form

$$g_\tau \phi(\mathbf{k}) = U^\dagger(g\mathbf{k})\phi(\mathbf{k}), \quad g_\tau \phi^\dagger(\mathbf{k}) = \phi^\dagger(\mathbf{k})U(g\mathbf{k}) \quad (\text{A10})$$

Due to the symmetry, the second quantization Hamiltonian (A3) is invariant under the crystalline symmetry operation

$$\begin{aligned} \sum_{\mathbf{k}} \phi^\dagger(\mathbf{k})H(\mathbf{k})\phi(\mathbf{k}) &= g_\tau \sum_{\mathbf{k}} \phi^\dagger(\mathbf{k})H(\mathbf{k})\phi(\mathbf{k}) \\ &= \sum_{\mathbf{k}} \phi^\dagger(g\mathbf{k})U(\mathbf{k})H(\mathbf{k})U^\dagger(\mathbf{k})\phi(g\mathbf{k}) \end{aligned} \quad (\text{A11})$$

Hence, the symmetry equation for the free fermion Hamiltonian is given by

$$H(g\mathbf{k}) = U(\mathbf{k})H(\mathbf{k})U^\dagger(\mathbf{k}). \quad (\text{A12})$$

We will frequently use this symmetry equation through the manuscript for the generalized no-go theorem.

Appendix B: The winding number connection between \mathbf{K}_0 and $g\mathbf{K}_0$

We provide the detailed derivations for the relations of the two winding numbers at \mathbf{K}_0 and $g\mathbf{K}_0$. First, let us show that the definition (7) of the winding number is equivalent to the one using the flattened Hamiltonian. The flattened Hamiltonian

$$Q(\mathbf{k}) = \sum_{0 < E_\alpha}^{N_+} |\Psi^\alpha(\mathbf{k})\rangle\langle\Psi^\alpha(\mathbf{k})| - \sum_{0 > E_\beta}^{N_-} |\Psi^\beta(\mathbf{k})\rangle\langle\Psi^\beta(\mathbf{k})| \quad (\text{B1})$$

where $|\Psi^\gamma(\mathbf{k})\rangle$ is the eigenstate of the $\mathcal{H}(\mathbf{k})$ with energy E_γ . Assuming the absence of zero-energy states, chiral symmetry leads to $N_+ = N_-$. Since the flattened Hamiltonian inherits chiral symmetry (3) from the original Hamiltonian by choosing a proper basis, chiral symmetry operator can be written as $S = \tau_z \otimes \mathbb{I}_{n \times n}$ and the flattened Hamiltonian has this off-diagonal form

$$Q(\mathbf{k}) = \begin{pmatrix} 0 & q(\mathbf{k}) \\ q^\dagger(\mathbf{k}) & 0 \end{pmatrix}. \quad (\text{B2})$$

Due to $Q^2 = \mathbb{I}_{2n \times 2n}$, $q(\mathbf{k})$ is a unitary matrix and invertible due to the absence of the zero-energy state. Using $q(\mathbf{k})$, the winding number is defined in a closed loop integral path in the BZ

$$\begin{aligned} \nu &= \frac{i}{2\pi} \oint d\mathbf{k} \cdot \text{Tr}[q^{-1}(\mathbf{k})\partial_{\mathbf{k}}q(\mathbf{k})] \\ &= \frac{i}{2\pi} \oint d\mathbf{k} \cdot \partial_{\mathbf{k}} \text{Tr}[\ln q(\mathbf{k})] \\ &= \frac{i}{2\pi} \oint d(\ln \det[q(\mathbf{k})]) \end{aligned} \quad (\text{B3})$$

This definition of the winding number is regularly used in the literature [5, 42].

To show that $h(\mathbf{k})$ and $q(\mathbf{k})$ lead to the same winding number, we choose the eigenstates as the basis and then prove that $\mathcal{H}(\mathbf{k})$ commutes with $Q(\mathbf{k})$ since

$$\begin{aligned} \mathcal{H}(\mathbf{k})Q(\mathbf{k}) &= \sum_{0 < E_\alpha}^{N_+} E_\alpha(\mathbf{k})|\Psi^\alpha(\mathbf{k})\rangle\langle\Psi^\alpha(\mathbf{k})| - \sum_{0 > E_\beta}^{N_-} E_\beta(\mathbf{k})|\Psi^\beta(\mathbf{k})\rangle\langle\Psi^\beta(\mathbf{k})| \\ &= Q(\mathbf{k})\mathcal{H}(\mathbf{k}) \end{aligned} \quad (\text{B4})$$

The commutation relation can be rewritten in the proper basis

$$\begin{aligned} 0 &= [\mathcal{H}(\mathbf{k}), Q(\mathbf{k})] \\ &= \begin{pmatrix} h(\mathbf{k})q^\dagger(\mathbf{k}) - q(\mathbf{k})h^\dagger(\mathbf{k}) & 0 \\ 0 & h^\dagger(\mathbf{k})q(\mathbf{k}) - q^\dagger(\mathbf{k})h(\mathbf{k}) \end{pmatrix}. \end{aligned} \quad (\text{B6})$$

One can obtain

$$\begin{aligned} \det[h(\mathbf{k})q^\dagger(\mathbf{k})] &= \det[q(\mathbf{k})h^\dagger(\mathbf{k})] \\ &= \det[(h(\mathbf{k})q^\dagger(\mathbf{k}))^\dagger] = \det[h(\mathbf{k})q^\dagger(\mathbf{k})]^*. \end{aligned} \quad (\text{B7})$$

The above equation implies that $\det[h(\mathbf{k})q^\dagger(\mathbf{k})]$ is a real number so that $\ln \det(h(\mathbf{k})) + \ln \det(q^*(\mathbf{k})) = \gamma(\mathbf{k})$ is a single-valued function, which leads to $\oint d\gamma(\mathbf{k}) = 0$. Using the property of the unitary matrix $q(\mathbf{k})$, we have $\ln \det(q^*) + \ln \det(q) = 0$. Hence, the winding number with the closed integral path $\Gamma(\mathbf{K}_0)$ can be directly written in form of $h(\mathbf{k})$

$$\begin{aligned} \nu(\mathbf{K}_0) &= \frac{i}{2\pi} \oint_{\Gamma(\mathbf{K}_0)} d(\ln \det[q(\mathbf{k})]) \\ &= \frac{i}{2\pi} \oint_{\Gamma(\mathbf{K}_0)} d(\ln \det[h(\mathbf{k})]) \end{aligned} \quad (\text{B8})$$

To connect the relation between $\nu(\mathbf{K}_0)$ and $\nu(\Gamma\mathbf{K}_0)$, we first consider $g_\tau = \{g|\tau\}$ with spatial translation τ as a 2D crystalline symmetry operator.

Since the matrix form of the symmetry operator commutes with chiral symmetry operator $S = \tau_z \otimes \mathbb{I}$, the unitary symmetry operator in the single-particle basis (or particle-hole basis for superconductors) is written in a generic form of

$$U_g^+(\mathbf{k}) = \begin{pmatrix} U_{g1}(\mathbf{k}) & 0 \\ 0 & U_{g2}(\mathbf{k}) \end{pmatrix}, \quad (\text{B9})$$

where $U_{gi}(\mathbf{k})$ is a momentum-dependent unitary matrix, which can describe a nonsymmorphic symmetry operation. The crystalline symmetry equation (14) connects the Hamiltonian at \mathbf{K}_0 and $g\mathbf{K}_0$

$$\begin{aligned} \mathcal{H}(g\mathbf{k}) &= U_g^+(\mathbf{k})\mathcal{H}(\mathbf{k})U_g^{+\dagger}(\mathbf{k}) \\ &= \begin{pmatrix} 0 & U_{g1}(\mathbf{k})h(\mathbf{k})U_{g2}^\dagger(\mathbf{k}) \\ U_{g2}(\mathbf{k})h^\dagger(\mathbf{k})U_{g1}^\dagger(\mathbf{k}) & 0 \end{pmatrix}. \end{aligned} \quad (\text{B10})$$

We have $h(g\mathbf{k}) = U_{g1}(\mathbf{k})h(\mathbf{k})U_{g2}^\dagger(\mathbf{k})$. The integral path $\Gamma(g\mathbf{K}_0)$ is an infinitesimal close loop encircling nodal point

$g\mathbf{K}_0$ and then the winding number at $\Gamma(g\mathbf{K}_0)$ is given by

$$\begin{aligned}\nu(g\mathbf{K}_0) &= \frac{i}{2\pi} \oint_{\Gamma(g\mathbf{K}_0)} d(\ln \det[h(\mathbf{k})]) \\ &= \frac{i}{2\pi} \oint_{\Gamma(\mathbf{K}_0)} \det(g) d(\ln \det[h(g\mathbf{k})]) \\ &= \frac{i}{2\pi} \oint_{\Gamma(\mathbf{K}_0)} \det(g) d(\ln \det[h(\mathbf{k})]) \\ &= \det(g)\nu(\mathbf{K}_0)\end{aligned}\quad (\text{B11})$$

We use the integral $\oint_{\Gamma(\mathbf{K}_0)} d(\ln \det U_{gi}(\mathbf{k})) = 0$ since $U_{gi}(\mathbf{k})$ does not collect additional $U(1)$ winding phase in the infinitesimal integral loop. The reason is that $\det(U_{g\pm}(\mathbf{k}))$ does not vanish to create a nodal point due to the nature of unitary matrix.

Secondly, consider time reversal symmetry operator T^+ commutes with chiral symmetry operator S

$$\mathcal{H}(-\mathbf{k}) = T\mathcal{H}(\mathbf{k})T^{-1} = U_T\mathcal{H}^*(\mathbf{k})U_T^\dagger, \quad (\text{B12})$$

where $T^+ = U_T\mathcal{K}$ and \mathcal{K} is the complex conjugate operator. The commutation relation between T^+ and S gives the form of

$$T^+ = \begin{pmatrix} U_{T1} & 0 \\ 0 & U_{T2} \end{pmatrix} \mathcal{K}, \quad (\text{B13})$$

where U_{Ti} is momentum-independent since time reversal symmetry operator is non-spatial. In 2D momentum space, time reversal operation is equivalent to the combination of C_2 rotation and complex conjugation. Therefore,

$$\begin{aligned}\nu(-\mathbf{K}_0) &= \frac{i}{2\pi} \oint_{\Gamma(-\mathbf{K}_0)} d(\ln \det[h(\mathbf{k})]) \\ &= \frac{i}{2\pi} \oint_{\Gamma(\mathbf{K}_0)} d(\ln \det[h^*(\mathbf{k})]) \\ &= \frac{-i}{2\pi} \oint_{\Gamma(\mathbf{K}_0)} d(\ln \det[h(\mathbf{k})]) \\ &= -\nu(\mathbf{K}_0)\end{aligned}\quad (\text{B14})$$

Hence, with the commutation relation between T^+ and S , time reversal operation flips the sign of the winding number for the nodal point at $-\mathbf{K}_0$.

On the other hand, when symmetry operator anticommutes with S , the relation of the winding numbers between \mathbf{K}_0 and $g\mathbf{K}_0$ flips the sign. Following the similar derivation, we have crystalline symmetry operator $U_g^-(\mathbf{k})$, which anticommutes with S , in the form of

$$U_g^-(\mathbf{k}) = \begin{pmatrix} 0 & V_{g1}(\mathbf{k}) \\ V_{g2}(\mathbf{k}) & 0 \end{pmatrix}, \quad (\text{B15})$$

where V_{gi} is a unitary matrix. This symmetry operator links the Hamiltonian at \mathbf{K}_0 and $g\mathbf{K}_0$

$$\begin{aligned}\mathcal{H}(g\mathbf{k}) &= U_g^-(\mathbf{k})\mathcal{H}(\mathbf{k})U_g^{+\dagger}(\mathbf{k}) \\ &= \begin{pmatrix} 0 & V_{g1}(\mathbf{k})h^\dagger(\mathbf{k})V_{g2}^\dagger(\mathbf{k}) \\ V_{g2}(\mathbf{k})h(\mathbf{k})V_{g1}^\dagger(\mathbf{k}) & 0 \end{pmatrix}.\end{aligned}\quad (\text{B16})$$

Using $h(g\mathbf{k}) = V_{g1}(\mathbf{k})h^\dagger(\mathbf{k})V_{g2}^\dagger(\mathbf{k})$ and following the similar derivation with $U_g^+(\mathbf{k})$, we have this relation of the winding numbers at the two nodal points

$$\begin{aligned}\nu(g\mathbf{K}_0) &= \frac{i}{2\pi} \oint_{\Gamma(\mathbf{K}_0)} \det(g) d(\ln \det[h(g\mathbf{k})]) \\ &= \frac{i}{2\pi} \oint_{\Gamma(\mathbf{K}_0)} \det(g) d(\ln \det[h^\dagger(\mathbf{k})]) \\ &= \frac{-i}{2\pi} \oint_{\Gamma(\mathbf{K}_0)} \det(g) d(\ln \det[h(\mathbf{k})]) \\ &= -\det(g)\nu(\mathbf{K}_0)\end{aligned}\quad (\text{B17})$$

For time-reversal symmetry operator T^- anticommutes with S , since the complex conjugate operator in T^- flips the sign of the winding number, the relation between \mathbf{K}_0 and $-\mathbf{K}_0$ with time-reversal symmetry is given by

$$\nu(-\mathbf{K}_0) = \nu(\mathbf{K}_0) \quad (\text{B18})$$

The results of the winding number relations are summarized in Eqs. 16, 17 and Table. II.

Appendix C: The algebra between chiral operator and time-reversal operator

We know that $T^2 = C^2 = \pm 1$ in class BDI, CII and $T^2 = -C^2 = \pm 1$ in class CI, DIII. Let us consider $T^2 = C^2 = \pm 1$. We can choose a proper basis and phase so that chiral operator S is hermitian and $S^2 = 1$. By sandwiching S^2 with T and C , we have

$$TC = TS^2C = T^2CTC^2 = CT. \quad (\text{C1})$$

This commutation relation leads to $0 = T[T, C] = [T, TC] = [T, S]$. That is, class BDI, CII preserve T^+ time-reversal symmetry. Following the similar derivation, we have T^- time-reversal symmetry for class CI, DIII.

Appendix D: Neutralized winding number summation

Each nodal point in the BZ is characterized by winding number. The essence of the no-go theorem is that the summation over winding numbers for all the nodal points must vanish. To prove the neutralization we simply write the definition of the winding number summation

$$\begin{aligned}\sum_i \nu(\mathbf{K}_0^i) &= \sum_i \frac{i}{2\pi} \oint_{\Gamma(\mathbf{K}_0^i)} d(\ln \det[q(\mathbf{k})]) \\ &= \frac{i}{2\pi} \oint_{\partial\text{BZ}} d(\ln \det[h(\mathbf{k})]) \\ &= 0,\end{aligned}\quad (\text{D1})$$

where \mathbf{K}_0^i represent all of the nodal points ($E = 0$) in the BZ. The integral path of the winding number for any nodal point is an infinitesimal loop counterclockwise encircling that nodal point. The integral path for all the nodal points can continuously deform to the boundary of the BZ (∂BZ) as illustrated in

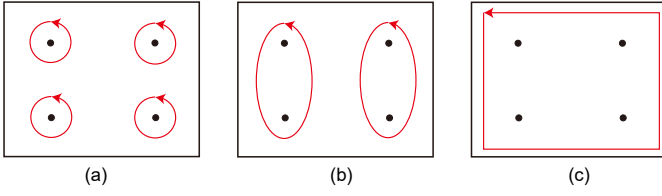


FIG. 17: (color online) The integral paths (red line) of the winding numbers for the nodal points (black dots) evolve in the BZ. The black box represents the entire boundary of the BZ. (a) The integral path of the winding number is an infinitesimal loop encircling a nodal point. (b) The integral path of the multiple loops grows without passing through any nodal point and through the deformation two loops form one big loop. (c) The integral path for all the nodal nodal is equivalent to the integral path along the boundary of the BZ, since through the deformation the path does not pass any nodal points. By using the periodic boundary condition of the BZ, this integral path vanishes.

Fig. 17. Importantly, the integral path never passes any nodal points during the deformation so that the total winding number is unchanged after the deformation; hence, the second line with ∂BZ in the equation holds. Since $h(\mathbf{k})$ can be a single-valued in the entire BZ, by using the periodic boundary, ∂BZ vanishes so that the summation must be zero.

Appendix E: Four Dirac nodes: WG#17 in class DIII

In all the WG symmetry classes, it is the most difficult task to find a tight-binding model for the minimal configuration of a nodal point with $\nu = 2$ located at Γ and two nodal points with $\nu = -1$ at K, K' in class DIII. In a 2-band model, time reversal symmetry ($T^2 = -1$) limits the winding number of the nodal point at Γ to an odd number. Hence, the 2-band model cannot host a nodal point at Γ carrying an even winding number. To find the minimal tight-binding model hosting this high-ordered nodal point, we start with a 4-band model consisting of two 6-Dirac-point Hamiltonians $H_6(\mathbf{k})$ (36) in class DIII. Since $H_6(\mathbf{k})$ possesses 6 Dirac nodes separately located at $\Gamma, M_{1,2,3}, K', K$, two of the twelve Dirac nodes at Γ carry $\nu = 2$ winding number together, two nodes at $M_{1,2,3}$ carry $\nu = -2$, and two nodes at K, K' carry $\nu = 2$. However, the nodal points at $M_{1,2,3}$ should be removed and the signs of the winding numbers at K, K' should be switched. To achieve this, we intentionally add $H_4(\mathbf{k})$ (39) from class CI with real coefficient α as a coupling between two $H_6(\mathbf{k})$'s. The 4×4 Hamiltonian is written in the form of

$$H_{4 \times 4}(\mathbf{k}) = \begin{pmatrix} 0 & h_6(\mathbf{k}) & 0 & \alpha h_4(\mathbf{k}) \\ h_6^*(\mathbf{k}) & 0 & -\alpha h_4^*(\mathbf{k}) & 0 \\ 0 & -\alpha h_4(\mathbf{k}) & 0 & -h_6(\mathbf{k}) \\ \alpha h_4^*(\mathbf{k}) & 0 & -h_6^*(\mathbf{k}) & 0 \end{pmatrix}. \quad (\text{E1})$$

Since time reversal symmetry with $T = i\tau_0\sigma_y\mathcal{K}$ and particle-hole symmetry $C = \tau_0\sigma_x\mathcal{K}$ are preserved, the system belongs to class DIII. Hence, chiral symmetry operator is

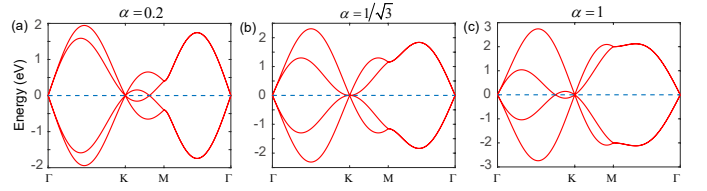


FIG. 18: The Dirac points move from $M_{1,2,3}$ as α varies from 0. (a) The Dirac node moves along \overline{MK} as $0 < \alpha < 1/\sqrt{3}$. (b) As $\alpha = 1/\sqrt{3}$, the moving Dirac node is located at K . The total winding number of the 4-fold degenerate nodal point becomes -1. (c) The Dirac point moves away from K toward Γ .

given by $S = \tau_0\sigma_z$. Furthermore, this is WG#17 with C_6 rotation and M_x generators since the Hamiltonian obeys $M_x H_{4 \times 4}(-k_x, k_y) M_x^{-1} = H_{4 \times 4}(k_x, k_y)$ with $M_x = \tau_z\sigma_y$ and $C_6 H_{4 \times 4}(\frac{k_x + \sqrt{3}k_y}{2}, \frac{k_y - \sqrt{3}k_x}{2}) C_6^{-1} = H_{4 \times 4}(k_x, k_y)$ with $C_6 = \cos \pi/6 \tau_z \sigma_0 - i \sin \pi/6 \tau_z \sigma_z$. The algebra between the generators and the chiral symmetry operator is given by M_x^- and C_6^+ . According to Table IV, this WG symmetry class can host a nodal point at Γ with $\nu = 2$, two nodal points with $\nu = -1$ at K, K' separately as the minimal configuration.

To realize the minimal configuration, we begin to increase α from 0, two Dirac points at each of $M_{1,2,3}$ points move toward K, K' along $\overline{MK}, \overline{MK}'$ separately as shown in Fig. 18(a). Since $h_4(0)$ vanishes, the node carrying $\nu = 2$ at Γ is intact. As $\alpha = 1/\sqrt{3}$, the moving Dirac points carrying $\nu = -1$ are exactly located at K, K' ; Fig. 18(b) shows the 4-fold degenerate point is located in K . Since originally each of K', K has +2 winding number and each of the Dirac nodes from $M_{1,2,3}$ carries $\nu = -1$, after merging with the three Dirac points from $M_{1,2,3}$, the 4-fold degenerate nodal point at K or K' carries $\nu = -1$ winding number in total. Thus, the Hamiltonian (E1) with $\alpha = 1/\sqrt{3}$ is the tight-binding model hosting the 4-fold degenerate node at Γ with $\nu = 2$ and the nodes at K, K' with $\nu = -1$. We note this is the minimal configuration is unstable. That is, as $\alpha > 1/\sqrt{3}$, from K or K' Dirac nodes separately move along $\overline{\Gamma K}$ or $\overline{\Gamma K}'$ toward Γ as shown in Fig. 18(c).

Appendix F: C_2T symmetry

Space-time inversion symmetry (C_2T) can protect 2D Dirac cones in the presence of disorders, and quantizes the \mathbb{Z}_2 Berry phase in the 1D integral path. Here, we provide the detailed deviations; the Berry phase with the closed integral path $\Gamma(\mathbf{K}_0)$ at the nodal point \mathbf{K}_0 can be written in Eq. 42.

Space-time inversion operator C_2T is the combination of a unitary matrix and complex conjugation $C_2T = V_{\mathbf{k}}\mathcal{K}$; the unitary matrix $V_{\mathbf{k}}$ might be \mathbf{k} -dependent and does not have any singularity point in the BZ. By assuming the absence of degenerate states, the relation of wavefunctions under C_2T symmetry is given by

$$|u_n(\mathbf{k})\rangle = e^{i\beta_{\mathbf{k}}^j} C_2T |u_n(\mathbf{k})\rangle = e^{i\beta_{\mathbf{k}}^j} V_{\mathbf{k}} |u_n^*(\mathbf{k})\rangle. \quad (\text{F1})$$

The Berry phase with a non-contractible integral path can be written as

$$\begin{aligned}
\gamma(\mathbf{K}_0) &= i \sum_{n \in \text{occ}} \oint \langle u_n(\mathbf{k}) | \partial_{\mathbf{k}} | u_n(\mathbf{k}) \rangle d\mathbf{k} \\
&= i \sum_{n \in \text{occ}} \oint \langle u_n^*(\mathbf{k}) | V_{\mathbf{k}}^\dagger e^{-i\beta_{\mathbf{k}}^j} \partial_{\mathbf{k}} e^{i\beta_{\mathbf{k}}^j} V_{\mathbf{k}} | u_n^*(\mathbf{k}) \rangle d\mathbf{k} \\
&= - \sum_{n \in \text{occ}} (\beta_+^j - \beta_-^j) + i \sum_{n \in \text{occ}} \oint \langle u_n^*(\mathbf{k}) | \partial_{\mathbf{k}} | u_n^*(\mathbf{k}) \rangle d\mathbf{k} \\
&\quad + i \sum_{n \in \text{occ}} \oint \langle u_n(\mathbf{k}) | V_{\mathbf{k}}^\dagger (\partial_{\mathbf{k}} V_{\mathbf{k}}) | u_n^*(\mathbf{k}) \rangle d\mathbf{k}, \quad (\text{F2})
\end{aligned}$$

where β_{\mp}^j represent the phases at the beginning and the end of the integration path respectively; since the integration path is a closed loop, the start point and the end point are identical. Hence, the first summation is $2m\pi$, where m is an integer. Furthermore, due to the absence of any singularity in $V_{\mathbf{k}}$, the third term vanishes. After using the identity

$$\langle \phi_{\mathbf{k},j}^* | \partial_{\mathbf{k}} | \phi_{\mathbf{k},j}^* \rangle = \langle \partial_{\mathbf{k}} \phi_{\mathbf{k},j} | \phi_{\mathbf{k},j} \rangle = - \langle \phi_{\mathbf{k},j} | \partial_{\mathbf{k}} | \phi_{\mathbf{k},j} \rangle, \quad (\text{F3})$$

we have the quantized Berry phase

$$\gamma(\mathbf{K}_0) = \sum_{n \in \text{occ}} (\beta_+^j - \beta_-^j) / 2 = 0, \pi \pmod{2\pi} \quad (\text{F4})$$

The modulo operation of 2π stems from gauge transform $|u_n^*(\mathbf{k})\rangle \rightarrow e^{i\theta} |u_n^*(\mathbf{k})\rangle$ by using \mathbf{K}_0 as the singularity point for the transformation; Hence, the two Berry phases differed by $2\pi l$ are equivalent.

The crystalline symmetry $\{g|\tau\}$ connects two nodal points \mathbf{K}_0 and $g\mathbf{K}_0$ so that the Hamiltonians at the two points obeys

$$\mathcal{H}(g\mathbf{k}) = U_g(\mathbf{k}) \mathcal{H}(\mathbf{k}) U_g^\dagger(\mathbf{k}), \quad (\text{F5})$$

where the crystalline symmetry operator $U_g(\mathbf{k})$ is a momentum-dependent unitary matrix. Therefore, the wavefunctions at the two points are connected by

$$|u_n(g\mathbf{k})\rangle = U_g(\mathbf{k}) |u_n(\mathbf{k})\rangle. \quad (\text{F6})$$

With this relation the Berry phases at $g\mathbf{K}_0$ point is written in the form of the Berry phase at \mathbf{K}_0

$$\begin{aligned}
&\gamma(g\mathbf{K}_0) \\
&= i \sum_{n \in \text{occ}} \oint_{\Gamma(g\mathbf{K}_0)} \langle u_n(\mathbf{k}) | \partial_{\mathbf{k}} | u_n(\mathbf{k}) \rangle \cdot d\mathbf{k} \\
&= i \det(g) \sum_{n \in \text{occ}} \oint_{\Gamma(\mathbf{K}_0)} \langle u_n(g\mathbf{k}) | \partial_{g\mathbf{k}} | u_n(g\mathbf{k}) \rangle \cdot dg\mathbf{k} \\
&= i \det(g) \sum_{n \in \text{occ}} \oint_{\Gamma(\mathbf{K}_0)} \langle U_g(\mathbf{k}) u_n(\mathbf{k}) | \partial_{\mathbf{k}} | U_g(\mathbf{k}) u_n(\mathbf{k}) \rangle \cdot d\mathbf{k} \\
&= i \det(g) \sum_{n \in \text{occ}} \oint_{\Gamma(\mathbf{K}_0)} \langle u_n(\mathbf{k}) | \partial_{\mathbf{k}} | u_n(\mathbf{k}) \rangle \cdot d\mathbf{k} \\
&= \det(g) \gamma(\mathbf{K}_0) \quad (\text{F7})
\end{aligned}$$

Here we use that $U_g(\mathbf{k})$ does not have any singularity in the BZ. Since the Berry phase is either 0 or π , the relation between \mathbf{K}_0 and $g\mathbf{K}_0$ can be simplified to

$$\gamma(g\mathbf{K}_0) = \gamma(\mathbf{K}_0). \quad (\text{F8})$$

Similarly, for time-reversal symmetry, the Berry phases at \mathbf{K}_0 and $-\mathbf{K}_0$ are related by

$$\gamma(\mathbf{K}_0) = \gamma(-\mathbf{K}_0) \quad (\text{F9})$$

-
- [1] N. P. Armitage, E. J. Mele, and A. Vishwanath, *Rev. Mod. Phys.* **90**, 015001 (2018).
- [2] Z. K. Liu, B. Zhou, Y. Zhang, Z. J. Wang, H. M. Weng, D. Prabhakaran, S.-K. Mo, Z. X. Shen, Z. Fang, X. Dai, Z. Hussain, and Y. L. Chen, *Science* **343**, 864 (2014).
- [3] S.-Y. Xu, I. Belopolski, N. Alidoust, M. Neupane, G. Bian, C. Zhang, R. Sankar, G. Chang, Z. Yuan, C.-C. Lee, S.-M. Huang, H. Zheng, J. Ma, D. S. Sanchez, B. Wang, A. Bansil, F. Chou, P. P. Shibayev, H. Lin, S. Jia, and M. Z. Hasan, *Science* **349**, 613 (2015).
- [4] B. Q. Lv, H. M. Weng, B. B. Fu, X. P. Wang, H. Miao, J. Ma, P. Richard, X. C. Huang, L. X. Zhao, G. F. Chen, Z. Fang, X. Dai, T. Qian, and H. Ding, *Phys. Rev. X* **5**, 031013 (2015).
- [5] C.-K. Chiu, J. C. Y. Teo, A. P. Schnyder, and S. Ryu, *Rev. Mod. Phys.* **88**, 035005 (2016).
- [6] M.-A. Miri and A. Alù, *Science* **363**, eaar7709 (2019).
- [7] L. Lu, Z. Wang, D. Ye, L. Ran, L. Fu, J. D. Joannopoulos, and M. Soljačić, *Science* **349**, 622 (2015).
- [8] S. Murakami, *New J. Phys.* **9**, 356 (2007).
- [9] K. Kawabata, T. Bessho, and M. Sato, *Phys. Rev. Lett.* **123**, 066405 (2019).
- [10] B. J. Wieder, B. Bradlyn, Z. Wang, J. Cano, Y. Kim, H.-S. D. Kim, A. M. Rappe, C. L. Kane, and B. A. Bernevig, *Science* **361**, 246 (2018).
- [11] C.-K. Chiu and A. P. Schnyder, *Phys. Rev. B* **90**, 205136 (2014).
- [12] Y. X. Zhao and Z. D. Wang, *Phys. Rev. Lett.* **116**, 016401 (2016).
- [13] Y. Cao, V. Fatemi, S. Fang, K. Watanabe, T. Taniguchi, E. Kaxiras, and P. Jarillo-Herrero, *Nature* **556**, 43 (2018).
- [14] P. Stepanov, I. Das, X. Lu, A. Fahimniya, K. Watanabe, T. Taniguchi, F. H. L. Koppens, J. Lischner, L. Levitov, and D. K. Efetov, *Nature* **583**, 375 (2020).
- [15] H. S. Arora, R. Polski, Y. Zhang, A. Thomson, Y. Choi, H. Kim, Z. Lin, I. Z. Wilson, X. Xu, J.-H. Chu, K. Watanabe, T. Taniguchi, J. Alicea, and S. Nadj-Perge, *Nature* **583**, 379 (2020).
- [16] U. Zondiner, A. Rozen, D. Rodan-Legrain, Y. Cao, R. Queiroz, T. Taniguchi, K. Watanabe, Y. Oreg, F. von Oppen, A. Stern, E. Berg, P. Jarillo-Herrero, and S. Ilani, *Nature* **582**, 203 (2020).
- [17] A. H. Castro Neto, F. Guinea, N. M. R. Peres, K. S. Novoselov, and A. K. Geim, *Rev. Mod. Phys.* **81**, 109 (2009).
- [18] C. L. Kane and E. J. Mele, *Phys. Rev. Lett.* **95**, 146802 (2005).
- [19] C. L. Kane and E. J. Mele, *Phys. Rev. Lett.* **95**, 226801 (2005).
- [20] C. Weeks, J. Hu, J. Alicea, M. Franz, and R. Wu, *Phys. Rev.*

- [X 1, 021001 \(2011\)](#).
- [21] S. Ryu and Y. Hatsugai, *Phys. Rev. Lett.* **89**, 077002 (2002).
- [22] S. Matsuura, P.-Y. Chang, A. P. Schnyder, and S. Ryu, *New J. Phys.* **15**, 065001 (2013).
- [23] M.-A. Miri and A. Alù, *Science* **363**, eaar7709 (2019).
- [24] H. Shen, B. Zhen, and L. Fu, *Phys. Rev. Lett.* **120**, 146402 (2018).
- [25] Z. Yang, A. P. Schnyder, J. Hu, and C.-K. Chiu, *Phys. Rev. Lett.* **126**, 086401 (2021).
- [26] H. Nielsen and M. Ninomiya, *Nuclear Physics B* **193**, 173 (1981).
- [27] H. Nielsen and M. Ninomiya, *Nuclear Physics B* **185**, 20 (1981).
- [28] H. Nielsen and M. Ninomiya, *Physics Letters B* **105**, 219 (1981).
- [29] Y.-H. Chan, C.-K. Chiu, M. Y. Chou, and A. P. Schnyder, *Phys. Rev. B* **93**, 205132 (2016).
- [30] K. S. Novoselov, A. K. Geim, S. V. Morozov, D. Jiang, M. I. Katsnelson, I. V. Grigorieva, S. V. Dubonos, and A. A. Firsov, *Nature* **438**, 197 (2005).
- [31] E. A. H. S. S. Cahangirov, M. Topsakal and S. Ciraci, *Phys. Rev. Lett.* **102**, 236804 (2009).
- [32] D. Malko, C. Neiss, F. Vines, and A. Gorling, *Phys. Rev. Lett.* **108**, 086804 (2012).
- [33] J. Kim, S. S. Baik, S. W. Jung, Y. Sohn, S. H. Ryu, H. J. Choi, B.-J. Yang, and K. S. Kim, *Phys. Rev. Lett.* **119**, 226801 (2017).
- [34] N. Okuma, K. Kawabata, K. Shiozaki, and M. Sato, *Phys. Rev. Lett.* **124**, 086801 (2020).
- [35] H. C. Po, H. Watanabe, and A. Vishwanath, *Phys. Rev. Lett.* **121**, 126402 (2018).
- [36] Y. Hwang, J. Ahn, and B.-J. Yang, *Phys. Rev. B* **100**, 205126 (2019).
- [37] Z. Song, L. Elcoro, N. Regnault, and B. A. Bernevig, arXiv e-prints, arXiv:1905.03262 (2019).
- [38] S. M. Young and C. L. Kane, *Phys. Rev. Lett.* **115**, 126803 (2015).
- [39] Y. J. Jin, B. B. Zheng, X. L. Xiao, Z. J. Chen, Y. Xu, and H. Xu, arXiv e-prints, arXiv:2008.10175 (2020), arXiv:2008.10175.
- [40] A. Kitaev, *AIP Conf. Proc.* **1134**, 22 (2009).
- [41] A. Altland and M. R. Zirnbauer, *Phys. Rev. B* **55**, 1142 (1997).
- [42] A. P. Schnyder, S. Ryu, A. Furusaki, and A. W. W. Ludwig, *Phys. Rev. B* **78**, 195125 (2008).
- [43] J. Ahn, S. Park, and B.-J. Yang, *Phys. Rev. X* **9**, 021013 (2019).
- [44] N. Okuma, K. Kawabata, K. Shiozaki, and M. Sato, arXiv:1910.02878.
- [45] H. Shen, B. Zhen, and L. Fu, *Phys. Rev. Lett.* **120**, 146402 (2018).
- [46] K. Kawabata, K. Shiozaki, M. Ueda, and M. Sato, *Phys. Rev. X* **9**, 041015 (2019).
- [47] F. Tang, H. C. Po, A. Vishwanath, and X. Wan, *Nature* **566**, 486 (2019).
- [48] T. Zhang, Y. Jiang, Z. Song, H. Huang, Y. He, Z. Fang, H. Weng, and C. Fang, *Nature* **566**, 475 (2019).
- [49] M. G. Vergniory, L. Elcoro, C. Felser, N. Regnault, B. A. Bernevig, and Z. Wang, *Nature* **566**, 480 (2019).
- [50] S. Ono, H. C. Po, and H. Watanabe, arXiv e-prints, arXiv:1909.09634 (2019).
- [51] M. Geier, P. W. Brouwer, and L. Trifunovic, arXiv e-prints, arXiv:1910.11271 (2019).
- [52] B. Béri, *Phys. Rev. B* **81**, 134515 (2010).
- [53] P. M. R. Brydon, A. P. Schnyder, and C. Timm, *Phys. Rev. B* **84**, 020501 (2011).
- [54] A. P. Schnyder and S. Ryu, *Phys. Rev. B* **84**, 060504 (2011).
- [55] H. Zhou, C. Peng, Y. Yoon, C. W. Hsu, K. A. Nelson, L. Fu, J. D. Joannopoulos, M. Soljačić, and B. Zhen, *Science* **359**, 1009 (2018).
- [56] G. van Miert and C. M. Smith, *Phys. Rev. B* **93**, 035401 (2016).
- [57] K. S. Novoselov, A. K. Geim, S. V. Morozov, D. Jiang, M. I. Katsnelson, I. V. Grigorieva, S. V. Dubonos, and A. A. Firsov, *Nature* **438**, 197.
- [58] Y. Zhang, Y.-W. Tan, H. L. Stormer, and P. Kim, *Nature* **438**, 201 (2007).
- [59] P. R. Wallace, *Phys. Rev.* **71**, 622 (1947).
- [60] S. Cahangirov, M. Topsakal, E. Aktürk, H. Sahin, and S. Ciraci, *Phys. Rev. Lett.* **102**, 236804 (2009).
- [61] D. Malko, C. Neiss, F. Viñes, and A. Görling, *Phys. Rev. Lett.* **108**, 086804 (2012).
- [62] H. Huang, W. Duan, and Z. Liu, *New Journal of Physics* **15**, 023004 (2013).
- [63] K.-H. Jin, H. Huang, Z. Wang, and F. Liu, *Nanoscale* **11**, 7256 (2019).
- [64] Y. Guo, Z. Lin, J.-Q. Zhao, J. Lou, and Y. Chen, *Scientific Reports* **9**, 18516 (2019).
- [65] S. V. Ramankutty, J. Henke, A. Schiphorst, R. Nutakki, S. Bron, G. Arazi-Kanoutas, S. K. Mishra, L. Li, Y. K. Huang, T. K. Kim, M. Hoesch, C. Schlueter, T. L. Lee, A. de Visser, Z. Zhong, J. van Wezel, E. van Heumen, and M. S. Golden, *SciPost Phys.* **4**, 010 (2018).
- [66] S. Guan, Y. Liu, Z.-M. Yu, S.-S. Wang, Y. Yao, and S. A. Yang, *Phys. Rev. Materials* **1**, 054003 (2017).
- [67] P. G. de Gennes, *Superconductivity Of Metals And Alloys* (Westview Press, 1999).
- [68] D. J. Van Harlingen, *Rev. Mod. Phys.* **67**, 515 (1995).
- [69] C. C. Tsuei and J. R. Kirtley, *Rev. Mod. Phys.* **72**, 969 (2000).
- [70] S. Sachdev, *Quantum Phase Transitions*, 2nd ed. (Cambridge University Press, 2011).
- [71] A. H. Castro Neto, F. Guinea, N. M. R. Peres, K. S. Novoselov, and A. K. Geim, *Rev. Mod. Phys.* **81**, 109 (2009).
- [72] The effective model is derived from discussions with Qiang Zhang, and their paper is in preparation.
- [73] J. Hu and H. Ding, *Scientific reports* **2**, 381 (2012).
- [74] C. K. Chiu, Y. H. Chan, and A. P. Schnyder, arXiv e-prints, arXiv:1810.04094 (2018), arXiv:1810.04094.
- [75] X.-F. Zhou, X. Dong, A. R. Oganov, Q. Zhu, Y. Tian, and H.-T. Wang, *Phys. Rev. Lett.* **112**, 085502 (2014).
- [76] L. Z. Zhang, Z. F. Wang, Z. M. Wang, S. X. Du, H.-J. Gao, and F. Liu, *The Journal of Physical Chemistry Letters* **6**, 2959 (2015).
- [77] L. Z. Zhang, Z. F. Wang, S. X. Du, H.-J. Gao, and F. Liu, *Phys. Rev. B* **90**, 161402 (2014).
- [78] Y. Gu, Q. Zhang, C. Le, Y. Li, T. Xiang, and J. Hu, *Phys. Rev. B* **100**, 165405 (2019).
- [79] J. Wang, S. Deng, Z. Liu, and Z. Liu, *National Science Review* **2**, 22 (2015).
- [80] Y. Li, X. Wu, Y. Gu, C. Le, S. Qin, R. Thomale, and J. Hu, *Phys. Rev. B* **100**, 214513 (2019).
- [81] C. M. Bender, *Rep. Prog. Phys.* **70**, 947 (2007).
- [82] N. Moiseyev, *Non-Hermitian Quantum Mechanics* (2011).
- [83] I. Rotter and J. P. Bird, *Rep. Prog. Phys.* **78**, 114001 (2015).
- [84] L. Feng, R. El-Ganainy, and L. Ge, *Nat. Photonics* **11**, 752 (2017).
- [85] R. El-Ganainy, K. G. Makris, M. Khajavikhan, Z. H. Musslimani, S. Rotter, and D. N. Christodoulides, *Nat. Phys.* **14**, 11 (2018).

- [86] S. K. Ozdemir, S. Rotter, F. Nori, and L. Yang, *Nat. Mater.* **18**, 783 (2019).
- [87] S. K. Gupta, Y. Zou, X.-Y. Zhu, M.-H. Lu, L. Zhang, X.-P. Liu, and Y.-F. Chen, (2018), [arXiv:1803.00794](https://arxiv.org/abs/1803.00794).
- [88] V. M. Martinez Alvarez, J. E. Barrios Vargas, M. Berdakin, and L. E. F. Foa Torres, *Eur. Phys. J. Spec. Top.* **227**, 1295 (2018).
- [89] A. Ghatak and T. Das, *J. Phys.*, 29 (2019).
- [90] C. M. Bender and S. Boettcher, *Phys. Rev. Lett.* **80**, 5243 (1998).
- [91] C. M. Bender, D. C. Brody, and H. F. Jones, *Phys. Rev. Lett.* **89**, 270401 (2002).
- [92] M. A. Stephanov, *Phys. Rev. Lett.* **76**, 4472 (1996).
- [93] N. Hatano and D. R. Nelson, *Phys. Rev. Lett.* **77**, 570 (1996).
- [94] M. S. Rudner and L. S. Levitov, *Phys. Rev. Lett.* **102**, 065703 (2009).
- [95] S. Longhi, *Phys. Rev. Lett.* **105**, 013903 (2010).
- [96] T. E. Lee, *Phys. Rev. Lett.* **116**, 133903 (2016).
- [97] D. Leykam, K. Y. Bliokh, C. Huang, Y. D. Chong, and F. Nori, *Phys. Rev. Lett.* **118**, 040401 (2017).
- [98] R. A. Molina and J. González, *Phys. Rev. Lett.* **120**, 146601 (2018).
- [99] V. Kozii and L. Fu, arXiv e-prints, [arXiv:1708.05841](https://arxiv.org/abs/1708.05841) (2017), [arXiv:1708.05841 \[cond-mat.mes-hall\]](https://arxiv.org/abs/1708.05841).
- [100] M. Papaj, H. Isobe, and L. Fu, *Phys. Rev. B* **99**, 201107 (2019).
- [101] H. Shen and L. Fu, *Phys. Rev. Lett.* **121**, 026403 (2018).
- [102] S. Yao and Z. Wang, *Phys. Rev. Lett.* **121**, 086803 (2018).
- [103] S. Yao, F. Song, and Z. Wang, *Phys. Rev. Lett.* **121**, 136802 (2018).
- [104] F. Song, S. Yao, and Z. Wang, *Phys. Rev. Lett.* **123**, 170401 (2019).
- [105] F. Song, S. Yao, and Z. Wang, *Phys. Rev. Lett.* **123**, 246801 (2019).
- [106] F. K. Kunst, E. Edvardsson, J. C. Budich, and E. J. Bergholtz, *Phys. Rev. Lett.* **121**, 026808 (2018).
- [107] K. Yokomizo and S. Murakami, *Phys. Rev. Lett.* **123**, 066404 (2019).
- [108] Z. Yang, K. Zhang, C. Fang, and J. Hu, arXiv e-prints, [arXiv:1912.05499](https://arxiv.org/abs/1912.05499) (2019), [arXiv:1912.05499 \[cond-mat.mes-hall\]](https://arxiv.org/abs/1912.05499).
- [109] K. Zhang, Z. Yang, and C. Fang, (), [arXiv:1910.01131](https://arxiv.org/abs/1910.01131).
- [110] Y. Xu, S.-T. Wang, and L.-M. Duan, *Phys. Rev. Lett.* **118**, 045701 (2017).
- [111] A. Cerjan, M. Xiao, L. Yuan, and S. Fan, *Phys. Rev. B* **97**, 075128 (2018).
- [112] J. Carlström and E. J. Bergholtz, *Phys. Rev. A* **98**, 042114 (2018).
- [113] Z. Yang and J. Hu, *Phys. Rev. B* **99**, 081102 (2019).
- [114] T. Liu, Y.-R. Zhang, Q. Ai, Z. Gong, K. Kawabata, M. Ueda, and F. Nori, *Phys. Rev. Lett.* **122**, 076801 (2019).
- [115] Z. Zhang, M. Rosendo López, Y. Cheng, X. Liu, and J. Christensen, *Phys. Rev. Lett.* **122**, 195501 (2019).
- [116] X.-W. Luo and C. Zhang, *Phys. Rev. Lett.* **123**, 073601 (2019).
- [117] C. H. Lee, L. Li, and J. Gong, *Phys. Rev. Lett.* **123**, 016805 (2019).
- [118] Z. Gong, Y. Ashida, K. Kawabata, K. Takasan, S. Higashikawa, and M. Ueda, *Phys. Rev. X* **8**, 031079 (2018).
- [119] H. Zhou and J. Y. Lee, *Phys. Rev. B* **99**, 235112 (2019).
- [120] C.-H. Liu, H. Jiang, and S. Chen, *Phys. Rev. B* **99**, 125103 (2019).
- [121] J. Y. Lee, J. Ahn, H. Zhou, and A. Vishwanath, *Phys. Rev. Lett.* **123**, 206404 (2019).
- [122] R. Hamazaki, K. Kawabata, and M. Ueda, *Phys. Rev. Lett.* **123**, 090603 (2019).
- [123] S. Longhi, *Phys. Rev. Lett.* **122**, 237601 (2019).
- [124] B. Höckendorf, A. Alvermann, and H. Fehske, *Phys. Rev. Lett.* **123**, 190403 (2019).
- [125] H. Shen, B. Zhen, and L. Fu, *Phys. Rev. Lett.* **120**, 146402 (2018).
- [126] K. Kawabata, T. Bessho, and M. Sato, *Phys. Rev. Lett.* **123**, 066405 (2019).
- [127] D. Leykam, K. Y. Bliokh, C. Huang, Y. D. Chong, and F. Nori, *Phys. Rev. Lett.* **118** (2017).
- [128] Y. Xu, S.-T. Wang, and L.-M. Duan, *Phys. Rev. Lett.* **118**, 045701 (2017).
- [129] K. Kanki, S. Garmon, S. Tanaka, and T. Petrosky, *Journal of Mathematical Physics* **58**, 092101 (2017).
- [130] A. Z. I.M. Gelfand, M.M. Kapranov, *Discriminants, Resultants and Multidimen* (Birkhauser, 1994).
- [131] H. Woody, “Polynomial resultants,”.
- [132] S. JANSON, “Resultant and discriminant of polynomials,” (2010).
- [133] X.-L. Qi, T. L. Hughes, and S.-C. Zhang, *Phys. Rev. B* **78**, 195424 (2008).
- [134] Z. Gong, Y. Ashida, K. Kawabata, K. Takasan, S. Higashikawa, and M. Ueda, *Phys. Rev. X* **8**, 031079 (2018).
- [135] T. Kariyado and A. Vishwanath, *Phys. Rev. Research* **1**, 033076 (2019).
- [136] J. Ahn and B.-J. Yang, *Phys. Rev. Research* **2**, 012060 (2020).